

8-2014

Dissecting The Roles Of Trim24 In Regulation Of Hepatic Lipid Metabolism And Inflammation

Lindsey C. Minter

Follow this and additional works at: https://digitalcommons.library.tmc.edu/utgsbs_dissertations



Part of the [Medical Genetics Commons](#)

Recommended Citation

Minter, Lindsey C., "Dissecting The Roles Of Trim24 In Regulation Of Hepatic Lipid Metabolism And Inflammation" (2014). *Dissertations and Theses (Open Access)*. 497.
https://digitalcommons.library.tmc.edu/utgsbs_dissertations/497

This Dissertation (PhD) is brought to you for free and open access by the MD Anderson UTHealth Houston Graduate School at DigitalCommons@TMC. It has been accepted for inclusion in Dissertations and Theses (Open Access) by an authorized administrator of DigitalCommons@TMC. For more information, please contact digcommons@library.tmc.edu.

**DISSECTING THE ROLES OF TRIM24 IN REGULATION OF HEPATIC LIPID
METABOLISM AND INFLAMMATION**

by

Lindsey Cauthen Minter, B.S., B.A.

APPROVED:

Advisory Professor, Michelle C. Barton, PhD

Joya Chandra, PhD

Nancy Jenkins, PhD

Guillermina Lozano, PhD

Stephanie Watowich, PhD

APPROVED:

Dean, The University of Texas
Graduate School of Biomedical Sciences at Houston

**DISSECTING THE ROLES OF TRIM24 IN REGULATION OF HEPATIC LIPID
METABOLISM AND INFLAMMATION**

A

DISSERTATION

Presented to the Faculty of
The University of Texas
Health Science Center at Houston
and
The University of Texas
MD Anderson Cancer Center
Graduate School of Biomedical Sciences
in Partial Fulfillment

of the Requirements

for the Degree of

DOCTOR OF PHILOSOPHY

by

Lindsey Cauthen Minter, B.S., B.A.

Houston, Texas

August, 2014

DEDICATION

To my Lord and Savior, Jesus Christ, Who has given me salvation, strength, and hope to continue in the face of seemingly impossible odds.

There have been many times that I have been afraid, and You have comforted me. You have been ever faithful to teach me the wonderfully complex and unsearchable mysteries of your Creation.

Not for a moment, have You forsaken me...

Be glorified and famous!

Psalm 91

ACKNOWLEDGEMENTS

To my husband: Andy, my best friend and the love of my life. Thank you for showing me how to trust and pray without fear. Your constant pursuit of God has greatly impacted my life, thank you for living with unwavering conviction, discipline, and purpose. I am so grateful for your love that has spoken truth in my life. You have walked with me and many times carried me through this time. I am honored to be your wife and look forward to the future with you. Many blessings and love to you, my heart.

To my parents: Pam and Tim Cauthen, true pillars of strength in faith, wisdom, and love. Thank you for your courage in the face of opposition and your commitment to your word and work. Your example of Godly character and living out your convictions has permanently impacted my life. Thank you for taking the time to show me what is right and wrong and for living the same way that you taught. You have supported and walked with me during both the best and worst times of my life. Thank you for always being there. I cannot adequately express my gratitude for the sacrifices that you have made on my behalf, but I will never forget them. I can only pray that I will come to have even a fraction of your character. All my love.

To my grandparents: Betty and Kenneth Cauthen, Grandmother and Granddaddy, two pillars of the faith and constant prayer warriors. Thank you for living the life of sacrifice to the Lord for all to see. I am eternally grateful for your

legacy that you have passed on to your family of the value of setting your sights on the things that are truly important in life. Your constant prayer and encouragement has carried me through many times of trial. Thank you for your wise counsel and for making time to teach me from your experience and wisdom. All my love.

To my grandparents: Faye and G.L. McCullough, Granny and Pops, who were some of my biggest cheerleaders and just missed the opportunity to see me finally receive this degree. I miss you both multiple times everyday. Thank you for teaching me the value of education and good work, unconditional support and love, to never give up, and how to laugh in just about any situation. Your generosity and love for people have left a lasting mark on my heart. Thank you for the time and love you lavished on me, your memory will always be in my heart. Here's to you, kids, I'll be looking for you with every eye! Until we meet again...

To my family: Ken and Peggy Cauthen, Will, Christie, Mason and Seth Cauthen, Jack, Katie, Hank, and Isaac Castilaw, Ty Cauthen, Jeremy, Stefanie, Triston, Austin, and Hudson Williams, Gladys Owens, Pam and Neil Glenn, Cathi and Mark Lippert, Donna, Keith, Kara, and Mikala Slaughter, Mindi, David, and Cameron Morgan, Stephen Skaggs, Laura, Jeff, Amanda, and Brody Weidle, Elceone and Johnny Roberts, Sue and Dean Essery. Thank you for your unfailing love, support, and prayers.

To my best friends: Tiffany Johnson, Rachel Iglesias. Thank you for speaking truth into my life! To all of the gang at Bay Area First Baptist and Newly One: thank you for your prayers, editing, love, and listening ears.

To those who have gone before: Larry Stafford, Jimmy Dean Graves, Jimmy Roberts, Rachel Viola and Emzy H. Patrick, Nora Emily McCullough, Troy Owens, Phillip Childree. Thank you for the legacy you have left behind.

To my donors: Schissler Foundation, Sylvan Rodriguez Foundation, and Hearst Foundation for the monetary support that has made this work possible.

To my mentor: Dr. Michelle C. Barton. Thank you for taking a chance on me and seeing me through to the end. Your faith in me has helped me to spread my wings. I appreciate your willingness to let me pursue my passions. Thank you.

To my committee members: Dr. Guillermina Lozano, Dr. Nancy Jenkins, Dr. Joya Chandra, and Dr. Stephanie Watowich. Thank you for being an inspiration, a wealth of knowledge, a sounding board, and for the support and time you have poured into me. Women in science ROCK!

To all the past and present members of the Barton laboratory, who have helped me in unfathomable ways: Dr. Shiming Jiang, Dr. Abhinav Jain, Sabrina Stratton, Kendra Allton, Hui Wei, Aundrietta Duncan, Dr. Ryan McCarthy, Dr. Srikanth Appikonda, Kaushik Thakkar, Jing Li, Dr. Teresa Yiu, Dr. Zeynep C. Akdemir. I would not have been able to get to this point without your help. Thank you for the support, teaching, listening, constructive criticism, and fun.

To my collaborators at MD Anderson Cancer Center and abroad: Dr. Huiyuan Zhang, Dr. Benny Chang, Dr. Richard Lee, and so many more. Without your incredible skill and wonderful passion for science, I would not have arrived at this point.

DISSECTING THE ROLES OF TRIM24 IN REGULATION OF HEPATIC LIPID METABOLISM AND INFLAMMATION

Lindsey Cauthen Minter, B.S., B.A.

Advisory Professor: Michelle C. Barton, Ph.D.

In this dissertation, I report the characterization of a new mouse model that recapitulates development of hepatocellular carcinoma (HCC) following spontaneous hepatic lipid accumulation, inflammation, and damage of liver tissue, due to complete loss of *Trim24* expression. In human HCC and other cancers, TRIM24 expression is aberrantly high, while deletion of TRIM24 in the mouse has been shown to act as a liver specific tumor suppressor. The hypothesis tested here was that TRIM24, the E3 ubiquitin ligase of p53, regulates genes that impact hepatic lipid inflammation and metabolism. I further dissected whether TRIM24 regulates immune cell populations that are commonly misregulated in nonalcoholic fatty liver disease (NAFLD) and nonalcoholic steatohepatitis (NASH). In the first part of my dissertation, I establish through global gene expression, chromatin enrichment, biochemical, and immunohistochemical analyses that TRIM24 represses hepatic lipid accumulation, inflammation, and fibrosis and damage in the murine liver. In the second part of my thesis, I show that loss of *Trim24* leads to increased hepatic macrophage populations and implicates crosstalk with the hematopoietic niche in the bone marrow. Intersections of RNA-seq and TRIM24 ChIP-seq datasets

yielded novel gene targets of TRIM24 in mouse liver. Furthermore, I show that TRIM24 is enriched at promoters of genes involved in oxidative stress control, inflammation, and glucose metabolism, all processes that are misregulated in NAFLD and NASH progression. Further, biochemical analyses showed increased glucose metabolism and insulin sensitivity coupled with a decrease in visceral adipose tissue upon loss of *Trim24*. These findings recapitulate those found in human studies of lean (non-obese) individuals with NAFLD. Thus, this dissertation shows that complete loss of *Trim24* offers a model of nonalcoholic fatty liver disease, steatosis, fibrosis and development of hepatocellular carcinoma in the absence of high-fat diet or obesity. In addition, this model offered an opportunity to identify specific immune cell populations, gene targets and metabolic pathways that are regulated by TRIM24.

DEDICATION.....	iii
ACKNOWLEDGEMENTS.....	iv-vii
ABSTRACT.....	viii-ix
TABLE OF CONTENTS.....	x-xiv
LIST OF FIGURES.....	xv-xix
LIST OF TABLES/APPENDICES.....	xx-xxi
ABBREVIATIONS.....	xxii-xxiii
CHAPTER I: INTRODUCTION AND RATIONALE FOR THE STUDY	
1.1. The liver: home to metabolism and immunity.....	2-7
<i>a. Zonal regions</i>	
<i>b. Cell specific functions</i>	
1.2. Transcription factors in the liver.....	8-10
<i>a. Lipid metabolism</i>	
<i>b. Inflammation</i>	
1.3. The “two-hit” theory of NAFLD.....	10
1.4. NAFLD, NASH, HCC disease spectrum.....	11-18
<i>a. Histological and pathological features</i>	
<i>b. Potential mechanisms and animal models</i>	
<i>c. Incidence, mutations, and ethnicities affected</i>	
<i>d. Diagnositic features</i>	
<i>e. Current treatment modalities</i>	
1.5. TRIM24 as a transcriptional co-regulator.....	19-21
1.6. Hypothesis and Aims of this work.....	22

CHAPTER II: MATERIALS AND METHODS

2.1. Generation of germline <i>Trim24</i> ^{dIE1} deficient mice.....	26-27
2.2. PCR analysis of <i>Trim24</i> genotypes.	27-29
<i>a. Germline deletion of Trim24</i>	
<i>b. Albumin-Cre; Trim24</i> ^{LoxP/LoxP}	
2.3. Southern blot analysis of <i>Trim24</i> genotypes.....	29
2.4. Western blot analysis of <i>Trim24</i> genotypes.....	30
2.5. RNA extraction and quantitative Real-time (qRT-PCR analysis).....	30-32
2.6. Histological and immunohistochemical studies.....	32-37
<i>a. Paraffin embedded sections</i>	
<i>b. Frozen tissue sections</i>	
<i>c. Oil red O staining</i>	
<i>d. Trichrome Staining</i>	
<i>e. PAS Staining</i>	
<i>f. Immunohistochemistry</i>	
2.7. Plasma collection.....	37
2.8. Serum collection.....	37
2.9. ALT/AST and Lipid profile analysis.	38
2.10. Glucose tolerance/Insulin tolerance testing (GTT/ITT testing)	38-39
2.11. Liver perfusion.....	39-40
2.12. Hepatic Immune Cell Isolation.....	40
2.13. Bone marrow collection.....	41
2.14. Flow Cytometry Analysis.....	41-42

a. <i>RBC Lysis</i>	
b. <i>Cell Fixation and Staining</i>	
c. <i>FlowJo Analysis</i>	
2.15. <i>CyTOF (sample preparation and analysis)</i>	42-44
a. <i>Antibody labeling.</i>	
b. <i>Sample staining and fixation</i>	
c. <i>Sample permeabilization and labeling</i>	
d. <i>IR-intercalator staining</i>	
e. <i>viSNE analysis</i>	
2.16. <i>Chromatin Immunoprecipitation (ChIP)</i>	45-49
a. <i>Making the liver lysate</i>	
b. <i>Testing the lysate</i>	
c. <i>MNase digestion, lysis, pre-clearing and addition of antibody to samples</i>	
d. <i>Washing and removal of RNA/protein from samples</i>	
e. <i>DNA extraction and qPCR</i>	
f. <i>Designing Primers for ChIP</i>	
2.17. <i>RNA-seq data analysis.</i>	49
2.18. <i>ChIP-seq data analysis.</i>	50
2.19. <i>Variant analysis</i>	51
2.20. <i>Statistical analysis</i>	51

CHAPTER III: TRIM24 SUPPRESSES DEVELOPMENT OF SPONTANEOUS HEPATIC LIPID ACCUMULATION AND HEPATOCELLULAR CARCINOMA IN MICE.

3.1. Introduction.....52-54

3.2. A *Trim24*^{-/-} mouse generated by deletion of promoter and exon 1.....54-59

3.3. *Trim24*^{-/-} mice develop hepatocellular lesions, steatosis and HCC.....59-72

3.4. Inflammation, injury and degeneration are increased in adult *Trim24*^{-/-} mice.....73-78

3.5. Genome-wide analysis of gene expression in *Trim24*^{-/-} liver reveals misregulation of lipid metabolism and inflammation.....79-80

3.6. Lipid metabolism and inflammation are aberrantly regulated in *Trim24*^{-/-} liver.....81

3.7. TRIM24 directly regulates genes in lipid metabolic, inflammation and damage pathways.....82-85

3.8. Discussion.....86-90

CHAPTER IV: TRIM24 SUPPRESSES PROGRESSIVE CHRONIC INFLAMMATION AND PROTECTS FROM SECONDARY METABOLIC DISORDERS ASSOCIATED WITH NASH PROGRESSION.

4.1. Introduction.....91-99

4.2. Germline deletion of TRIM24 causes an increase in hepatic macrophage populations.....100-103

4.3. Intersection of RNA-seq and ChIP-seq datasets reveals differentially expressed TRIM24 bound metabolic and inflammatory target genes.....	104-110
4.4. <i>Trim24</i> ^{-/-} mice exhibit increased glucose metabolism and insulin sensitivity.....	111-117
4.5. Loss of TRIM24 causes a decrease in visceral body fat.....	118-121
4.6. Overlap of RNA-seq and ChIP-seq analysis reveals differentially expressed TRIM24 bound lipid and glucose metabolic target genes.....	122-123
4.7. Discussion.....	124-126

CHAPTER V: DISCUSSION AND FUTURE DIRECTIONS

5.1. TRIM24 and metabolism...a balancing act?.....	127-133
5.2. Do specific domains of TRIM24 regulate inflammatory and lipid metabolic processes in the liver?.....	133-135
5.3. Does TRIM24 impact crosstalk between hepatocytes and immune cells in liver disease?.....	135-147
5.4. Links between TRIM24, p53 and HCC?.....	147
5.5. Implications for inflammasome-directed crosstalk between bone marrow and liver leading to progression of the NAFLD, NASH, HCC spectrum.	148
5.6. TRIM24 and human NAFLD, NASH, and HCC.....	149
CONCLUSIONS	150-153
CONTRIBUTIONS	154
APPENDIX	176-179
BIBLIOGRAPHY	180-203
VITA	204

LIST OF FIGURES

Chapter I

Diagram 1. Zonal anatomy and functions of the liver. anatomy and functions of the liver.....	6
Diagram 2. Cells of the liver.....	7
Diagram 3. Hepatic Transcription factors and fatty acid metabolism.....	9
Diagram 4: Hits in the progression of the NAFLD, NASH, HCC spectrum.....	13
Diagram 5. TRIM24 protein structure.....	23
Diagram 6. Model summarizing the hypothesis that TRIM24 was a hepatoprotective role the against the hallmarks of NAFLD, NASH, and HCC.....	24

Chapter III

Figure 1. Scheme for generation of the <i>Trim24</i> ^{-/-} mouse.....	55
Figure 2. PCR Genotyping analysis confirming deletion of <i>Trim24</i> exon 1.....	56
Figure 3. Confirmation of <i>Trim24</i> deficiency.....	57
Figure 4. Loss of <i>Trim24</i> RNA expression in <i>Trim24</i> ^{-/-} liver: RNA-seq of <i>Trim24</i> ^{-/-} and WT.....	58
Figure 5. Deletion of TRIM24 has no effect on TRIM28/33 expression.....	61
Figure 6. Lipids and fibrosis increase in aging <i>Trim24</i> ^{-/-}	62
Figure 7. Normal morphology, lipid accumulation and fibrosis in age-matched <i>Trim24</i> ^{+/+} livers (6 months).....	63
Figure 8. Lipid accumulation in <i>Trim24</i> ^{-/-} livers.....	64
Figure 9. Fibrosis is not evident in young <i>Trim24</i> ^{-/-} livers.....	65

LIST OF FIGURES (continued)

Chapter III (continued)

Figure 10. Fibrosis gene expression is upregulated upon loss of <i>Trim24</i>	67
Figure 11. Liver index is increased in <i>Trim24</i> ^{-/-} mice.....	68
Figure 12. Aging <i>Trim24</i> ^{-/-} mice develop hepatocellular carcinoma.....	69
Figure 13. Normal morphology in livers of <i>Trim24</i> ^{+/+} and <i>Trim24</i> ^{+/-} mice.....	70
Figure 14. Distribution of HCC progression in aging <i>Trim24</i> ^{-/-} livers.....	71
Figure 15. <i>Trim24</i> ^{-/-} mouse survival curve.....	72
Figure 16. Hepatocellular damage and dysfunction in 2 month <i>Trim24</i> ^{-/-}	75
Figure 17. Abdominal peripheral fat is decreased in <i>Trim24</i> ^{-/-} mice.....	76
Figure 18. <i>Trim24</i> ^{-/-} livers show evidence of increased hepatocellular damage..	77
Figure 19. Apoptosis and fibrosis related genes are upregulated in <i>Trim24</i> ^{-/-} liver.....	78
Figure 20. Loss of TRIM24 causes hepatic misregulation of lipid metabolic, stress, and inflammatory related gene expression.....	80
Figure 21. Loss of TRIM24 causes misregulation of inflammatory, stress, and lipid metabolic related gene expression indicative of NAFLD/NASH.....	84
Figure 22. TRIM24 regulates hepatic lipid metabolism, stress and inflammation genes.....	85
Figure 23. Retro-viral associated gene expression is increased in <i>Trim24</i> ^{-/-} mice.	89
Figure 24. Retinoid responsive genes are misregulated in <i>Trim24</i> ^{-/-} livers at 3 and 10 weeks of age.....	90

Chapter IV

Figure 25. Glycolysis, TCA cycle, and Fatty Acid Regulation.....	97
Figure 26. Hepatic macrophages are increased in <i>Trim24</i> ^{-/-} liver.....	101
Figure 27. Hepatic macrophages are increased in <i>Trim24</i> ^{-/-} liver.....	102
Figure 28. Hepatic myeloid cells are increased in <i>Trim24</i> ^{-/-} liver.....	103
Figure 29. Integrated RNA- and ChIP-seq and identification of TRIM24 bound, differentially expressed gene targets that are repressed by TRIM24.....	107
Figure 30. Integrated RNA- and ChIP-seq and identification of TRIM24 bound, differentially expressed gene targets that are activated by TRIM24.....	108
Figure 31. TRIM24 binds oxidative stress response and inflammatory factors in the liver.....	110
Figure 32. Workflow of glucose and insulin tolerance tests (GTT/ITT).....	113
Figure 33. Glucose metabolism and insulin sensitivity increases in male 2, 4, and 6 month <i>Trim24</i> ^{-/-} mice.....	114
Figure 34. Glucose metabolism is relatively unchanged and insulin sensitivity increases in female 2, 4, and 6 month <i>Trim24</i> ^{-/-} mice.....	115
Figure 35. Hepatic gene expression levels of glycolysis related factors are decreased upon loss of <i>Trim24</i>	116
Figure 36. Loss of TRIM24 leads to decreased glycogen metabolism during aging.....	117
Figure 37. Loss of TRIM24 causes a decrease in total body weight during aging.....	119

Figure 38. Loss of TRIM24 causes a decrease in visceral white fat weight during aging.....120

Figure 39. Loss of TRIM24 has no effect on liver index prior to HCC progression.....121

Figure 40. TRIM24 binds lipid and glucose factors in the liver.....123

Chapter V

Diagram 7. Future direction studies128

Figure 41. Bone marrow derived macrophages have increased M2 macrophage associated gene expression in *Trim24*^{-/-}138

Figure 42. Analysis (PCR, qPCR, and IHC) confirming Cre expression and localization in *Albumin-Cre; Trim24*^{LoxP/LoxP} liver139

Figure 43. Timeline of disease progression and incidence of HCA and HCC in *Trim24*^{-/-} versus *Albumin-Cre; Trim24*^{LoxP/LoxP}140

Figure 44. Hepatocellular damage and dysfunction in 2 month *Albumin-Cre; Trim24*^{LoxP/LoxP} mice.....141

Figure 45. Liver-specific deletion of *Trim24* increases the abundance of myeloid lineage precursor cells in the bone marrow143

Figure 46. Liver-specific TRIM24 knockout induces an inflammatory response in the bone marrow and increases the abundance of myeloid lineage precursor cells.....144

Chapter VI

Diagram 8. Working model summarizing the effects of TRIM24 loss in the mouse model.....	153
---	-----

LIST OF TABLES

Table 1: Mouse models of NAFLD/NASH.....	15
Table 2: Sequences of 5' probe and 3' probe used for Southern blot.....	155
Table 3: Primers for real-time PCR analysis of mRNA expression.....	156-157
Table 4: Primers for CHIP PCR analysis.....	158-159
Table 5: Pathology report and diagnosis of aging <i>Trim24</i> ^{-/-} mice.....	160-167
Table 6: Top up- and down-regulated categories from <i>Trim24</i> ^{-/-} vs. <i>Trim24</i> ^{+/+} RNA-seq.....	168-169
Table 7: Lipid and Inflammatory genes activated and repressed in <i>Trim24</i> ^{-/-}	170
Table 8: Comparison of phenotypic characteristics in DE4 and DE1 <i>Trim24</i> ^{-/-} mice.....	171
Table 9: <i>Trim24</i> variants and predicted products upon deletion of E4.....	172-173
Table 10: Glucose transporter genes expressed in the liver.....	98
Table 11: Top 5 IPA categories and gene targets from integration of RNA- and CHIP-seq in mouse liver.....	109
Table 12: Predictive factors of NAFLD in lean compared to obese patients.....	126
Table 13: Current mouse models available in the Barton laboratory for further studies.....	132
Table 14: Flow Cytometry Antibodies.....	174
Table 15: CyTOF Antibodies.....	175

LIST OF APPENDICES

Appendix 1: Solution list for ChIP.....	176-179
---	---------

LIST OF ABBREVIATIONS

KC – Kupffer Cells

NAFLD – Nonalcoholic fatty liver disease

NASH - Nonalcoholic steatohepatitis

HCC – Hepatocellular carcinoma

ALT – alanine aminotransferase

AST – aspartate aminotransferase

US – Ultrasound

TG – Triglycerides

IHC – Immunohistochemistry

CytoF – Mass spectrometry cell time of flight

FACS- Flow analysis of cell sorting

visNE - Visual Stochastic Neighbor Embedding

GTT- Glucose tolerance test

ITT – Insulin tolerance test

HSC – Hematopoietic stem cell

CFU- GM – Colony forming unit, granulocyte/macrophage

IL – Interleukin

CFU-M – Colony forming unit – macrophage

Arg1 –Arginase-1 enzyme

CSF1/M-CSF – macrophage colony stimulating factor 1

TNF- α – Tumor necrosis factor – α

CXCL/CCL – Chemokines

RANKL – Receptor activator of NF- κ B ligand

IFN- γ – Interferon gamma

List of Abbreviations (continued)

SR – Scavenger receptors

GM-CSF – Granulocyte macrophage colony stimulating factor

RNS – Reactive nitrogen series

ROS – Reactive oxygen series

NR – Nuclear Receptor

RAR- α – Retinoic Acid Receptor alpha

ER- α – Estrogen Receptor alpha

RXR/LXR – Retinoid X receptor/Liver X receptor

CHAPTER I

INTRODUCTION

BACKGROUND AND RATIONALE FOR THE STUDY

1.1. The liver: a fine tuned balance between metabolism and immunity

The liver, the largest solid organ in the body, houses an incredibly complex system that metabolizes carbohydrates, protein, lipids and glucose, and produces bile acids to aid in the breakdown of food for usable energy that is utilized by multiple organs in the body. In addition to these metabolic processes, the liver serves as an immune organ by filtering toxins from the blood and protects the body [1]. Patterns of signaling, import, and export are kept in perfect balance through these liver processes. Blood, containing hydrophilic nutrients from the intestine, enters the liver via the hepatic portal vein, these nutrients are metabolized, and then distributed to the rest of the body through the central vein [2]. Oxygenated blood enters the liver through the hepatic artery, which resides within the portal triad (bile duct, portal vein, hepatic artery). Based upon the boundaries outlined by the hepatic vasculature, the liver is divided into functional units that are composed of lobules that surround a central vein and the borders are composed of portal tracts [3]. K. Jungermann proposed the use of “zones, ” after discovering that hepatocytes have specialized functions based upon their proximity to different vasculature [4] [5] . There are 3 zones in each lobule (Diagram 1): 1) periportal, 2) midportal, and 3) pericentral, with portal zones (1,2) being closest to the periphery and the central zone (3) being nearest to the central vein. Blood flows from the portal vein and hepatic artery to the central vein (zones 3 to 1), while bile flows in the opposite direction (zones 1 to 3). The various functions of the liver are carried out by either parenchymal (hepatocytes) or non-parenchymal cells. The bulk of the liver is composed of hepatocytes (parenchyma) that extend along the hepatic plate (from

the portal triad to the vein), and whose primary function is to maintain metabolic homeostasis and to proliferate upon damage [1] (Diagram 1). Lipogenesis occurs in zone 1, while fatty acid degradation occurs in zone 2 [2]. Additional zonation of metabolic functions applies to ammonia and glutamine metabolism/transport, glucose/energy metabolism, and drug metabolism (Diagram 1). Synthesis of serum proteins and albumin are common metabolic processes performed by all hepatocytes that occur across zones [2].

While most of the liver is composed of parenchymal cells, non-parenchymal cells also play a critical role in homeostasis by moderating hepatic immune response. Non-parenchymal cells can be sub-divided into: stellate, endothelial, and Kupffer cells (Diagram 2). Stellate cells are found in the Space of Disse, between hepatic endothelial and epithelial cells and represent approximately 5-8% of the cells in the liver. While their main function is to store lipid droplets, stellate cells also store a large amount of vitamin A [6]. Upon liver damage, activated stellate cells respond to immune signals at the source of the injury and produce extracellular matrix (ECM) to form a scar, which can lead to fibrosis [7]. Fibrosis is defined as excessive deposition of the extracellular matrix (ECM), eventually leading to destruction and impairment of organ structure and organ function that can lead to various liver disease such as HCC [8]. Activated hepatic stellate cells and fibroblasts cause an increase in proliferation, fibrogenesis, contractility, matrix degradation, chemotaxis and cytokine release [9]. While still under debate, it is thought that activated fibroblasts arise from hepatic stellate cells [10]. Recent studies have shown that hepatic stellate cells are stimulated by platelet-derived growth factor (PDGF)-BB

and transforming growth factor (TGF)-1, and/or epithelial growth factor (EGF) led to an increase in both migratory capacity and matrix metalloproteinase (MMP) 2-activity [9]. Further studies establish a connection between hepatic fibroblasts and hepatocytes in progression of fibrosis. In the past, direct contribution of hepatocytes to liver fibrosis was thought be relatively minor, studies by Kalluri et al. (2007) demonstrated that TGF- β 1, a pro-fibrotic growth factor, induces adult mouse hepatocytes to undergo morphological and functional changes that are hallmarks of epithelial to mesenchymal transition (EMT) and is inhibited by bone morphogenic protein-7 (BMP7) [10]. Additionally hepatocytes that undergo EMT contribute to increase populations of activated fibroblasts in CCL₄-induced liver fibrosis, thus linking hepatocytes, stellate cells, and fibroblasts to progression of hepatic fibrosis. In addition to functions in fibrotic progression, stellate cells secrete cytokines and growth factors to aid in regeneration of hepatic epithelial cells, such as cholangiocytes (bile cells) and hepatocytes [10]. Other non-parenchymal cells also serve important functions in the liver. Endothelial cells reside in the sinusoid of the liver and arise from hepatoblast cells during embryonic development [11]. Oval cells are intrahepatic endothelial “stem cells” that are thought to interact with hepatocytes to aid in liver regeneration following liver damage or surgical resection. Kupffer cells (KC,macrophages), which reside in the sinusoids, are the first macrophages that come into contact with foreign bacteria or material via the blood from the intestine circulated through the portal vein [12]. Hepatic KCs constitute 80-90% of the macrophages present in the body and, as suggested, are members of the immediate (innate) immune response to foreign, potentially dangerous material [13]. It is

thought that KCs arise from circulating monocytes that migrate from the bone marrow to the blood and transform to macrophages that then migrate to different organs such as the liver [14]. Normally, KCs compose about 35% of the non-parenchymal cells in the liver of adult mice. KCs in the liver increase in cell density and are activated following damage or interactions with foreign material (i.e. bacteria) and are associated with acute hepatitis (human) or chemical injury (rodents) [15, 16].

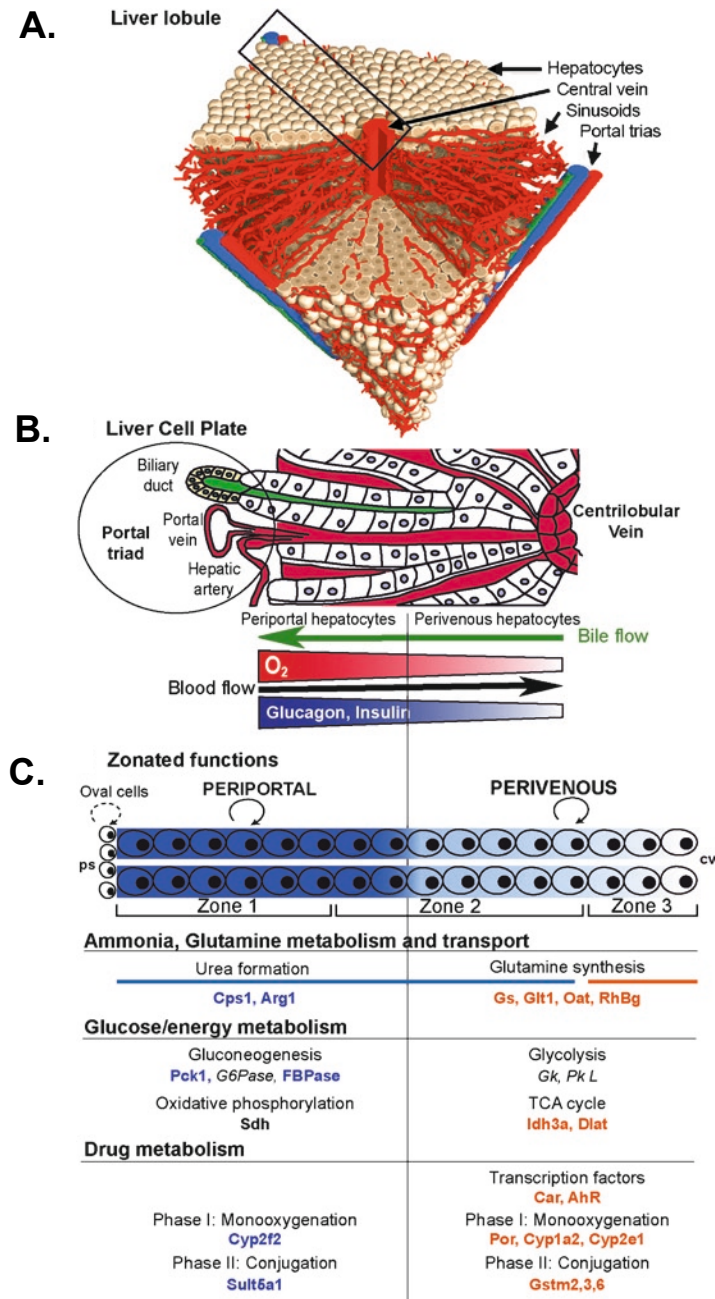


Diagram 1. Zonal anatomy and functions of the liver. **A)** The liver lobule with cut away view to show architecture and arrangement. **B)** View of the portal triad organization composed of biliary duct, portal vein and hepatic artery. Blood flows from the portal triad into the centrilobular vein, while bile, oxygen, glucagon and insulin flow/produced in the opposite direction. **C)** Zones of the liver and their related functions in metabolism. (Reprinted with permission from Monga, P.S. Ed. *Springer Press. Molecular Pathogenesis of Liver Diseases. 2011*) [2]

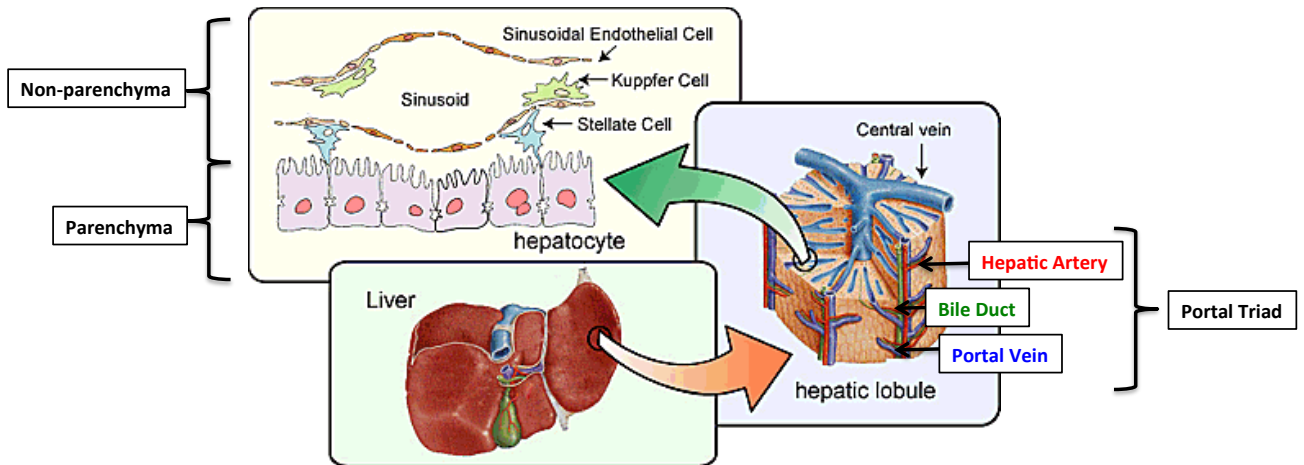


Diagram 2. Cells of the liver. Each hepatic lobule contains a complex organization of hepatic cells composed mostly of hepatocytes (parenchyma) and stellate cells (non parenchyma) bordering the sinusoids that transfer bile and blood in and out of the liver, respectively. Non-parenchymal sinusoidal endothelial cells line the sinusoids and Kupffer cells reside within the sinusoids. (Modified from www.rutlandherald.typepad.com).

1.2. Transcription factors in the liver

The liver is responsible for a multitude of metabolic processes and efficiently converts food into usable energy for the body. Several key nuclear receptor transcription factors such as: PPAR (α , β , γ 1, and γ 2), HNF4 (α and γ), retinoid X-receptor (RXR) α , and liver X receptor (LXR) (α and β) regulate fatty acid metabolism, which is one of the most utilized processes in the liver [17] (Diagram 3). Nonesterified fatty acids (NEFAs) bind to the ligand-binding domain of each of these nuclear receptors and function like hydrophobic hormones to control the function of the receptor. Dietary polyunsaturated fatty acids (PUFAs) function to suppress key transcription factors that control hepatic lipid metabolism and inflammation such as: SREBP-1, carbohydrate regulatory element-binding protein (ChREBP), max-like factor X (MLX), and nuclear factor κ B (NF κ B) [17]. The first transcription factors that are activated following liver resection or damage, along with NF κ B, are Stat3 and AP-1 [18, 19] [20]. Additionally, gluconeogenesis in the liver is controlled by the forkhead box O1 (FoxO1) transcription factor and its coactivator, PGC1 α [17]. Under normal conditions, these processes work in conjunction to effectively regulate both the metabolic and immune processes of the liver. However, upon misregulation of these processes, disease progression occurs. The presence of lipid peroxidation, which is the oxidative degradation of lipids, is indicative of oxidative stress [17]. These stress responses are linked to inflammatory responses that are controlled by transcription factors such as NF κ B and are implicated in progression and pathogenesis of various diseases such as non-alcoholic fatty disease (NAFLD) [17].

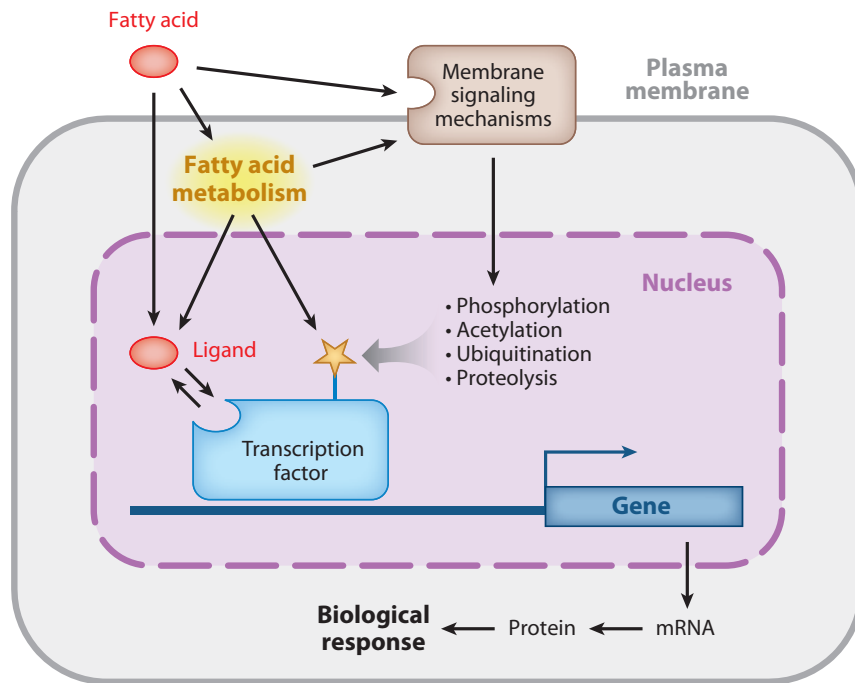


Diagram 3. Hepatic Transcription factors and fatty acid metabolism. Hepatic fatty acid metabolism overview. (Reprinted with permission from *Annu. Rev. Nutr.* 2013. 33:249–69) [17].

The progression of NAFLD has been connected with both misregulation of lipid metabolism, oxidative stress and damage in the liver and recruitment of Kupffer cells and leukocytes. The paracrine signaling from these cells releases cytokines such as interleukin 6 (IL-6) and tumor necrosis factor (TNF), which in turn cause progression of the disease in the surrounding parenchymal and stellate cells [17-19]. Chronic hepatic inflammation is known to be a causative factor in permanent hepatocyte damage, which in turn sets the stage for development of HCC.

1.3. The two-hit theory in Non-alcoholic fatty liver disease (NAFLD) and Non-alcoholic steatohepatitis (NASH).

In the disease progression spectrum from steatosis to steatohepatitis, a long-standing theory was proposed by Christopher Day and coined the “two-hit theory”. This theory suggests that the “first hit” in the disease progression is the development of hepatic steatosis (lipid accumulation) [21]. If there are no other changes in the organ environment, genetic or otherwise, the disease usually does not progress. However, if a “second hit” is present, such as increased oxidative stress, DNA damage, or fibrosis, and the disease progresses to the more aggressive steatohepatitis [21]. Steatohepatitis is a condition that is defined by retention of lipids in the liver that causes a chronic inflammatory disorder, which left unchecked, progresses to cirrhosis. While the initial theory was proposed in cases of alcohol related disease progression, the same tenets have been cited in non-alcoholic fatty liver disease (NAFLD) and non-alcoholic steatohepatitis (NASH).

1.4. NAFLD, NASH, HCC disease spectrum

NAFLD is now the most common liver disease in the Western world, however prevalence varies within different ethnic populations, genders, and spectrum of health [22]. NAFLD is defined by an excessive accumulation of triglycerides (TG) in the liver (steatosis) of individuals who do not consume excessive amounts of alcohol [23]. It is known to be the most common cause for liver damage (due to abnormal liver biochemistry and cirrhosis) and frequently causes the need for liver transplantation [24]. Histological standards dictate that over 5% of hepatocytes must possess steatosis to corroborate a diagnosis of NAFLD [25]. By definition, steatosis is the presence of vacuoles that contain lipid deposits in varying degrees of severity. These lipid-filled vacuoles are either distributed in small amounts throughout the cytoplasm (microvesicular steatosis) or completely engulf the cytoplasm and displace the nucleus (macrovesicular steatosis) [26]. There are two sub-types of NAFLD: (1) patients that present with solely steatosis and (2) the 10-20% with nonalcoholic steatohepatitis (NASH), a more aggressive disease, due to chronic inflammation and hepatocellular injury [27, 28].

NASH is further defined by liver-specific misregulation of cholesterol homeostasis, lipid accumulation, aberrant glucose metabolism, insulin resistance, and inflammation, which leads to a chronic state of metabolic imbalance [27, 28]. Histologically, NASH is defined by steatosis in hepatocytes and hepatocellular damage due to inflammation as evidenced by hepatic ballooning, Mallory bodies, infiltration of neutrophils, macrophages, and lymphocytes [26]. Additionally, megamitochondria and abnormal iron deposition are frequently present. Hepatic

ballooning is most prevalent near areas of steatosis, while Mallory bodies are structures that arise due to eosinophilic infiltration. While all of these conditions can occur in specific zones (1&3) of the liver, they are not restricted to these areas [3].

NASH patients have a higher rate of cirrhosis, liver failure and hepatocellular carcinoma (HCC), compared to individuals with NAFLD [29]. While the processes causing progression from NAFLD to NASH are reversible, most patients have progressed to the irreversible state of cirrhosis or HCC by the time of diagnosis (Diagram 4).

Many patients present with hepatic steatosis but do not progress to chronic inflammation or fibrosis (NASH) [30]. However, there are 10-20% of patients who do progress from NAFLD to NASH [31]. Most studies have focused on either genetics or diet as the cause of NAFLD incidence and progression to NASH and more advanced disease. Activation of the oxidative stress response has been connected with inflammatory processes due to misregulated lipid metabolism [32]. Recent studies suggest that the reactive oxygen series (ROS), products of lipid peroxidation (lipotoxicity), and tumor necrosis factor- α (TNF- α) are responsible for the transition from steatosis to NASH [33]. Furthermore, progression of fibrosis has been shown to increase the risk of HCC 25-fold [34]. While poorly understood, it seems that these elements are instrumental in progression of NASH and setting the stage for HCC.

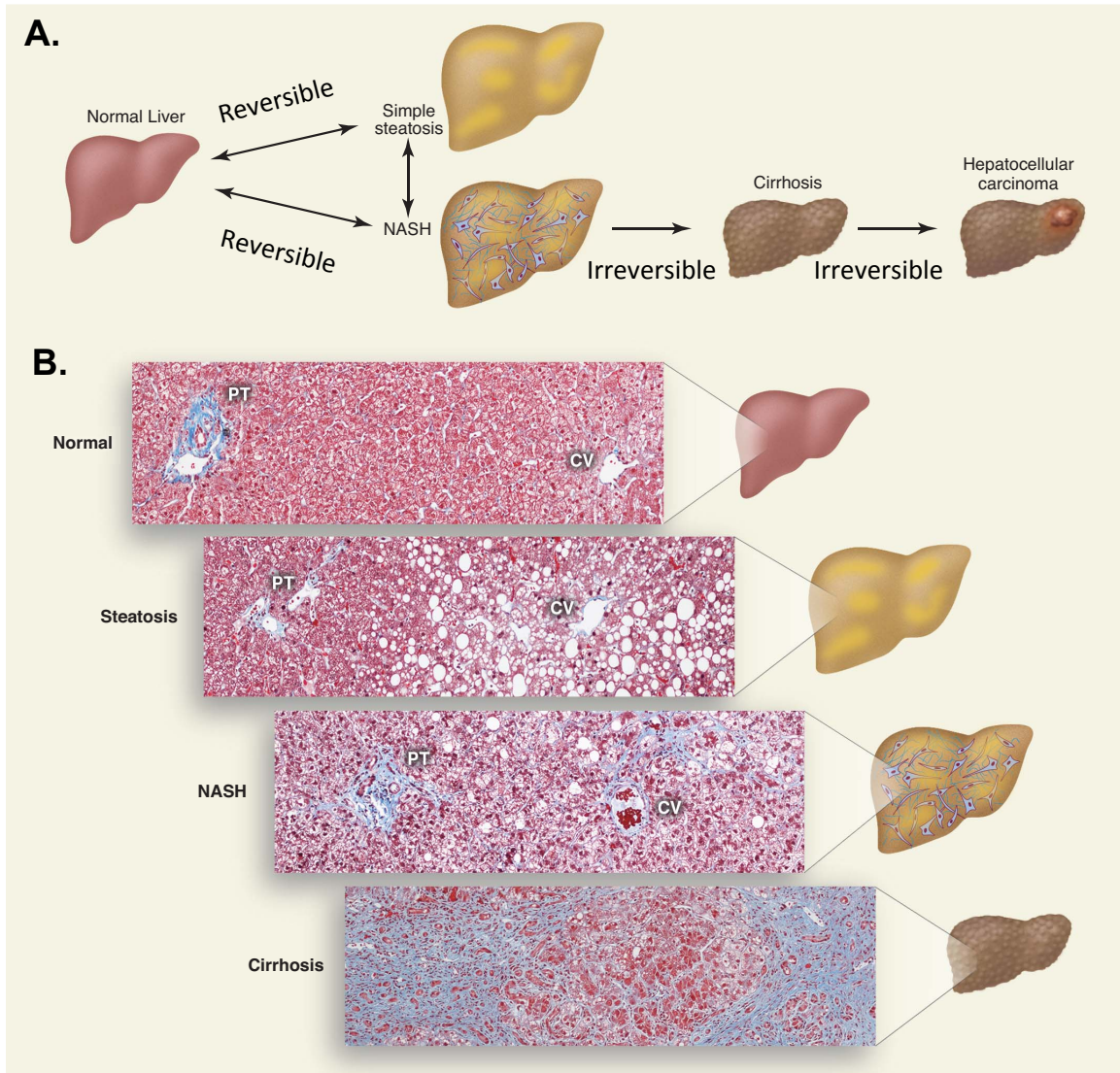


Diagram 4: Morphological changes during NAFLD, NASH, and HCC progression. **A)** Progressive disease begins with accumulation of simple steatosis due to TG accumulation in hepatocytes (NAFLD). NASH develops due to lipotoxicity associated with TG accumulation that causes inflammation, hepatocellular damage/apoptosis, and fibrosis (reversible processes). These processes are reversible, as the arrows illustrate. NASH commonly progresses to cirrhosis, and a higher risk of HCC development (non-reversible processes), which are irreversible processes. **B)** Microscopic sections representing the disease spectrum from normal liver, steatosis, NASH, and cirrhosis. Masson's trichrome was used to stain collagen fibers (blue). PT (portal triad=hepatic artery, bile duct, portal vein), CV (Central Vein). Modified from *Science*, 2011: Vol. 332 no. 6037 pp. 1519-1523. Reprinted with permission from AAAS [29].

In order to better understand the pathways and possible mechanisms underlying disease progression, several mouse models have been created to study NAFLD and NASH (Table 1). Various methods have been used to recapitulate disease progression in the mouse model such as genetic, nutritional, chemically induced damage, and a combination of these factors. The goal of mouse models is to reflect the elements of human disease: histologically, biochemically, and metabolically. Thus, an effort has been made to create models that possess the hallmarks of NAFLD and NASH, such as metabolic syndrome, obesity, insulin resistance, chronic inflammation, hepatocellular damage, and eventual progression to HCC. Genetic models have focused mainly on altering expression of transcription factors connected to metabolism and inflammatory processes in the liver (Table 1). Nutritional models typically employ the high fat (Western), methionine and choline deficient, cholesterol and cholate or fructose diet to replicate the metabolic syndrome, obesity, histology, and progression of human disease. In damage-induced models, ethanol or CCL4 are typically administered, often along with altered diet. While many models have presented elements of the disease, none have completely replicated the entire spectrum of the human disease.

Gene/Model	Modification	NASH	Fibrosis	Liver tumors	Observations in human liver disease
PI3K/AKT signaling					
<i>Pik3ca</i>	Liver-specific transgenic overexpression of activated mutant	No	No	Yes	Transgenic allele modeled after mutation detected in HCC
<i>Pten</i>	Liver-specific knockout	Yes	Yes	Yes	Decreased expression in NAFLD; Loss of function common in HCC
<i>Akt</i>	Liver overexpression via adenoviral or hydrodynamic injection	Yes	No	Yes	Increased expression in HCC associated with upregulation of lipogenic genes
JAK/STAT signaling					
<i>IL-6</i>	Constitutive knockout	Yes	No	No	^a Increased expression in obesity and type 2 diabetes
<i>Il6st</i>	Constitutive knockout	Yes	Yes	No	^a Activating mutations detected in liver cancer
<i>Jak2</i>	Liver-specific knockout	Yes	Yes	No	Sequence variants associated with metabolic syndrome risk
<i>Stat5</i>	Liver-specific knockout	No	No	Yes	Pathway activation associated with cirrhosis risk in NAFLD
PPAR signaling					
<i>Acox1</i>	Constitutive knockout	Yes	Yes	Yes	Sequence variants in PPAR associated with NAFLD
<i>Lgals3</i>	Constitutive knockout	Yes	Yes	Yes	Sequence variants in PPAR associated with NAFLD
NF-κB signaling					
<i>NEMO</i>	Liver-specific knockout	Yes	Yes	Yes	Decreased expression in HCC
<i>Atg5</i>	Systemic mosaic deletion	Yes	No	Yes	Autophagy is decreased in NAFLD and HCC
<i>Atg7</i>	Liver-specific knockout	Yes	No	Yes	Autophagy is decreased in NAFLD and HCC
<i>Becn1</i>	Systemic heterozygosity	Yes	No	Yes	Autophagy is decreased in NAFLD and HCC
Polygenic					
FLS strain	Selective breeding	Yes	Yes	Yes	
TSOD strain	Selective breeding	Yes	Yes	Yes	
SAM metabolism					
<i>Mat1a</i>	Constitutive knockout	Yes	No	Yes	Hypermethylation and decreased expression in NAFLD, cirrhosis, and HCC
<i>Bhmt</i>	Constitutive knockout	Yes	No	Yes	Decreased expression and loss-of-function mutation in HCC
<i>Gnmt</i>	Constitutive knockout	No	Yes	Yes	Hypermethylation and decreased expression in NAFLD, cirrhosis, and HCC

NAFLD non-alcoholic fatty liver disease, NASH non-alcoholic steatohepatitis, HCC hepatocellular carcinoma

^a Observation in humans is discordant with mouse model

Table 1: Mouse models of NAFLD/NASH. Mouse models are divided into genetically modified (1-8) and diet induced (9-13). Resulting phenotype with relation to disease spectrum is shown in the table. Modified from: Riordan, JD, et al, *Mamm Genome*. 2014 [35].

In human disease progression, there is a significant difference in occurrence between different ethnicities. Drawing from previous studies that linked two single nucleotide polymorphisms (SNPs) reference samples (rs) 738409 and 2281135, in the *PNPLA3* locus [36] and elevated ALT [37] with induction of NAFLD, Li et al. presents a statistical model based upon these disease risk factors in the Hispanic American population [38]. This population was found to have a high prevalence of elevated ALT (39%), obesity (49%), and diabetes (30%), which are strongly associated with NAFLD [38]. Additionally, the study found that high rates of end-stage liver disease were significantly higher in males than in females and Hispanics compared to other ethnicities [38]. While end-stage liver disease rates were higher in males, the SNP associated with NAFLD in *PNPLA3* (rs738409) was only seen in females. African-American patients were found to have a lower prevalence of NAFLD than Caucasians [39]. Due to these differences in NAFLD and NASH incidence by race, the distribution of disease incidence may be explained by distribution of adipose tissue, triglycerides, and SNPs.

It is worth noting that lean individuals also develop NAFLD, although at a lower rate of incidence than obese individuals – 7% NAFLD incidence in lean individuals as compared to 28% NAFLD incidence in obese individuals [40]. Most of these lean patients with NAFLD were younger, Hispanic, and had lower prevalence of metabolic syndrome accompanied by better insulin sensitivity when compared to obese NAFLD patients [40]. Interestingly, most of the individuals who are diagnosed with non-obese NAFLD were female. Most mouse model studies have focused on

obesity-related NAFLD and NASH; however, further studies are needed to better understand the complexities associated with non-obese disease progression.

To date, there are several methods employed to diagnose NAFLD, but pathological assessment from biopsy is still the most widely accepted method for a definitive diagnosis of NAFLD and differentiation from NASH, due to the ability to study the tissue for presence and extent of fibrosis [24, 41]. Histological scoring methods such as the non-alcoholic liver disease activity score (NAS) [42] and histopathological algorithms for evaluation of liver lesions in morbidly obese patients [43] are being implemented to obtain a better evaluation of disease status in patients. However, there are many problems such as potential complications due to the complexity of the disease and invasiveness of the biopsy, cost, and inconvenience to the participant, making it a very unpopular means of diagnosis [38]. Thus, in most cases, other means must be used in diagnosis such as: magnetic resonance imagery (MRI), measurement of organic compounds in the breath [44], and the FIB-4 test (analyzes ALT, AST, platelet number, and age) [45]. The most common methods are ultrasound (US) measurement of alanine aminotransferase (ALT) and aspartate aminotransferase (AST) levels, both of which have numerous problems [24]. Previous studies have shown that US is unable to detect low grade or very small amounts of hepatic steatosis [24]. Additionally, relying solely on ALT and AST levels to determine diagnosis has been shown to be unreliable as these levels fluctuate within normal range in both NAFLD and NASH [46].

Treatment options for NAFLD and NASH are very limited and have varying levels of success. Since most patients are obese, weight management and

increased physical activity have been shown to improve liver histology by reducing hepatocellular damage due to lipid accumulation, while delaying progression [47]. Frequently, morbidly obese patients undergo bariatric surgery to reduce their weight and reduce excess lipid as a reservoir of disease [48]. When high-risk patients with metabolic syndrome are observed, preventative agents such as ursodeoxycholic acid (UDCA), omega-3 polyunsaturated fatty acids (*N*-3 PUFA), statins and pre- and probiotics are implemented with varying success [47]. In patients with accompanying metabolic disorders, such as insulin resistance, insulin-sensitizing agents such as metformin and thiazolidinediones (TZD) are prescribed. To combat oxidative stress and reduce hepatic fibrosis, vitamin E is the treatment modality of choice [48]. Surgical procedures such as liver transplantation are considered the last resort for irreversible end-stage cirrhosis and HCC. Thus, a combination of methods, not merely diagnostic but also genetic in nature must be employed to provide a better screening method in order to treat this disease prior to progression. Manipulation of key lipid metabolic and inflammatory related genes in the mouse model have provided information regarding NAFLD and HCC disease progression that has contributed to the field of knowledge regarding better diagnostic and treatment modalities. However, a mouse model that develops spontaneous disease progression through the entire spectrum of NAFLD, NASH, and HCC, following genetic manipulation, has not been achieved.

1.5. TRIM24 as a transcriptional co-regulator

The Tripartite motif (TRIM) protein family is defined by conserved N-terminal domains of RING (Really Interesting New Gene), two B-boxes, a coiled-coil domain and variable C-terminal domains, which contribute to TRIM protein functions in differentiation, development, oncogenesis and apoptosis. In mammals, TRIM24 is a member of the Transcription Intermediary Factor (TIF1) sub-family including TRIM24 (TIF1 α), TRIM28 (TIF1 β /KAP1) and TRIM33 (TIF1 γ), a subset within the larger TRIM family of 70 proteins [49]. This family of proteins is known to interact with each other and, in the case of TIF1 γ , to have functions in epigenetic silencing, E3-SUMO-ligase activity, as well as interaction with MDM2 and E2F1 [50-52]. In our laboratory, TRIM24 was discovered to be a previously unknown negative regulator of p53 by Allton et al. (2009). Utilizing mass spectrometry data from mouse and stem cell models that implemented C-terminal tandem affinity purified (TAP) tag fusion with the open reading frame (ORF) of *Trp53*, a mouse model was created that expressed endogenously regulated p53 (p53-TAP^{K1}). Additional experiments showed TRIM24 negatively regulates p53 through E3 ubiquitin ligase activity via the N-terminal RING domain. Studies of the TRIM24 *Drosophila* homolog, *Bonus*, showed that mosaic clones, mutated in *Bonus*, were highly apoptotic. This phenotype was rescued by depletion of p53. Further studies in various human cancer cell lines cemented the conclusion upon depletion of *TRIM24*, led to p53-dependent apoptosis. TRIM24 has also been identified as a co-regulator of retinoid signaling, highly expressed in a profile of tumors, and associated with fusion partners such as *Braf* (T18) and *Ret* oncogenes in acute promyelocytic leukemia and papillary thyroid carcinoma [53-56].

In addition to these functions, TRIM24 is a co-regulator of nuclear receptors via the LXXLL motif and a Plant Homeodomain (PHD)/Bromodomain histone “reader” of histone modifications: H3K4me0 and H3K23ac [57-60] (Diagram 5). The evolutionarily conserved LXXLL motif is essential for interaction with nuclear receptors (NRs) [61]. NRs are defined as ligand-inducible transcription factors that function to regulate transcription of target genes through binding of DNA sequences as homo/heterodimers [55]. NR homo- and heterodimers such as: RAR α (Retinoic acid receptor alpha)/RXR (Retinoid X receptor), Androgen (AR), Estrogen (ER α), Progesterone (PR), and Vitamin D3 (VDR) [54, 55, 59, 62-64] have been shown to interact with the LXXLL motif of TRIM24.

In a mouse model targeting exon 4 of TRIM24 for germline deletion (*Trim24*^{dIE4/dIE4}), it was discovered that RAR-mediated signaling was reactivated, through re-expression of RAR α and repressed genes in the liver, leading to eventual HCC [65, 66]. Subsequent studies in *Trim24*^{dIE4/dIE4} mice showed that *Trim24* represses the vitamin D receptor (VDR) pathway in the kidney, suggesting up-regulation of calcium sensor receptor (*Casr*) expression, which could account for the arterial calcifications (not seen in the liver) in this mouse [66]. Additionally, *Trim24* was shown to suppress HCC progression by inhibition of the IFN/STAT pathway via RAR dependent regulation of the *Stat1* promoter [58]. Taken together, these findings suggested that *Trim24* is a tumor suppressor and an “essential brake” for retinoic acid-induced transcription that protects against HCC and arterial calcification [65].

Conversely, our laboratory discovered that TRIM24 is a co-activator of ER α -mediated activation of transcription in human breast cancer cells. We further

established this transcriptional activation is facilitated by recognition of a unique histone signature H3K4me0/H3K23ac via the Plant Homeodomain (PHD) and Bromodomain. Depletion of TRIM24 by shRNA led to decreased breast cancer cell survival, which was exacerbated by addition of the ER α inhibitor, 4-OH-tamoxifen [59]. Breast cancer patient samples showed a positive correlation between TRIM24 expression (immunohistochemistry) and poor prognosis [59]. Recent studies in immortalized human mammary epithelial cells (HMECs) show that TRIM24 expression causes progression from a non-transformed to cancerous phenotype [67]. Furthermore, ectopic expression of TRIM24 led to malignant transformation in both cell line and xenograft models [67]. Over expression of TRIM24 led to increased glycolytic and tricarboxylic acid (TCA) cycle gene expression in these transformed HMECs, suggesting a new role for TRIM24 in breast cancer progression and metabolism. Additional studies in MCF7 breast cancer cell lines, which harbor wild-type p53, showed that TRIM24 responds to stress and damage by negatively regulating p53 through an autoregulatory feedback loop [68]. This feedback loop was found to be independent of MDM2 and dependent upon direct binding of p53 to p53 response elements (p53 REs) in the distal promoter region of TRIM24 [68]. Thus, our laboratory has discovered numerous roles of TRIM24 as an oncogene in breast cancer, as well as mechanistic functions of TRIM24 and p53. However, we were interested in the dichotomy that existed between the role of TRIM24 as an oncogene in breast cancer and a tumor suppressor in a mouse model of HCC. Upon further examination of the *Trim24*^{dIE4/dIE4} mouse model, we observed that the RING domain, located in exon 1 of *Trim24* could possibly remain active in

this model. As our laboratory had established that the RING domain is essential for E3-ubiquitin ligase mediated inhibition of p53, we reasoned that p53 could still be active in the *Trim24*^{dIE4/dIE4} model. To better understand how this could be contributing to disease progression, and to better understand the dichotomy between dual role of *Trim24* as an oncogene (breast) and a tumor suppressor (liver) we developed a mouse model targeting the promoter region and exon 1 of *Trim24* for germline deletion (*Trim24*^{dE1/dE1}, referred to here as *Trim24*^{-/-}).

1.6. Hypothesis and Aims of this work

Upon aging, the *Trim24*^{-/-} mouse exhibited spontaneous development of hepatic lesions and HCC. Further studies showed that these hepatic lesions were filled with lipid and both hepatic lipid metabolic and inflammatory related gene expression were misregulated in these mice as well as NAFLD and NASH. These preliminary findings led me to hypothesize that the E3 ubiquitin ligase of p53, TRIM24, regulates genes that impact hepatic lipid inflammation and metabolism. Furthermore, I reasoned that TRIM24 could also be regulating specific systemic and hepatic immune cell populations, ultimately leading to development of NAFLD, NASH and HCC (Diagram 6). The goal of this study was to characterize this novel mouse model and to determine the role of *Trim24* in regulating mechanisms that protect the liver from aberrant lipid and glucose metabolism, chronic inflammatory damage and, ultimately, tumorigenesis.

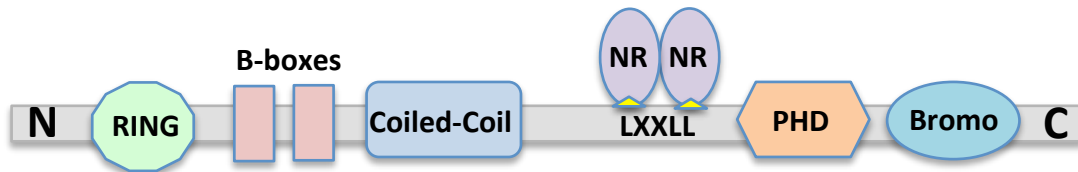


Diagram 5. TRIM24 protein structure- Diagram of TRIM24 protein structure and domains. NR- Nuclear receptor.

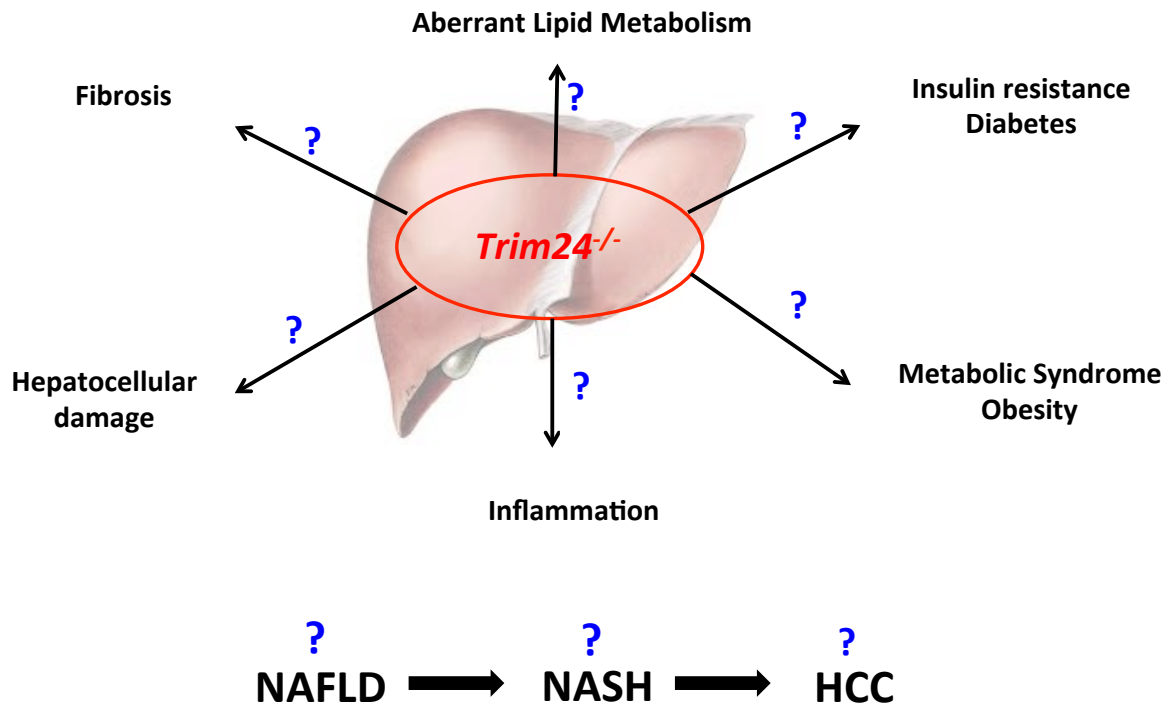


Diagram 6. Model of the hepato-protective role of TRIM24 against the hallmarks of NAFLD, NASH, and HCC. Modified from www.uscs.surgery.edu.

CHAPTER II

MATERIALS AND METHODS

2.1. Generation of germline *Trim24*^{dlE1} deficient mice. (Resource previously available in the laboratory, in collaboration with the Lozano laboratory, MD Anderson Cancer Center)

A conditional targeting vector (Fig. 1A) was constructed to delete the genomic fragment containing the core promoter and exon 1 of the *Trim24* gene by insertion of two LoxP sites for homologous recombination. The 5' arm (5182bp) was cloned by PCR with sense primer: AGGGTACCTGCGTCTGCTCT and antisense primer with an EcoR V site: ATGATATCATTCCAGGCCAGCCTGCTCTA. LoxP sites were introduced into the promoter fragment (1.7kb up-stream of transcriptional start site (TSS) and into intron 1 for a total knockout arm length of 2651bp with the primer pair: sense primer with EcoRV site and LoxP sequence: ATGATATCATAACTTCGTATAATGTATGCTATACGAAGTTATTCAGAGATCTGCC TGCCTCT and antisense primer with Xho I site: TTCTCGAGAAACAGACGGCAGCCAATCTG. The neomycin resistance gene (Neo) was fused to the phosphoglycerokinase (PGK) promoter (pGK-Neo) and inserted behind the LoxP site in intron 1 and flanked by two FRT sites for FLP-mediated excision. The 2858bp fragment in intron 1 was cloned as 3' arm using primer pair: sense primer with Sac II site: GATTCGCCGCGGCGAATCTTGTGCGTTCCGGG and antisense primer with Sal I site: AACGTCGACGTTCCGGCTGCCTTCATACCA. Deletion of the knockout arm resulted in a frame shift, completely disrupting the remaining protein coding sequence.

To generate *Trim24*-null mice, the linearized targeting vector (Fig. 1A) was electroporated into embryonic stem cells (ES, TC-1, MD Anderson Cancer Center) and positive ES cell clones were used to generate chimeric mice. Progeny were backcrossed to C57BL6/J mice (The Jackson Laboratory) for *Trim24*^{LoxPNeo/+} mice. *Trim24*^{LoxPNeo/+} mice were crossed to ROSA26-FLPeR mice (The Jackson Laboratory) to delete the Neomycin cassette: *Trim24*^{LoxP} mice. *Trim24*^{LoxP} mice were crossed to the zona pellucida 3 promoter-driven *Cre*-line (*Zp3-Cre*, The Jackson Laboratory): *Trim24*^{dIE1} mice. The *Trim24*^{dIE1/+} offspring were intercrossed to result in *Trim24*^{+/+}, *Trim24*^{+/dIE1} and *Trim24*^{dIE1/dIE1}. Mice were monitored for survival over a time-course of 585 days. For subsequent experiments, mice were backcrossed to 129S1 (Jackson laboratory) mice and then intercrossed with C57BL6/J mice to create B6:129 mice. All animal experiments were approved by the IACUC of the University of Texas MD Anderson Cancer Center.

2.2. PCR analysis of *Trim24* genotypes.

a. Genotyping of germline deletion.

Genomic DNA was isolated by Proteinase K digestion and phenol-chloroform extraction, followed by PCR amplification. The primer targeting sites are shown in Fig 1 and sequences are: f1: ATGGAGATGAAGTGATGGGGGAT; f2: CAAGTCTTTGGGGAATTACAGA; r1: CCTGGTAACATAAGCAAAGGA; r2: AGGTTTACAGAAGGAGACAAT; r3: CTAGTGAGACGTGCTACTTCCATTTG and r4: AAATCTCCGAAAGCAGCAGA. For detecting *Trim24*^{LoxPNeo} germline transition, f1/r1 primer pair for *Trim24*^{+/+} (WT) allele and f1/r3 primer pair for *Trim24*^{LoxPNeo} allele were used. The amplified fragment of 319bp (WT) and ~450bp (*Trim24*^{LoxPNeo}) were

obtained. To confirm the deletion of Neomycin cassette, primer pair f1/r4 was used to yield products of 175bp for WT and ~320bp for *Trim24*^{LoxP} (Floxed) mice. For detecting the deletion of proximal promoter and exon 1, PCR was performed with primer pairs f2/r2 and f2/r1 for WT and *Trim24*^{dIE1} alleles, respectively and the PCR products of 384bp (WT) and ~650bp (dIE1) were obtained. PCR conditions for all primer sets were 32 cycles of 95°C 4 min for preheating, then 95°C 30 seconds, 65°C 45 seconds, and 72°C 45 seconds followed by 72°C for 5 minutes.

b. Genotyping of liver specific deletion.

Albumin-Cre mice were obtained from Jackson Laboratory (B6.Cg-Tg (Alb/Afp-cre)21Mgn/J003574, referred to throughout the paper as Albumin-Cre). These mice were bred to *Trim24*^{LoxP} mice to obtain *Albumin-Cre; Trim24*^{LoxP/LoxP/+} (*HKO/+*-Hepatocyte specific Knockout/+, B6:129) mice. These mice genotypes were confirmed by ear punch and PCR for positive Cre and *LoxP* expression. *HKO/+* mice were intercrossed to obtain *HKO/HKO* mice (*Albumin-Cre; Trim24*^{LoxP/LoxP} /*Albumin-Cre; Trim24*^{LoxP/LoxP}). These mice are viable and can be bred through homozygous stock, litters were validated for positive Cre and *LoxP/LoxP* expression via ear punch. All mice were mixed B6:129 background. Integration of Cre expression was determined using primers: oMIR 1084 5'-GCGGTCTGGCAGTAAAACTATC (sequence from Jackson Labs), oMIR 1085 3'-GTGAAACAGCATTGCTGTCACCTT (sequence from Jackson Labs). PCR conditions were: 37 cycles of 94°C 3 min for preheating, then 94°C 30 seconds, 51.7°C 1

minute, 72°C 1 minute, (cycles 2-4 repeated 35 cycles), 72°C 2 minutes. Cre bands were located at 150 bp (Fig. 31).

2.3. Southern blot analysis of *Trim24* genotypes (Resource previously available in the laboratory)

For detecting the homologous recombination of *Trim24*^{LoxpNeo} in ES cells, genomic DNA was digested with SpeI, analyzed by electrophoresis on a 1% agarose gel and blotted onto an Amersham Hybond™-N+ membrane (GE Healthcare, Cat. # RPN303B). The duplicated blots were then hybridized to 5' and 3' external probes respectively. The 5' external probe was obtained by PCR amplification using primer set 5'-GGTAACCAAGGAATGTGGGTCT and 5'-GCCTGGTTTCTCATCATCTTTCCCT; and 3' external probe was obtained by PCR amplification using primer set 5'-CCCATTGGTCCAGTCAGAACAT and 5'-GGGGAGGGGAATGAAGATAA. The detailed probe sequences are listed in Table 2. Probes were labeled by EasyTides®, Deoxycytidine 5'triphosphate, [α 32P] (PerkinElmer, Cat. #BLU513H250UC) using Amersham™ Rediprime™ II Random Prime Labeling System (GE Healthcare, Cat. # RPN1633), followed by purification with illustra™ ProbeQuant™ G-50 Micro Columns (GE Healthcare, Cat. #28-9034-08). The correct patterns of hybridization were then visualized by exposing washed membranes to X-ray films (Kodak, Cat. #829 4985).

2.4 Western blot analysis of *Trim24* genotypes (Resource previously available in the laboratory)

For protein analyses of TRIM24, TRIM28 and TRIM33 expression in mouse embryo fibroblasts (MEFs), two lines of early passages of *Trim24*^{+/+} and ^{-/-} MEFs (passage 2) were plated in 6-well plates and incubated for two days. The whole cell lysates (50 µg) were separated by SDS-PAGE on 7.5% gel, transferred to nitrocellulose membranes and immunoblotted with primary antibody overnight (1:5000 dilution). The primary antibodies are anti-TRIM24 (Proteintech Group, 14208-1-AP), anti-TRIM28 (KAP1) (Abcam, ab22553), anti-TRIM33 (Abnova, H0005-1592-M01), and anti-β-actin (Sigma-Aldrich, A1978). After washing, the membrane was incubated with IRDye@800CW conjugated goat anti-rabbit IgG (LI-COR, 926-32211) or IRDye@680LT conjugated anti-mouse IgG (LI-COR, 926-68020) (1:20,000 dilution) as appropriate. The membranes were scanned and quantified with ODYSSEY CLx Infrared Imaging System.

2.5. RNA extraction and quantitative Real-time (qRT-PCR analysis).

Briefly, total RNA from cryopulverized, homogenized mouse liver was extracted with 1 mL of TRIzol reagent (Life Technologies, Invitrogen) per (0.2 g amount of tissue. TRIzol and sample were pipetted up and down about 20X at room temperature. 200 µl of chloroform (Fisher) was added per sample and the sample was vigorously shaken for 1 minute. Following a 3 minute incubation at room temperature, the samples were centrifuged for 15 minutes at 10,000XG, 4°C. The aqueous phase was moved to a new tube and 500 µl of 100% isopropanol (Fisher) was added, the samples were shaken for 1 min, and then incubated at room

temperature for 10 minutes. Following centrifugation, (10 minutes at 10,000XG, 4°C), the supernatant was discarded and the pellet was washed twice with 1 mL of 75% ethanol (Pharmco-AAPER) (Vortex, 7500XG centrifugation, 5 min, 4°C). The ethanol was then removed and the RNA pellet was dried on ice and resuspended in 20-50 µl DEPC (Sigma) water, depending on the size of the pellet. To determine RNA concentration and purity, the resuspended RNA pellet was diluted 1:1 in 2X TE buffer (10 mM Tris-HCL pH 7.5 -Fisher, 1 mM EDTA pH 8.0 - Fisher) and analyzed on the NanoDrop spectrometer. RNA with an absorbance curve of 1.85 or above was accepted as pure. 2.5 µg of RNA was added to 1 µl 10X DNase Buffer (Promega), 1 µl DNase (Promega) and DEPC water to a total volume of 9 µl. The samples were spun down and incubated for 20-30 minutes at 37°C. The DNase reaction was stopped with 1 µl 25mM EDTA and then the samples were moved to 65°C for 10 minutes after a brief spin. After the samples were incubated on ice for >1 minute. The DNased RNA (dRNA) 8 µl was added to 1.5 µl Random Hexamers (Invitrogen), 1.5 µl dNTP (Bioline), and DEPC water 1.5 µl and the sample was spun down and incubated for 65°C for 5 minutes, followed by >1 minute on ice. 4 µl of 5X First Strand Synthesis Buffer (Invitrogen), 2 µl 0.1 M DTT (Invitrogen), and 0.5 µl RNase inhibitor (Roche) was added to each sample, followed by a quick spin and 2 minute incubation at 42°C. Finally, 1 µl of Single Strand Reverse Transcriptase (Invitrogen) and 0.5 µl of DEPC water was added to the sample and the PCR settings were: 42°C for 50 minutes, 70°C for 15 minutes.

Primers were designed bridging two exons using the mouse database in Ensembl (NCBI) to visualize the sequence for each gene. Exon sequences were

entered into the primer design software, OligoArhcitect (Sigma) and primer pairs were checked for specificity using BLAST (NCBI). Upon receipt, primers were resuspended in sterile water at a concentration of 100 μ M and diluted 1:10 for working stock. To ensure that primers were specific, a standard curve experiment was performed using pooled cDNA from various mouse tissues and diluting primers 1:1000, 1:100, and 1:10. For qPCR analysis, samples were prepared with 0.2 μ l of each primer (Forward and Reverse), 5 μ l SYBR green PCR mastermix (Bio-Rad) and 1.6 μ l of sterile water to 7 μ l per well in addition to 3 μ l of cDNA (1:10) (10 μ l total/well) in a 96-well PCR plate (Life Technologies) Real-time qPCR was performed using primers for the indicated genes with the following cycles: 95°C 5 minutes, 95°C 30 seconds, 55-60°C 30 seconds, 72°C 30 seconds for 40 cycles (Table 3). Levels of RNA were normalized by comparison to *Hprt*.

2.6. Histological and immunohistochemical studies

a. Paraffin embedded sections.

Mouse tissues were fixed in 4% paraformaldehyde (PFA, Sigma) in PBS overnight, dehydrated in ethanol, embedded in paraffin using standard procedures. Sections (5 μ m) were cut, deparaffinized, rehydrated, and stained with hematoxylin/eosin (H&E) using standard procedures in the MD Anderson Cancer Center Veterinary Medicine Pathology Core.

b. Frozen tissue sections

Liver samples were fixed with 4% paraformaldehyde (PFA) in PBS over night at 4°C, incubated in 30% sucrose in cold room with shaking overnight, embedded with

O.C.T compound (Tissue-Tek, #4583), frozen on dry ice and stored at -80°C before use. Frozen tissues were cut at a thickness of 10 µm at 12°C, air-dried on the slide for 30 to 60 minutes.

c. Oil red O staining

Frozen sections were used for this procedure. The slides were incubated in 4% PFA for 10-15 minutes to dissolve the O.C.T. compound. Then, the slides were washed in PBS, followed by rinsing with water 3X for 5 minutes. Then, the slides were dipped quickly in 60% isopropanol and stained with freshly prepared ORO working solution (Electron Microscopy Science, #26503-02) for 7 minutes. After staining, the slides were quickly dipped in 60% isopropanol, washed immediately with water, counterstained for nuclear staining with Mayer's Hematoxylin solution (Sigma-Aldrich, #MHS16) for 5 minutes and sealed with mounting medium (Invitrogen, #P36930).

d. Masson's Trichrome Staining

Paraffin sections were used for this procedure. The slides were deparaffinized using histoclear (National Diagnostics), 3X for 10 minutes. Then, the slides were rehydrated through alcohol: 100% ethanol (2X 5 minutes), 95% ethanol (2X 5 minutes), 70% ethanol (2X 5 minutes), changing to fresh solution in between each time and finally to distilled water. The slides were incubated in Bouin's Fixative (EMS) overnight at room temperature. Following the incubation, the slides were

washed in running water until the yellow color was no longer visible. After drying around the sample, but not allowing it to completely dry, a hydrophobic Pap Pen (Research Products International) was used to draw a circle surrounding the sample. Next, the slides were stained in Weigert's Iron Hematoxylin Working solution (A + B solution, EMS) for 5 minutes, within the Pap Pen circle and then rinsed in running, distilled water for 10 minutes. The slides were then stained in Biebrich Scarlet-acid Fuchsin (EMS) for 15 minutes, Phosphomolybdic Acid-Phosphotungstic Acid (EMS) for 15 minutes, Aniline Blue Solution (EMS) for 10-20 minutes and finally rinsed with distilled water. 1% Acetic Acid (Sigma) was used to differentiate the slides for 3 to 5 minutes, followed by dehydration (95% ethanol, 100% ethanol, 2X each quickly changing), clearing 2X quickly in histoclear, and mounting with Cytoseal Mounting Media (EMS) after drying around the sample. If the staining was faint, samples were rinsed in water for shorter periods of time and dried at 50°C from 1 hour to overnight before mounting (instead of dehydrating and clearing) to preserve the staining. The protocol was modified from Electron Microscopy Services (EMS) protocol.

e. PAS Staining

Periodic Acid Schiff (PAS) staining was used to determine glycogen and carbohydrate levels in cells. Paraffin sections were deparaffinized and rehydrated through xylenes and alcohol as stated previously. The slides were placed in 0.5% aqueous periodic acid (Sigma) for 5 minutes and then rinsed in tap water and deionized water for 5 minutes each. Then, the slides were placed in freshly made Schiff's reagent for 15 minutes (5 g Sodium Metabisulfite-Sigma, 5 g pararosaniline-

Sigma, in 1 liter of 0.15M HCl, - Fisher, filtered with 3 g of activated charcoal (Sigma), cooled and stored away from light at 4°C), followed by rinsing twice in deionized water (5 minutes each). The slides were then counterstained by dipping in filtered Harris hematoxylin (Protocol) for 2-3 seconds and rinsing in running tap water for 3 minutes. Then, the slides were decolorized by dipping in acid alcohol for 2 seconds. The slides were developed in running tap water for 3 minutes to blue the hematoxylin. Finally, the slides were dehydrated through alcohols and xylene as stated previously and mounted. The protocol was modified from Current Protocols in Molecular Biology, 2007.

f. Immunohistochemistry

Paraffin sections were deparaffinized and rehydrated through xylenes and alcohol as stated previously. Antigen retrieval was performed using 100X Sodium Citrate Buffer (Vector) , diluted in water. 250 ml of this solution was heated for 3 minutes in the microwave in a slide container and then moved to a rice cooker that was heated to boiling. The slides were then placed in the boiling Sodium Citrate Buffer and steamed in the rice cooker for 30 minutes. The slides were cooled under running water. The area around the sample was dried, being careful not to allow the sample to dry and a Pap Pen was used to draw a circle around the sample. Next, the sample was blocked (against ubiquitous background signal) with 3% BSA (Jackson Labs ImmunoResearch) in PBS-Tween (0.1% Tween-20, Fisher in PBS) and 150 µl of goat serum from the Vectastain ABC Kit (Rabbit, PK-610) for 30 minutes to 1 hour at room temperature on a nutator.in a humidifying chamber (slide box with

moistened Whatman paper under slides). Next, the primary antibody, diluted in Blocking solution, was applied to the slides (immediately after removing the blocking solution) and the slides were incubated overnight at 4°C. Antibodies used for immunohistochemistry were anti-TRIM24 antibody (1:250, ProteinTech 14208-1-AP), anti-cleaved CASPASE 3 antibody (1:500, Cell signaling, #9661), and anti-F/480 antibody (Affymetrix 1:250 14-4801). Following the overnight incubation, the slides were washed 3X 5 minutes in PBS. The secondary antibody was then applied (For TRIM24 and CASPASE 3 - anti-Rabbit serum (Vectastain Kit) 1:1000, diluted in blocking solution, F4/80 – anti-rat serum (Vector BA-9401) 1:1000) and incubated in 1-1.5 hours at room temperature on a nutator in a humidifier chamber. The ABC blocking reagent (Vectastain) was prepared with 5ml of PBS and 1 drop A reagent + 1 drop B reagent (Vectastain) and incubated for 30 minutes at room temperature. During this incubation, the secondary antibody was removed in PBS (3X 5 minutes, shaking on a nutator, room temperature). Then, the ABC reagent was added to each slide and the slides were incubated for 30 minutes at room temperature. Following this incubation, the slides were washed in PBS (3X5 minutes) and moved to sterile water. The slides were then developed with DAB staining solution using the DAB reagent kit (Vector SK-4100) using 2 drops buffer, 4 drops DAB, 2 drops hydrogen peroxide, 2 drops Nickel, and mixed with 2.5 ml of sterile water. The slides were then developed until the desired contrast was achieved (-10-20 minutes). Following checking contrast levels under the microscope, the slides were washed with running water in a slow and steady stream from the frosted glass portion to the end of the slide until all reagent was removed. Next, the slides were counterstained with

Mayer's Hematoxylin (EMS, cleaved CASPASE 3) or Nuclear Fast Red (Vector, TRIM24). The counterstaining with Hematoxylin was achieved using the same method implemented in DAB staining. Nuclear Fast Red staining utilized a very short incubation period (10 seconds to 1 minute). The slides were then washed in running tap water for 5 minutes and dehydrated through alcohols, cleared, mounted as described previously.

2.7. Plasma collection.

2 month old *Trim24^{-/-}* and *Trim24^{+/+}* mice were fasted for 4 hours with water *ad libitum* (for metabolic, such as lipid panels, other tests used mice that were not fasting). Submandibular blood collection was performed, following administration of anesthesia (Isoflurane, Isothesia, Butler-Schein), using a 5 mm lancet (Goldenrod). Samples were collected with 4.5% EDTA to prevent clotting, incubated on ice, and centrifuged at 10,000 rpm, 10 minutes at 4°C to separate plasma and either snap frozen and stored at -80°C or submitted for analysis.

2.8. Serum collection.

The same protocol used in plasma collection was implemented in serum collection, except blood was collected without EDTA (Fisher). Samples were allowed to clot and were then centrifuged at 10,000 rpm, 10 minutes at 4°C to separate serum and either snap frozen and stored at -80°C or submitted for analysis.

2.9. ALT/AST and Lipid profile analysis.

AST, ALT, total plasma cholesterol (TPC), plasma TG, non-HDL-C, and HDL-C were quantitated using an Olympus clinical analyzer (Olympus) [69] by either the MD Anderson Cancer Center Veterinary Core or by Dr. Richard G. Lee (Isis Pharmaceuticals). Hepatic lipid profiles were assessed using the Folch liver lipid extraction method [70] by collaborator Dr. Richard G. Lee (Isis Pharmaceuticals).

2.10. Glucose tolerance/Insulin tolerance testing (GTT/ITT testing).

2, 4, and 6 month old *Trim24^{-/-}* and *Trim24^{+/+}* mice were fasted for 6 hours with water *ad libitum* beginning at 4 am in order to clear undigested food. At this time, both the top and bottom of the cage were changed to ensure that all food sources were removed. A glucose solution of 2 g glucose (Sigma) in 10 ml sterile water was dissolved and filter sterilized using a .22 filter μ m (Millipore). Just prior to the beginning of the test, each mouse was weighed to determine the amount of glucose per mouse to inject (Ex: 10X body weight = 25 g mouse \rightarrow 250 μ l of glucose). For insulin injections, 5 μ l of insulin (0.75 U/kg, Humulin-N, Eli Lilly) was diluted 1:1000 in sterile PBS on ice. The amount needed for injection per mouse was calculated based upon body weight (Ex: Weight in grams/1000 X 7500 = dose in μ l per mouse). A baseline blood glucose reading was taken via tail snip on a glucometer (One Touch Ultra Mini) prior to injection, after 6 hours of fasting. Insulin syringes (Becton Dickinson) were loaded with the correct amount of either glucose or insulin (kept on ice) for each mouse and the solution was injected into the abdomen via interperitoneal injection. Blood glucose readings were taken at 0, 15, 30, 60, 120

minutes following injection. Mice were allowed to recover for 1 week in-between testing sessions and were sacrificed after a week of recovery from the final test (Fig. 38).

2.11. Liver perfusion.

2 month old *Trim24^{-/-}* and *Trim24^{+/+}* mice were anesthetized using Isoflurane (Butler-Schein) and were checked for pedal reflexes. Under continued anesthesia, mice were restrained and the abdominal cavity was exposed. A 24G catheter (Terumo) was inserted into the inferior vena cava to the junction superior to the kidneys. Upon removal of the needle, the catheter was then attached to tubing fed through a peristaltic pump and cleared with freshly prepared Pre-clearing solution kept in a circulating water bath at 42°C (1X PBS, no calcium/magnesium, 0.2 M EGTA, pH 8.0, 1M HEPES pH 7.6) (Thermo Scientific, Sigma, MP Biomedicals). Sufficient blood clearance of the liver was closely monitored and the hepatic portal vein was clipped as an exit point for the clearing solution. Following sufficient hepatic blood clearance, freshly prepared Perfusion solution, also kept in a circulating water bath at 42°C (1X PBS without calcium/magnesium, 1M CaCl₂, 1M MgCl₂, 70 mg Collagenase IV) (Thermo Scientific, Sigma, Worthington) was pumped through the vena cava to digest the liver *in situ*. The gall bladder was removed and discarded. The liver was removed and transferred to a 50 ml conical tube (Becton Dickinson) with William's E media 500 mL (Sigma) supplemented with 5 mL of Insulin-transferrin-selenium (ITS, Sigma), 5 mL Gentamicin-glutamate (G/G, Sigma), 10 % Fetal Bovine Serum (FBS, Gemini), and 5 mL Penicillin-Streptomycin (P/S,

Mediatech), on ice. After vigorously shaking to suspend the cells, the suspension was poured through a 100 um filter (BD Falcon) and a cotton tipped applicator (Fisher Scientific) was used to mix remaining tissue in order to ensure that the majority of cells were filtered. The suspension was centrifuged at 4°C 50G for 2 min. The bottom layer of cells (hepatocytes) and the supernatant (non-parenchymal cells, immune cell portion) were separated with the supernatant and removed to a new tube.

2.12. Hepatic Immune Cell Isolation.

The supernatant fraction collected in the previous protocol (liver perfusion protocol) was washed with PBS and cells were pelleted at 2000G for 10 min (4°C). Prior to preparing the Percoll cushion, the solutions were pH adjusted with PBS in a 1:10 dilution at room temperature. The 37% and 70% solutions were prepared with PBS. The cells were then resuspended in 37% Percoll (Sigma) and layered onto a 70% Percoll cushion. The bottom layer of Percoll was kept at half the volume of the top layer of Percoll containing the supernatant. Cells were centrifuged through this Percoll gradient at 2000G for 20 minutes, with no brake. Following centrifugation, a bulb pipet (Fisher) was used to gently remove the intermediate layer between the 37% and 70% layers of Percoll, which contained the immune cell population. DMEM (Sigma) + 10% FBS (Gemini) + P/S (Mediatech) was added to the cell fraction and the mixture was centrifuged at 2000G for 5 minutes at 4°C. The cell pellet was resuspended in media on ice.

2.13. Bone marrow collection.

Femora and tibiae of 2 month old *Trim24^{-/-}* and *Trim24^{+/+}* mice were collected and the muscle was removed. The ends of the bones were removed and PBS + 2% FBS with 2mM EDTA (Fisher) was flushed through the bone shaft using a 22G needle (Becton Dickinson). Bone marrow was collected following the flushing of the bone and cells were disaggregated by gently pipetting up and down several times. The bone marrow was then pelleted by centrifugation at 300G for 10 minutes and was either snap frozen for storage at -80°C or resuspended in buffer for analysis.

2.14. Flow Cytometry Analysis.

a. RBC Lysis.

To remove red blood cell contamination, cells were pelleted by centrifugation (300-400xg) at 4°C, the supernatant was removed, and the cells were resuspended in Lysis Buffer (eBioscience). Following incubation on ice for 4-5 minutes with occasional shaking, the reaction was stopped by diluting the Lysis Buffer (1:6) with 1X PBS. The cells were centrifuged as previously and resuspended in Flow Cytometry Staining Buffer (eFluor® NC Flow Cytometry, eBioscience) so that the cell count was approximately 2×10^7 /mL.

b. Cell Fixation and Staining.

The antibodies in Table 14 were used for analysis and were combined with the Flow Cytometry Staining (FCS) buffer to the appropriate concentration. A 1:1 combination of cells and the antibody mixture was incubated for 30 minutes (dark, on ice). The

cells were then washed twice by adding the FCS buffer and subsequent centrifugation (300-400xg), 4°C for 5 minutes (supernatant was discarded). Cells were resuspended in the fixing buffer composed of 4% formalin/PBS (Fisher). The samples were then analyzed on the flow cytometer and gated using FlowJo software.

c. FlowJo Analysis. (This analysis was done in collaboration with Huiyuan Zhang, MD/PhD).

Briefly, samples were analyzed using forward and side scatter analysis to determine the cutoff for live versus dead cells. Then, the channels using the conjugated antibodies (Table 9) were compared to the CD45 status (Y-axis) of the cells to determine which cells were hematopoietic versus non-hematopoietic. Cells were then sorted and gated based upon cell surface markers for lineage and identification (Table 14).

2.15. CyTOF (sample preparation and analysis)

a. Antibody labeling.

For each antibody (Table 15, DVS Sciences), labeling was achieved using the MaxPar Metal Labelling Kit (DVS Sciences).

b. Sample staining and fixation.

Cells harvested from either the liver or bone marrow were resuspended in William's E media or DMEM, respectively (Invitrogen), and washed with PBS. Following washing, the cells were resuspended in serum-free media and an equal amount of 50 μM cisplatin (Sigma Aldrich) was added dropwise to a final concentration of 25 μM to stain for cell viability. After a 1 minute incubation and quenching with PBS + 1% BSA (Equitech-Bio Inc), cells were centrifuged and resuspended in serum free medium. 100 μM Iododeoxyuridine (IdU) (Sigma Aldrich) was added in serum free medium to label cells in S-phase. Following subsequent incubation and centrifugation and washing with PBS+1%BSA, cells were fixed with PBS + 1.5% paraformaldehyde (Sigma Aldrich) for 10 minutes at room temperature. Cells were incubated and then washed and resuspended in PBS.

c. Sample permeabilization and labeling.

Cells were centrifuged, washed with PBS, vortexed, permeabilized with methanol (MeOH) (Fisher) and incubated at 4°C for 1 hour to overnight (depending on the tissue). On the day of analysis, approximately 1.5 million cells stored in MeOH were centrifuged, MeOH was decanted, and cells were washed with wash buffer (PBS+0.5% BSA+0.02% sodium azide) and PBS. Then previously labeled antibodies were pooled per analysis and added to the washed cells, which were then incubated with gentle rocking for 45 min-1 hour at room temperature, followed by additional washes in wash buffer and PBS.

d. IR-intercalator staining.

Note: The following steps were performed immediately before the samples were analyzed.

IR-intercalator (DVS Sciences) was diluted 1:1000 in PBS+1.6% formaldehyde (Sigma Aldrich), added to the labeled cells, and incubated for 20 minutes at room temperature with gentle rocking. Following incubation, samples were washed with wash buffer. Immediately prior to analyzing each sample, the cells were resuspended in bead solution (DVS Sciences) and filtered using Falcon round bottom tubes with cell-strainer cap (BD Biosciences) submitted for CyTOF analysis.

e. viSNE analysis. (This data analysis was performed by Ryan McCarthy, PhD)

The Visual Stochastic Neighbor Embedding (viSNE) figures were generated using the t-Distributed Stochastic Neighbor Embedding (t-SNE) algorithm to visualize the high dimensional data on a two dimensional map as previously described [71]. The viSNE plots were generated based on data from the cell surface markers listed in Table 15 to group cells that shared phenotypically similar characteristics. Cell type identity in the viSNE plot was manually annotated based upon markers expression of markers listed in Table 15.

2.16. Chromatin Immunoprecipitation (ChIP). Modified from protocol in Kurinna, et al., *Hepatology*, 2010 [72].

a. Making the liver lysate.

Wild-type (*Trim24^{+/+}*) quiescent liver samples from 2 month old mice (pooled genders) were cyropulverized and weighed to approximately 0.5g per mouse (total volume was 2 g) on ice. The samples were then rinsed with cold PBS (sterile) and centrifuged at 50XG, 2 minutes at 4°C twice to remove residual blood. The samples were cross-linked with 556 µl of 37% Formaldehyde (Sigma) in 20 ml of sterile water and rotated at room temperature for 15 minutes. The cross-linking process was stopped with 6.8 ml of 0.5 M Glycine (Fisher) while rotating for 10 minutes at room temperature. Next, the samples were centrifuged at 2000 rpm, 7 minutes at 4°C and the supernatant was discarded. The liver pellet was resuspended using a wide bore pipet, in 4 ml of 1X PBS with 40 µl protease inhibitors (PI's, Sigma) and 4 µl of PMSF (MG/ICN), 0.1M in 100% ethanol). The samples were then dounced in a tissue homogenizer (Wheaton, Tight) 7 times on ice. The homogenate was then transferred to a 15 ml conical tube (Becton Dickson) and centrifuged at 2000 rpm, 7 minutes at 4°C. The pellet was then resuspended in 4 ml of Cell Lysis Buffer (Appendix 1) with PI and PMSF. The sample was again dounced 4 times on ice (Wheaton, tight) and divided into tubes so that the final volume was maximum of 800 µl per tube. The lysates were incubated on ice for 15 minutes and centrifuged at 5000 rpm, for 5 minutes at 4°C. The supernatant was discarded and the pellet was resuspended in 250 µl of Nuclear Lysis Buffer (Appendix 1) with PI and PMSF and

incubated for 10 minutes on ice (vortexing every 2 minutes). 0.1 g of acid washed glass beads (Sigma) were added per tube and samples were transferred to a programmable Bioruptor machine (Diagenode) to sonicate and shear the chromatin fragments in the samples. The machine was sufficiently cooled and set as follows: 30 cycles, 30 seconds on, 30 seconds off, rest for 30 minutes to cool down and repeat. Samples were then centrifuged at 14000 rpm for 30 minutes at 4°C and the supernatant was pooled and then divided into 200-300 µl aliquots per tube. The samples were snap frozen and stored at -80°C.

b. Testing the lysate.

To test the size of the chromatin fragments, 20 µl of lysate was added to 20 µl 2X SM2 buffer (Appendix 1) and 1 µl of 150U MNase (micrococcal nuclease-Worthington) at room temperature in tubes labeled for the following timepoints in minutes: 0 (Stop solution of 1/10th volume of 10X EDTA/EGTA – Appendix 1 already in tube), 15, 30, 45. At the end of each timepoint, the stop solution (see previous) was added and 300 µl of TE Buffer with 1.5 µl of RNase A (10mg/ml, Worthington) was added to digest RNA and the sample was incubated for 30 minutes at 37°C. Then, 15 µl of 10% SDS (Bio-Rad) and 7.5 µl Proteinase K (MP Biomedicals, 10 mg/ml) was added to the sample to digest proteins and the sample was incubated for 4 hours (minimum) at 37°C. The crosslinks were reversed overnight at 65°C. The samples were then extracted with 400 µl of Phenol:Chloroform (1:1 Buffered Phenol - Fisher, Chloroform – Fisher), vortexed vigorously, and centrifuged at 13,000 rpm for 5 minutes. The supernatant was removed to a new tube, where the

Phenol:Chloroform extraction was repeated as above. Next 400 μ l of chloroform was added to the sample and extracted as above. The upper phase was removed to a new tube with a final volume of approximately 200-250 μ l and DNA was precipitated with 1/10 volume of 3M Sodium Acetate (Fisher), 2 volumes of 100% ethanol, and 20 μ g glycogen (Sigma). The tubes were inverted to mix and incubated at -20°C for >1 hour (or -80°C for 1 hour), followed by centrifugation 13,000 rpm for 15 minutes at room temperature. After the supernatant was removed, the DNA pellet was washed twice with 70% ethanol, inverting the tube and centrifuging at 13,000 rpm for 2 minutes. The pellet was then air dried and resuspended in sterile water to a final volume of approximately 50 μ l. The DNA samples (0, 15, 30, 45 minutes of MNase digestion) were ran on a 2.0% agarose gel (composed of Agarose – Gene Mate and 1X T β E (10X to 1 L – Tris, Boric Acid –Sigma, 0.5M EDTA)) and visualized using ethidium bromide staining to determine which sample had the correct amount of digestion to achieve chromatin fragments on average 500bp (ranges from 150bp-1kb). The optimal timepoint for MNase digestion was 15 minutes.

c. MNase digestion, lysis, pre-clearing, and addition of antibody to the samples.

Protein A sepharose beads (GE Healthcare) were swollen in water over night at 4°C. The beads were then washed and resuspended in Lysis Buffer (Appendix 1) with PI's and PMSF to make a 50% slurry and kept on ice. MNase digestion was performed as described in the previous section using the digestion timepoint of 15 minutes. The input sample tube was placed at -80°C. The remaining samples were brought to a final volume of 500 μ l with Lysis Buffer (Appendix 1) and PI's with

PMSF. The lysates were then pre-cleared with 3 μ l of normal sheep IgG (Fisher) for 1 hour at 4°C on the nutator. 50 μ l of the bead slurry was added to each of the pre-clearing tubes were rotated for another hour at 4°C on the nutator. The samples were then centrifuged at 5000 rpm for 3 minutes at 4°C. The supernatant was transferred to a new tube and 4-5 μ g of TRIM24 (Proteintech) antibody to the allotted tubes. For binding controls, 3 μ l was IgG alone was added to a tube and 5 μ g histone H3 antibody (anti-Rabbit pAb Abcam ab1791) alone was added to another tube. Samples were rotated overnight at 4°C.

d. Washing and removal of RNA/Protein from samples.

The samples were centrifuged at 13,000 rpm for 2 minutes at 4°C. The supernatant was transferred to a new tube and 50 μ l of Protein A bead slurry was added using a wide bore pipet. The samples were then rotated for 1 hour at 4°C. Then, the samples were washed at 4°C, rotating with the following solutions (Appendix 1) : RIPA Buffer – 10 minutes, High Salt Solution – 10 minutes, LiCl Wash – 5 minutes, and TE Buffer – 2X 10 minutes. In between each wash, the samples were centrifuged at 5000 rpm for 3 minutes and the supernatant was carefully removed and discarded without disturbing the beads. Following these washes, 300 μ l of TE and 1.5 μ l of RNase A (10 mg/mL) was added to digest RNA to both the sample and Input tubes, which were then incubated for 30 minutes at 37°C. Then, 15 μ l of 10% SDS and 7.5 μ l of Proteinase K (10mg/mL) was added to the samples

to digest any residual protein and incubated at 37°C for a minimum of 4 hours. Finally, the cross-links were reversed by incubation at 65°C for 6 hours to overnight.

e. DNA extraction and qPCR.

For extraction methods, see previous section. Following extraction, 2 µl DNA was added to 8 µl Real time qPCR mastermix (see qPCR methods section) per well in a 96 well plate.

f. Designing primers for ChIP.

ChIP primers for potential Trim24 binding in promoter regions (half-sites for RARE or NR binding) of genes associated with lipid regulation are listed in Table 4. Primers for top gene candidates (*Nrf2*, *Saa1*, *Lpin1*, *Gck*, **Gbe1*, and *Jun**) are listed in Table 4.

*Data not shown.

2.17. RNA-seq data analysis. (This data analysis was preformed by Zeynep C. Akdemir, PhD)

The sequencing of 6 RNA-Seq samples (3 biological replicates of RNA samples from livers of *Trim24*^{-/-} and *Trim24*^{+/+} mice) produced Illumina 75 bp paired-end sequenced reads. These reads were aligned to the mouse genome (mm9), through the use of TopHAT 1.4.1 with -r 150 -G UCSC_genes.gtf (downloaded from UCSC mm9 July 2007) parameters[73]. EdgeR was applied to determine differentially expressed genes between *Trim24*^{-/-} and *Trim24*^{+/+} samples at a false discovery rate (FDR) adjusted p-value (q-value) of 1%[74]. DAVID functional annotation tool was

employed to establish biological functional annotation of differentially expressed genes in *Trim24*^{-/-} samples compared to *Trim24* samples. UCSC genome browser was used to visualize RNA-Seq reads along *Trim24*, using Mouse July 2007 (NCBI37/mm9) assembly[75, 76].

2.18. ChIP-seq data analysis. (This data analysis was preformed by Zeynep C. Akdemir, PhD)

ChIPseq was performed with pooled liver tissue from five mice at 10 wks of age (male and female). After sequencing, mapped reads are aligned to the genome and TRIM24 chromatin-enrichment profiles are generated using peak-calling programs (MACS or MACS2) in comparison to Input. TRIM24 binding was determined relative to transcription start sites (TSS's) of RefSeq genes, defined on the UCSC genome browser site. Programs such as MEME-Chip or TRAP are used to analyze DNA regions at binding peaks for transcription factor consensus binding motifs [77, 78]. This approach nominates candidate regulatory proteins that are likely recruited by TRIM24 to chromatin and that play key roles in each biological function and pathways. As a first approach to identifying the genes regulated by TRIM24, we used nearest neighbor within 10kb of TRIM24 binding. This data was further overlapped with 2 month old male and female RNA-seq analysis using the list comparison program from the Whitehead Institute for Biomedical Research. Following integration, the gene lists were analyzed using Igenuity Pathway Analysis (IPA) and DAVID to determine associated biological pathways with most significantly misregulated genes.

2.19. Variant analysis.

Ensembl Nucleotide (<http://www.ensembl.org/Multi/blastview>) and Blast databases (<http://www.ncbi.nlm.nih.gov/>) were used to predict *Trim24* spliced variants and their expressed protein isoforms.

2.20. Statistical analysis.

Student's *t* test was used in all statistical analysis and data were represented as mean \pm STDEV. Differences at $P < 0.05$ with two-sample unequal variance were considered to be statistically significant for RNA analysis, with $P < 0.1$ considered statistically significant for RNA-Seq analysis.

CHAPTER III

TRIM24 suppresses development of spontaneous hepatic lipid accumulation and hepatocellular carcinoma in mice

3.1. Introduction

TRIM24 is highly expressed in multiple types of human cancers, including breast [59, 79], head and neck [80], non-small cell lung [81], glioblastoma [82], and HCC [83]. In contrast to apparent oncogenic functions of TRIM24 in humans, analysis of a mouse model with *cre*-mediated excision of exon 4 of *Trim24* (*Trim24^{dIE4/dIE4}*) suggested that TRIM24 is a liver-specific, retinoid-dependent tumor suppressor [84]. However, recent evidence shows that the *Trim24^{dIE4/dIE4}* mouse is not null for *Trim24* in the liver, as it retains normal levels of *Trim24* RNA lacking exon 4 [85]. Additionally, I used utilized Ensembl and BLAST databases to predict that alternative start sites of *Trim24* transcription could yield native isoforms of *Trim24* lacking E4, as expressed in the *Trim24^{dIE4/dIE4}* mouse [85]. These isoforms are in frame and are predicted to produce proteins known as TRIM24 variants 1 and 3, which have high similarity to *BRAF* (Variant 1: 84% protein identity, Variant 3: 64% protein identity) (Table 9). HCC occurs in the *Trim24^{dIE4/dIE4}* mouse without apparent progression from NAFLD, due to activation of retinoid-dependent enhancers present in endogenous, murine VL30-retroviral transposons inserted across the mouse genome [85]. These long terminal repeat (LTR) enhancers are repressed by TRIM24/TRIM33 heteromeric complexes, similar to silencing of proviral DNA expression by TRIM28 [86]. In this mouse model, loss of TRIM24/TRIM33-mediated repression causes aberrantly high expression of inflammatory pathway genes linked to neoplastic inflammation in the liver.

The expression of *Trim24* RNA lacking exon 4 (E4), as observed in *Trim24^{dIE4/dIE4}* mice [85], leaves unresolved whether this aberrant RNA or encoded protein isoforms

exhibit dominant negative or gain-of-function, contributing to the observed HCC phenotype. These unknowns and, importantly, the documented over expression of TRIM24 in human cancers, including HCC [83], led us to create a conditional knockout mouse that is null for *Trim24* expression by genetic targeting of the promoter and first exon (*Trim24*^{dIE1/dIE1}).

3.2. A *Trim24*^{-/-} mouse generated by deletion of promoter and exon 1.

We engineered a conditional knockout mouse of *Trim24* by genetic targeting of the transcription start site and first exon (Fig. 1). To generate germline *Trim24* deletion, *Trim24*^{LoxP} mice were bred with *Zp3-Cre*–expressing mice to obtain *Trim24*^{+/-dIE1} progeny. *Trim24*^{+/+}, *Trim24*^{+/-dIE1} and *Trim24*^{dIE1/dIE1} progeny were confirmed by PCR analysis (Fig. 2) and were viable and fertile in both males and females. Deletion of *Trim24* occurs without allelic compensation, shown by protein and RNA analyses of mouse embryonic fibroblasts (MEFs) (3B), from *Trim24*^{+/+}, *Trim24*^{+/-dIE1} and *Trim24*^{dIE1/dIE1} E12.5 embryos (Fig. 3A), adult whole liver and hepatocytes as evidenced by immunohistochemistry (Fig. 3C-E).

Deep sequencing of RNA (RNA-seq), from *Trim24*^{+/+} and *Trim24*^{dIE1/dIE1} liver (2 mos), showed no detectable expression across the *Trim24* locus in *Trim24*^{-/-} (Fig. 4). Quantitative RT-PCR analysis of all three, potential protein-coding isoforms of *Trim24* (<http://useast.ensembl.org/>) with primers covering *Trim24* exon 2/3, exon 7/8, exon 11/13, and the 3'UTR (Table 3) confirmed complete loss of *Trim24* RNA expression in MEFs (Fig. 3B). Since our analyses of *Trim24* expression show that the *Trim24*^{dIE1/dIE1} mouse is truly null for *Trim24* expression, it is further discussed as *Trim24*^{-/-}

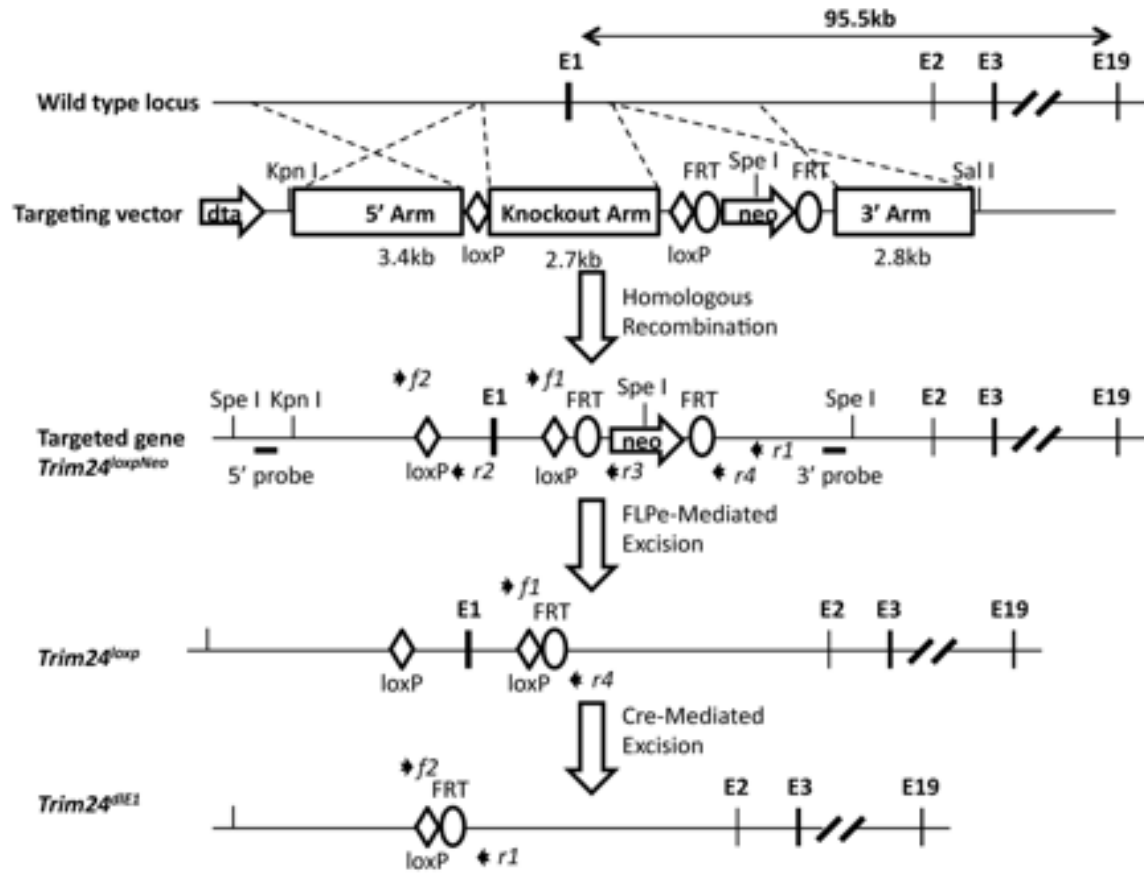


Figure 1. Scheme for generation of the *Trim24*^{-/-} mouse. Murine *Trim24* gene exons (E1-E19), Southern blot -5'/ 3' probes, and primers (f1, f2, r1, r2, r3, r4) for genotyping are shown with diagrams of crosses to delete E1 and promoter. Dta – Diphtheria toxin subtype A, Neo – Neomycin cassette, FRT – Flippase recognition target, LoxP – Locus of X over P1. Diamond = LoxP sites, Circle = FRT sites.

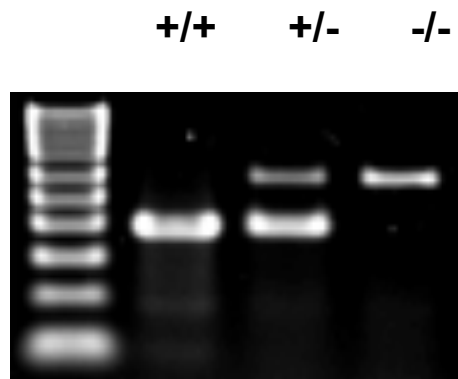


Figure 2. PCR Genotyping analysis confirming deletion of *Trim24* exon 1. Samples were obtained from tail snips. $+/+$ = Wild-type, $+/-$ = Heterozygous, $-/-$ = Null. PCR products of 384bp (WT) and ~650bp (dIE1) were obtained using primer pairs targeting f2/r2 and f2/r.

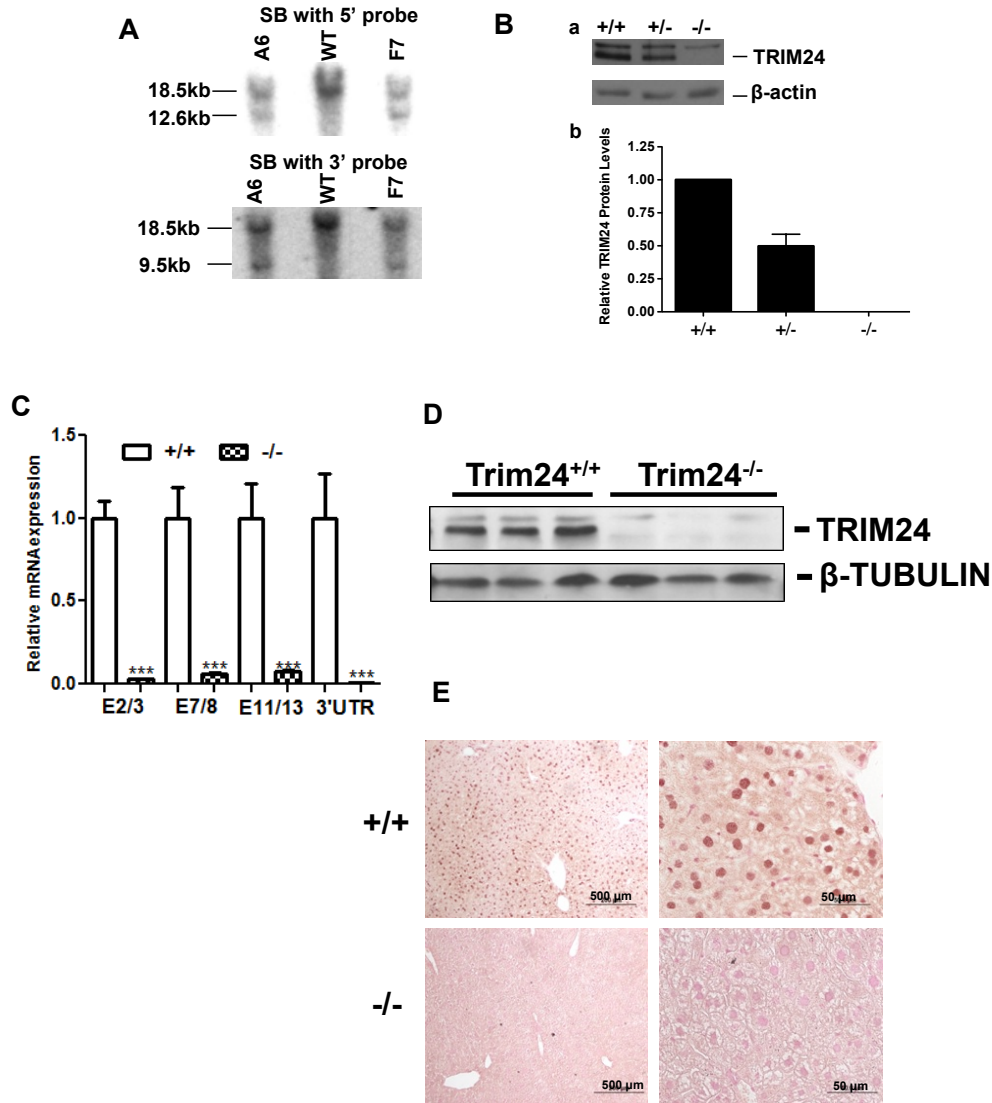


Figure 3. Confirmation of *Trim24* deficiency. **A)** Southern blot. DNA extracted from ES cell clones was digested with Spe I and analyzed with the 5' and 3' probes. Clone A6 and F7 showed the appropriate bands. **B)** (a) Western blot analysis of TRIM24 protein expression in MEFs of the indicated genotype. β -actin, as a loading control. (b) Relative TRIM24 protein levels in $Trim24^{+/+}$, $Trim24^{+/-}$, and $Trim24^{-/-}$ MEFs. **C)** Real-time PCR analysis revealed all isoforms were deleted in $Trim24^{-/-}$ liver (n=3) using primers targeting Exon2/3, Exon7/8, Exon 11/13, and 3'UTR. **D)** Western blot analysis for TRIM24 protein expression in $Trim24^{+/+}$ and $Trim24^{-/-}$ liver (n=3), compared to β -tubulin control. **E)** TRIM24 immunohistochemistry analysis using TRIM24 (Protein tech) antibody in $Trim24^{+/+}$ and $Trim24^{-/-}$ liver (n=3) at 2 months of age. Bar: 4X: 500 μ m; 40X: 50 μ m.

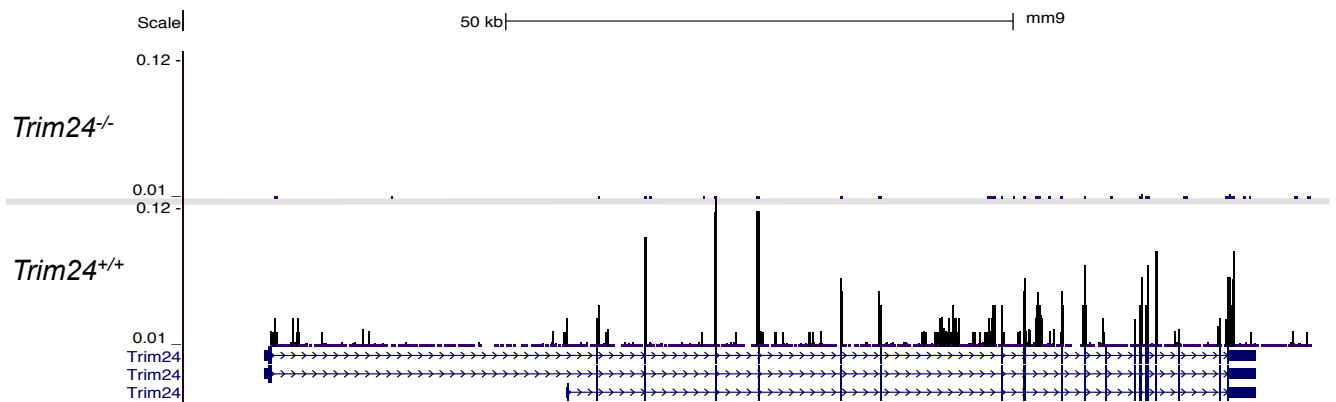


Figure 4. Loss of *Trim24* RNA expression in *Trim24*^{-/-} liver: RNA-seq of *Trim24*^{-/-} and WT. The figure represents a UCSC genome browser snapshot of the sequencing and positive peaks for *Trim24* expression in *Trim24*^{+/+} and *Trim24*^{-/-} mouse liver at 10 weeks of age. Vertical lines are peaks that denote positive expression of the gene coinciding with specific regions of the gene (exons and introns), as shown in the *Trim24*^{+/+} mouse liver, whereas in the *Trim24*^{-/-} mouse liver, lack of positive expression/peaks confirm complete deletion of the gene.

TRIM24 belongs to the TRIM protein TIF1 subfamily (C-VI) of which there are three members: TRIM24, TRIM28 and TRIM33 [87]. These proteins have a high degree of homology and form heteromeric complexes that vary according to cell type [87]. TIF1 α (TRIM24) and TIF1 β (TRIM28) amino acid sequences share 32% identity and 54% similarity over their entire length [55]. Most of the homology is stronger in the N- and C- terminal regions than in the central region. In the N-terminal region, homology exists between several evolutionarily conserved domains: the RBCC subfamily of RING finger proteins, one to two B box-type fingers, and a putative coiled-coil domain [54, 88]. The C-terminal region contains homology in the zinc or PHD finger and bromodomain regions, respectively [55]. Further studies showed that in addition to these conserved domains, TIF1 γ (TRIM33) and TIF1 α share a 25 amino acid-long, tryptophan- and phenylalanine-rich sequence downstream from the coiled coil motif. This sequence is highly conserved between all three TIF1 proteins and identical between TIF1 α and TIF1 γ (TRIM33) [61].

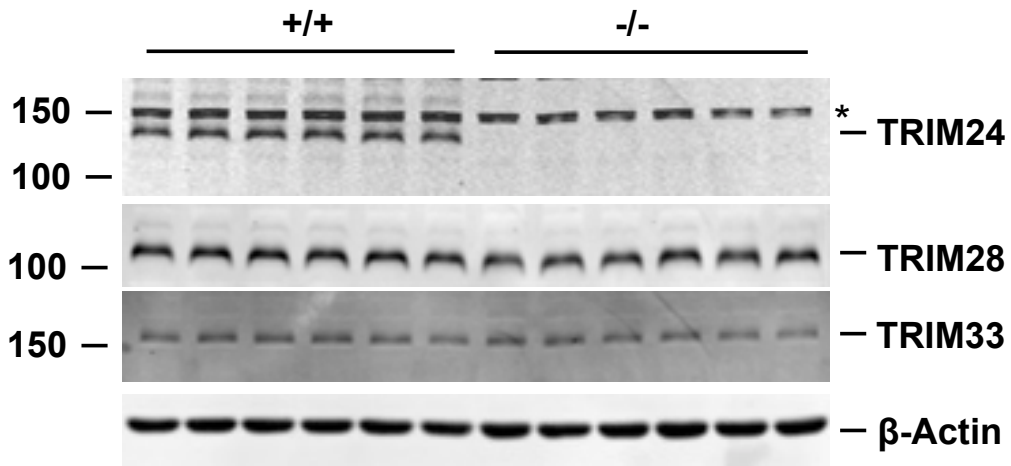
We determined if other TIF1 subfamily members potentially compensate for loss of *Trim24* [3][89], and analyzed *Trim28* and *Trim33* RNA and protein from wild type (WT) and *Trim24*^{-/-} MEFs (Fig. 5). These analyses showed no significant differences; therefore, it is unlikely that any phenotype of the *Trim24*^{-/-} mouse is due to compensatory functions of TRIM28 or TRIM33.

3.3. *Trim24*^{-/-} mice develop hepatocellular lesions, steatosis and HCC.

A major phenotype of *Trim24*^{-/-} mice is development of macroscopic white lesions in the liver by 4-6 months of age (Fig. 6A; a), compared to the normal morphology of *Trim24*^{+/-} liver and *Trim24*^{+/+} liver (Fig. 6A; b, 7). H&E staining showed

that *Trim24*^{-/-} liver lesions are composed of both micro- and macro-vesicular steatosis (Fig. 6A; c, d). Oil Red O (ORO) staining revealed that all hepatocytes within the lesions of *Trim24*^{-/-} liver are filled with lipid (Fig. 6A; e, f) in contrast to *Trim24*^{+/+} liver (Fig. 7). Further, hepatic lipid accumulation can be seen as early as 2 weeks of age (Fig. 8A) with significant accumulation of lipid in foci at 2 and 4 months of age (Fig. 8B, C). Trichrome staining to assess fibrotic progression was negative for collagen and mucin in *Trim24*^{-/-} liver at 3 and 10 weeks of age (Fig. 9A,B), when lipid accumulation is already obvious, but was positive for fibrosis by 6 months (Fig. 6A; g, h). *Trim24*^{+/+} liver remains negative at all ages (Fig. 9).

A



B

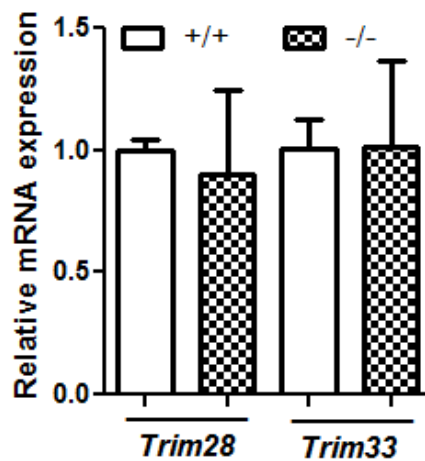


Figure 5. Deletion of TRIM24 has no effect on TRIM28/33 expression. A) Western blot analysis of TRIM24, 28, and 33 protein expression in MEFs. β -actin - loading control and * - non-specific. **B)** *Trim28* and *Trim33* expression in MEFs (RT-qPCR).

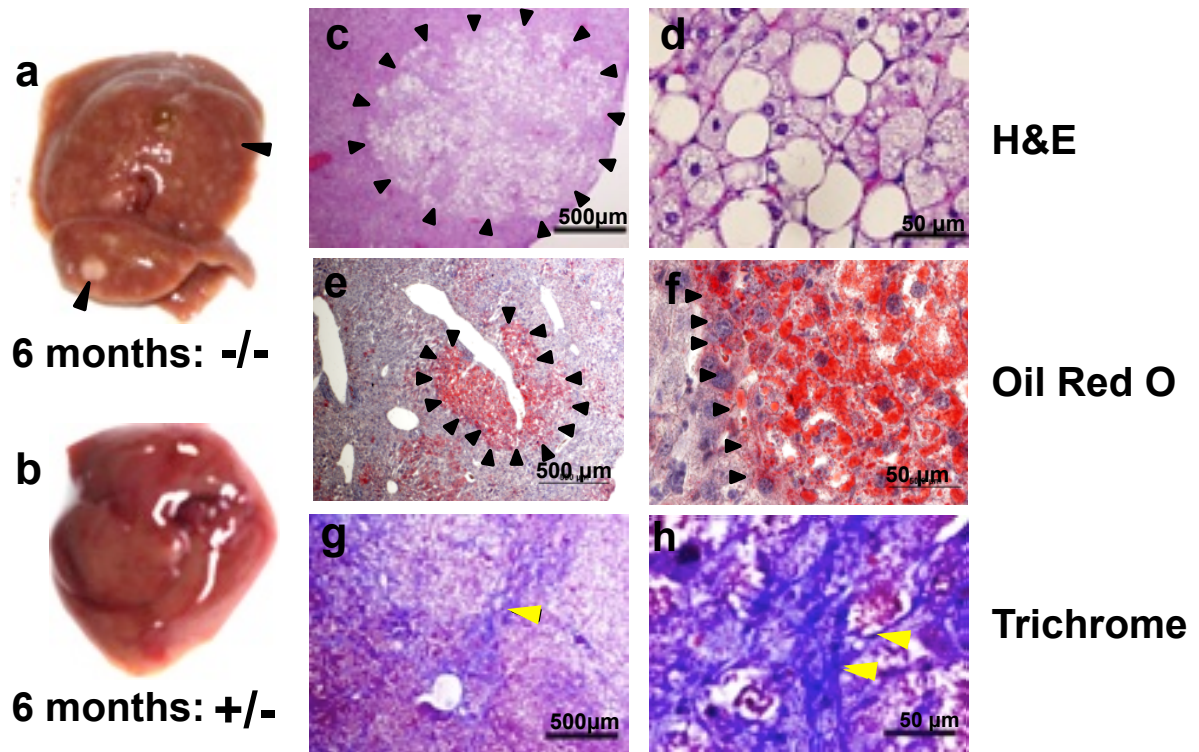


Figure 6. Lipids and fibrosis increase in aging *Trim24*^{-/-}. 6 month liver, lesions (arrows) (a) *Trim24*^{-/-}, (b) *Trim24*^{+/-}; (c,d) Vacuolated lesions with steatosis (H&E, black arrows indicate borders of lipid filled lesions). (e,f) Lipid accumulation using Oil Red O staining (black arrows indicate borders of lipid filled lesions). (g,h) Fibrosis (arrows indicate positive staining, Trichrome). Bar: 500 μm (4X) and 50 μm (40X).

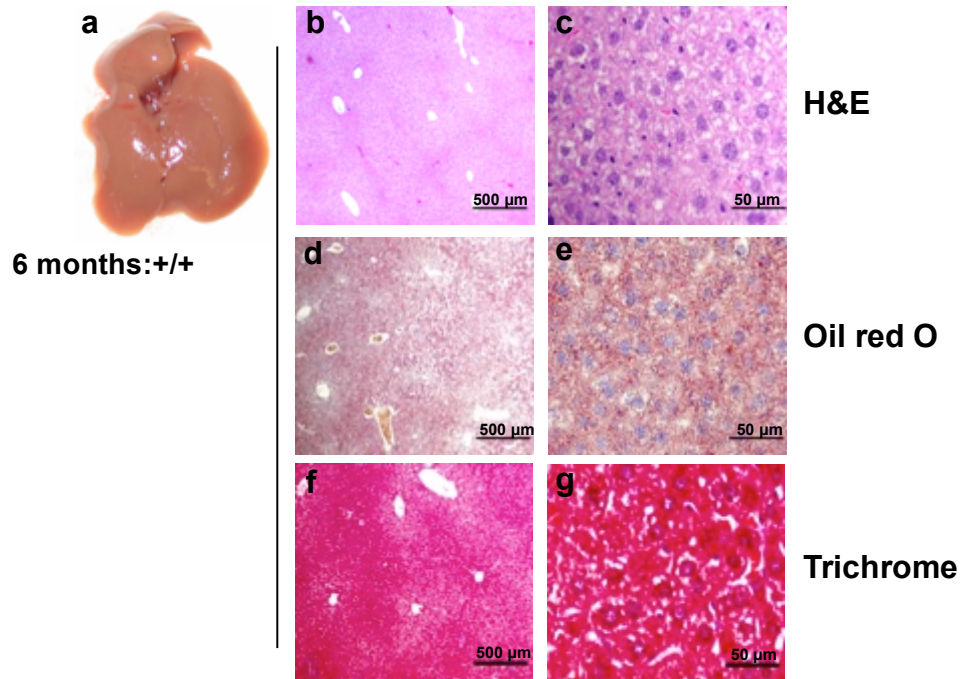


Figure 7. Normal morphology, lipid accumulation and fibrosis in age-matched *Trim24*^{+/+} liver (6 months). (a) Macroscopic analysis, (b, c) Histologic analysis by H&E staining, (d, e) Lipid accumulation analysis by Oil Red O staining, and (f, g) Fibrosis analysis by Trichrome staining. Bar: 4X: 500 μm; 40X: 50 μm.

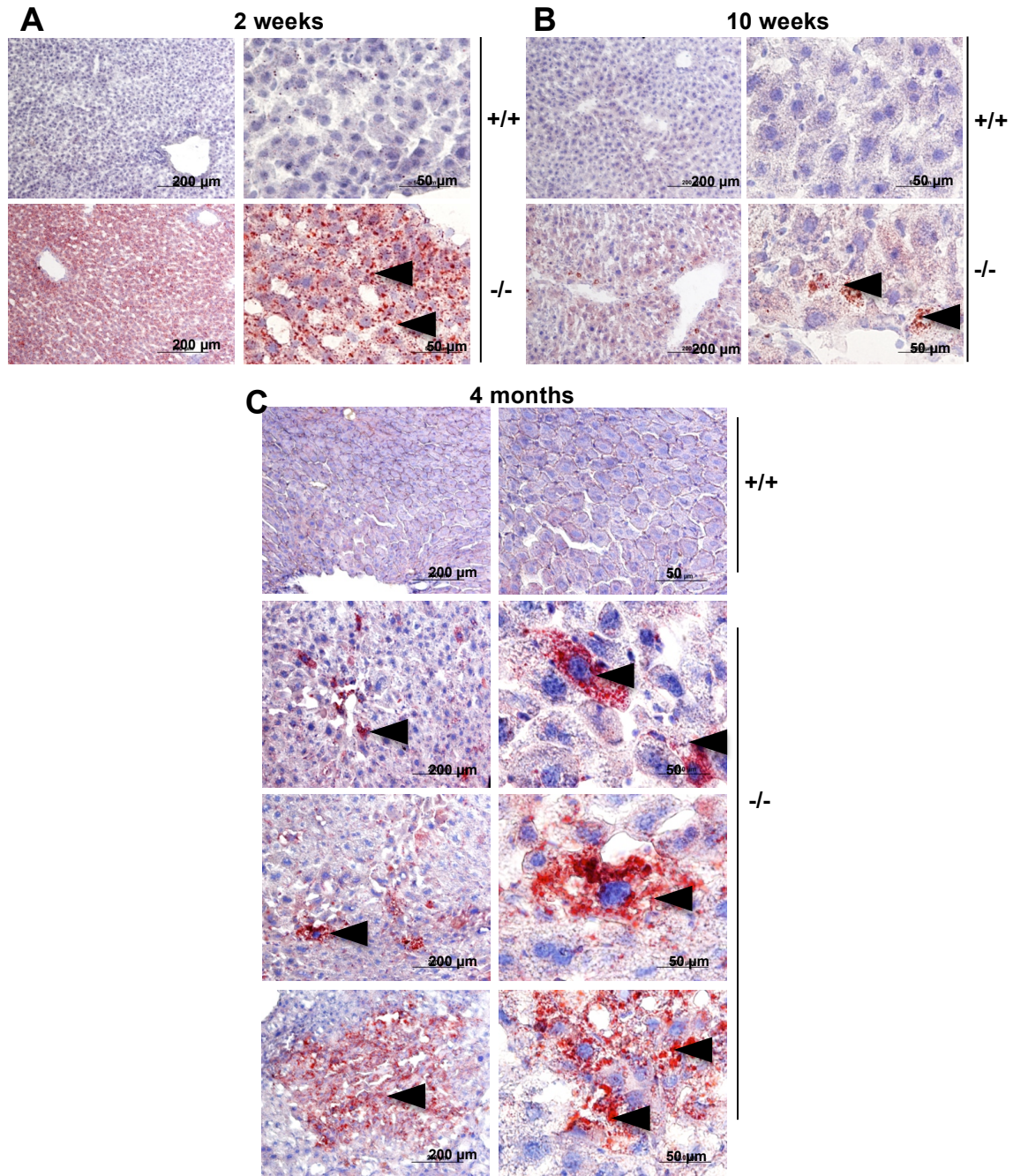


Figure 8. Lipid accumulation in *Trim24*^{-/-} livers. (A-C) Oil Red O staining of liver sections from *Trim24*^{-/-} **A)** 2 weeks, **B)** 10 weeks, and **C)** 4 months. Arrows indicate positive staining for accumulation of lipids. Bar: 200 μm for 10X and 50 μm for 40X.

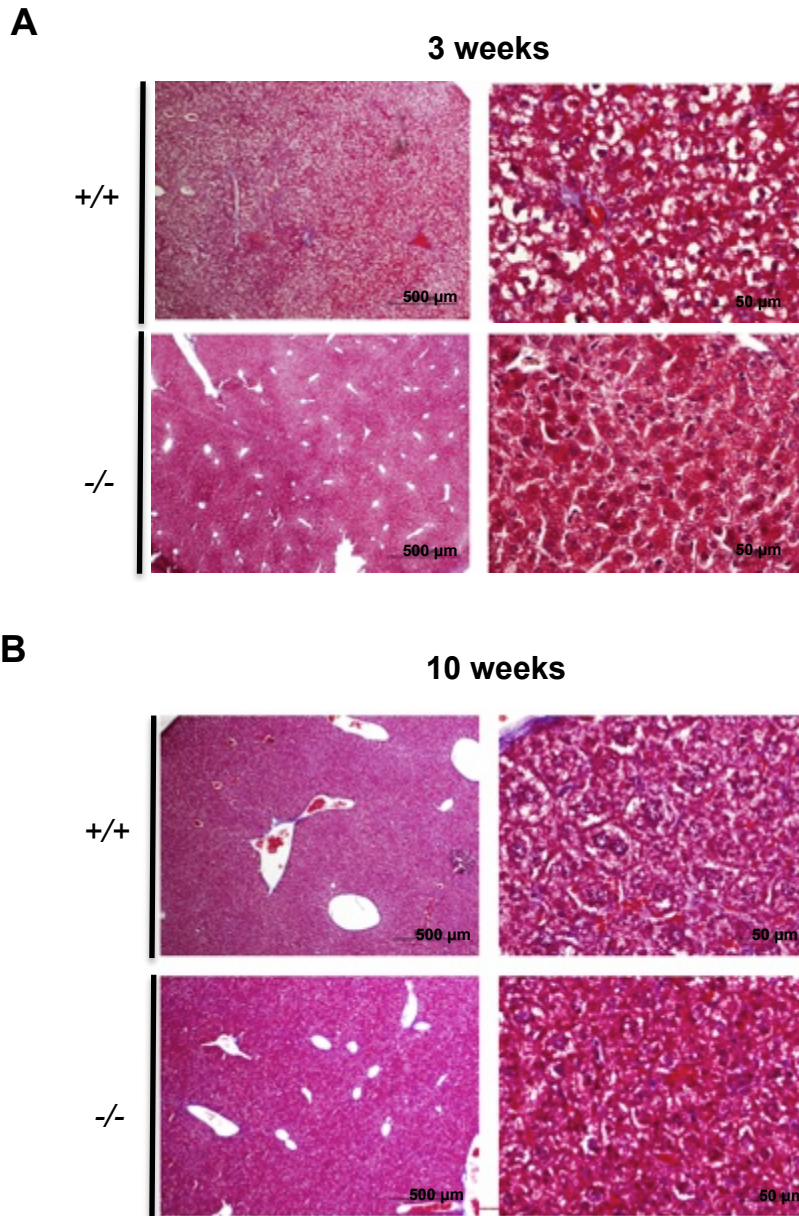


Figure 9. Fibrosis is not evident in young *Trim24*^{-/-} livers. Trichrome staining of liver sections from *Trim24*^{-/-} compared to *Trim24*^{+/+} (a-b) 3 weeks and (c-d) 10 weeks. Bar: 500 μm for 4X and 50 μm for 40X (n>5). Positive staining is dark blue and is not evident in these sections. For reference section, please consult Fig. 6h.

Significantly increased RNA levels of several collagen and matrix metalloproteinase (*Mmp*) genes and transforming growth factor- β receptor 2 (*Tgfb2*) indicate upregulation of fibrotic and damage-related pathways at 10 weeks of age, but fibrosis is not apparent until 6 months of age (Fig. 6,9,10). We saw progression of liver disease: between 9 and 23 months, the liver to body weight ratio (liver index) of *Trim24*^{-/-} mice increased 2.7 fold, compared to *Trim24*^{+/+} and *Trim24*^{+/-} mice (Fig. 11). Numerous macroscopic hepatic tumors (>2mm) were present in all *Trim24*^{-/-} mice (29/29), regardless of gender (Fig. 12). In contrast, there was no evidence of hepatic tumors or anomalies in age- and background-matched *Trim24*^{+/+} (0/17, 12-15 months) and *Trim24*^{+/-} (0/11, 12-18 months) mice (Table 5, Fig. 13). At 18 months, *Trim24*^{-/-} liver showed a spectrum of hyperplastic lesions, preneoplastic foci of cellular alteration (FCA) and neoplastic lesions of hepatocellular adenoma (HCA) with and without fatty changes (Fig. 12, a-i). The non-nodular or nodular HCA lesions had a vacuolated cell mass compressing the non-tumoral parenchyma (Fig. 12D; b,c). ORO staining revealed lipid accumulation in vacuolated cells of the tumor (Fig. 12D; d, e). Locally invasive hepatocellular carcinoma (HCC) with nodules (Fig. 12D; f, g) or without nodules (Fig. 12D; h, i) was seen in terminal mice. The relative presence or absence of nodules is evidence of both nodular and non-nodular HCC, therefore suggesting a heterogeneous tumor population. The distribution of tumor pathologies in *Trim24*^{-/-} mice, ages 9-21 months (n=27), were 26% HCA, 33% HCC with HCA, 22% HCC without HCA, and 19% indeterminate (other) (Fig. 14). *Trim24*^{-/-} mice have a median survival time of 409 days as compared to *Trim24*^{+/+} (no deaths at 585 days) (Fig. 15).

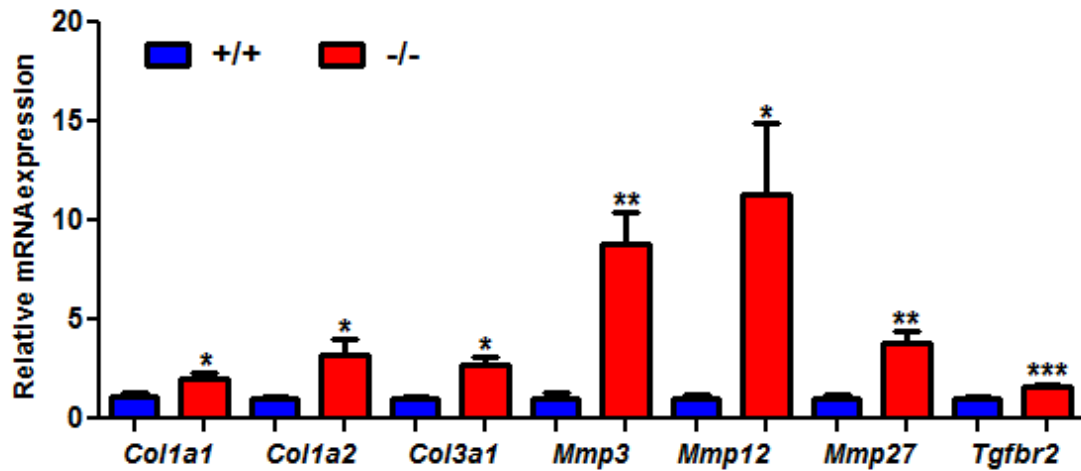


Figure 10. Fibrosis gene expression is upregulated upon loss of *Trim24*. Fibrosis genes up-regulated in 10 week *Trim24*^{-/-} liver: n=6, *p<0.05; **p<0.01; ***p<0.005.

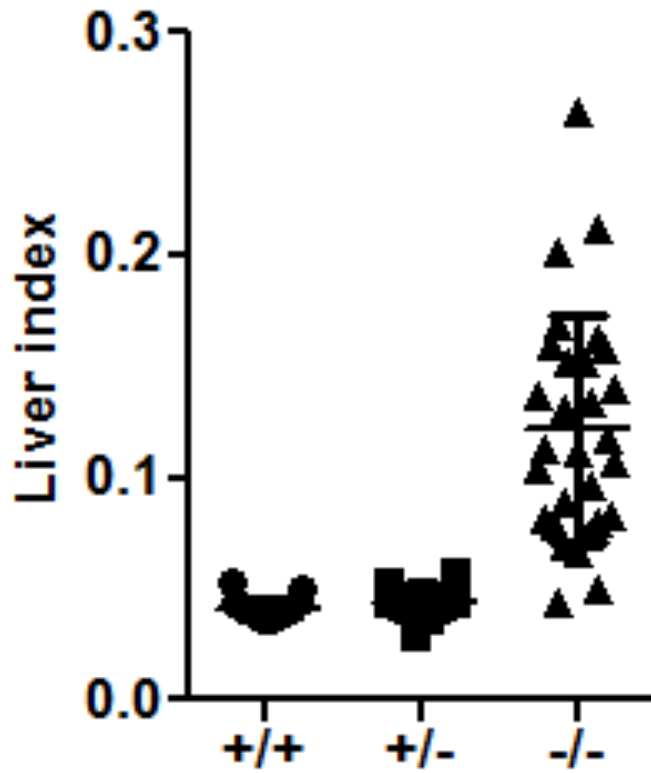


Figure 11. Liver index is increased in *Trim24*^{-/-} mice. *Trim24*^{-/-} (n=29), *Trim24*^{+/+} (n=17) and *Trim24*^{+/-} (n=11). ***p<6.7E-08. Mean ± SD.

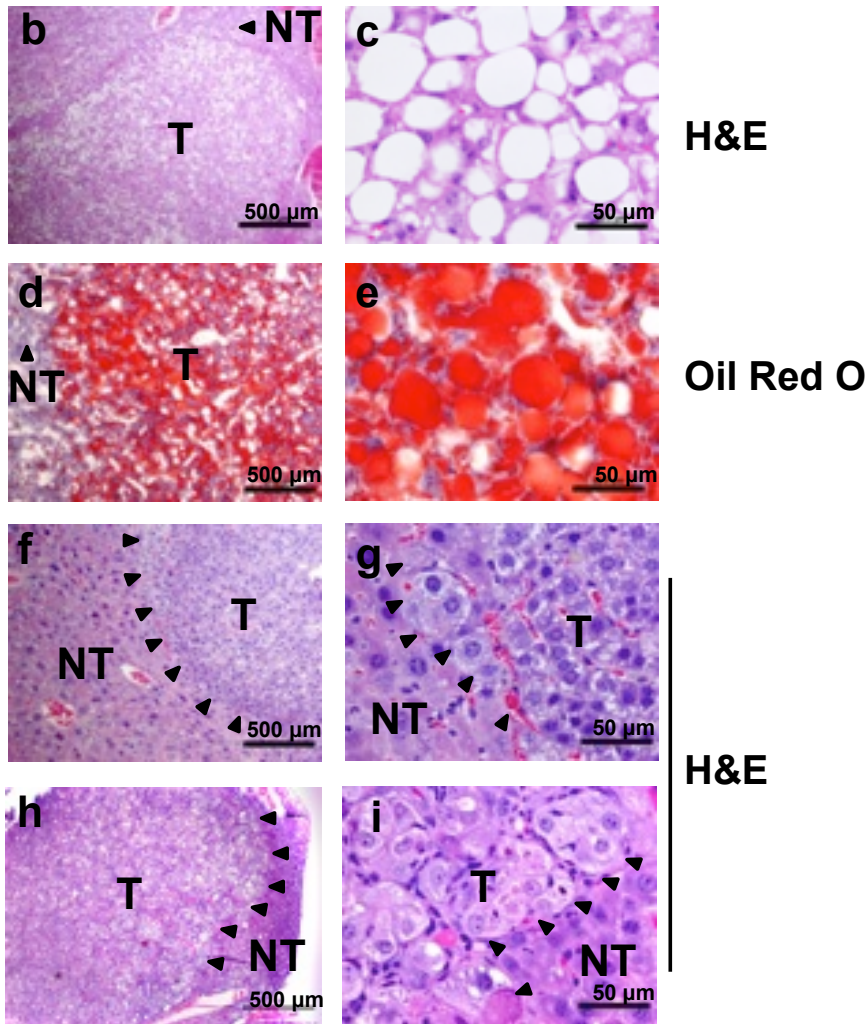
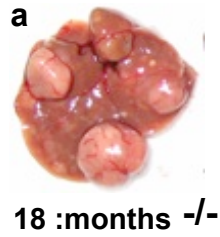


Figure 12. Aging *Trim24*^{-/-} mice develop hepatocellular carcinoma (HCC). 18 month *Trim24*^{-/-}: Multiple, large lesions (Hepatocellular adenoma – HCA) (b, c) Vacuolated (d, e) Lipid positive. (f,g) Invasive HCC without nodules. (h, i) Nodules. (Black Arrows = Boundary. T, tumor; NT, non-tumor). Bar: 500 μm (4X) and 50 μm (40X).

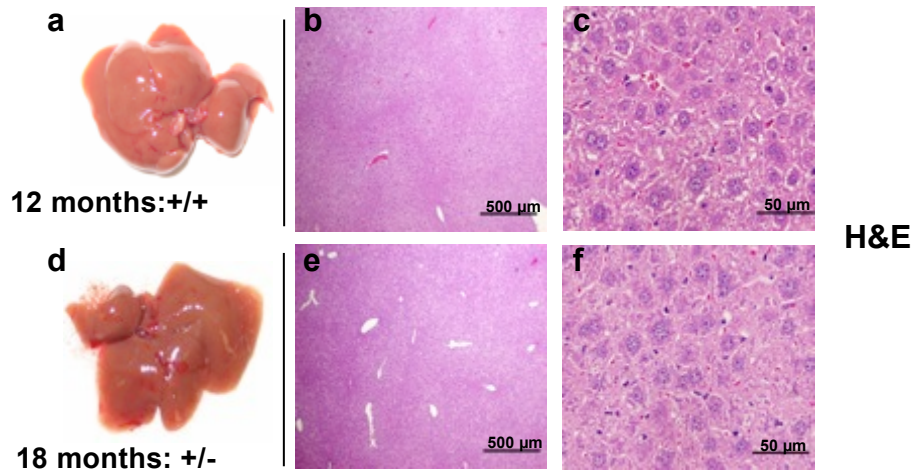


Figure 13. Normal morphology in livers of $Trim24^{+/+}$ (a, 12 months) and $Trim24^{+/-}$ (d, 18 months) mice. (A) Histological analysis of liver sections from (b,c) aging $Trim24^{+/+}$, (e,f) $Trim24^{+/-}$, in lower (4X: b,e) and higher (40X: c,f) magnification of H&E stain, respectively. Bar: 500 μm for 4X and 50 μm for 40X.

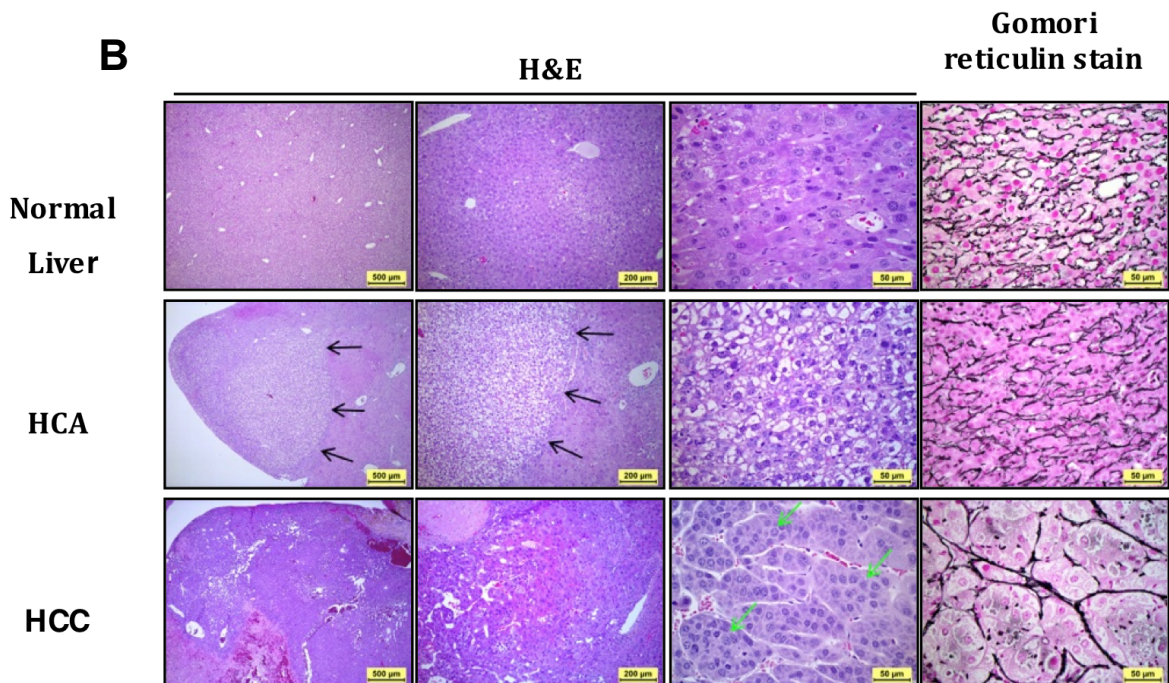
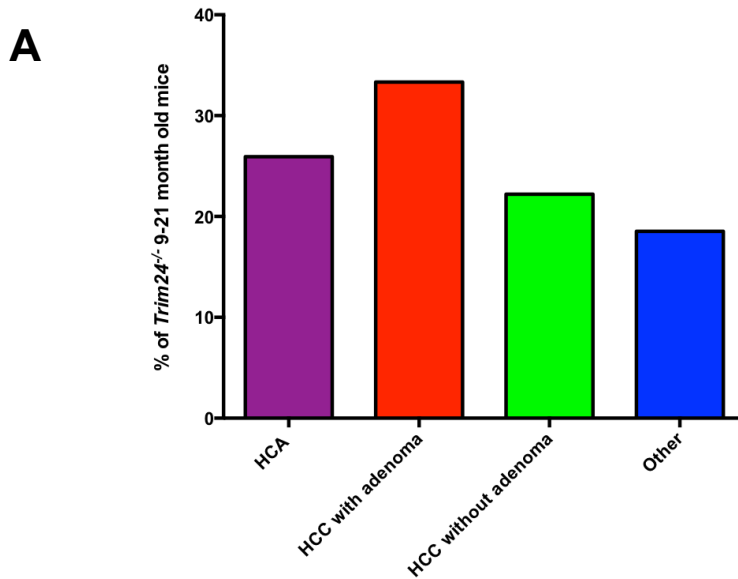


Figure 14. Distribution of HCC progression in aging *Trim24*^{-/-} livers. (A-B) *Trim24*^{-/-} mice ages 9-21 months (n=27) Findings are reported as % of total. Hepatocellular Adenomas (HCA) have distinct borders (black arrows) with minimal cellular atypia of hepatocytes, and minimal or no disruption of the basement membrane (black reticulin stain). Hepatocellular Carcinomas (HCC) have poorly defined borders, high degree of cellular atypia, marked disruption of the basement membrane and loss of normal tissue architecture, with formation of thick trabeculae (green arrows) of multiple layers of neoplastic hepatocytes. Bar: 4x: 500 μ m; 10x: 200 μ m; 40x: 50 μ m.

Trim24^{-/-} Mouse Survival

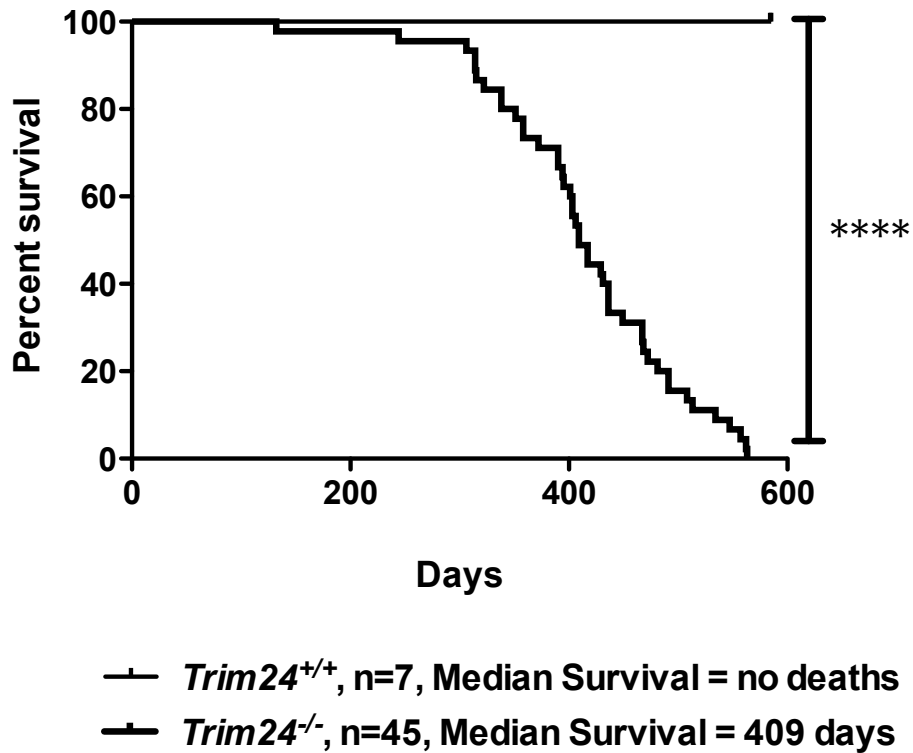


Figure 15. *Trim24*^{-/-} mouse survival curve. *Trim24*^{-/-} mice (n=45) have a median survival time of 409 days compared to *Trim24*^{+/+} (n=7) with no deaths at 585 days. ****p<0.0001.

3.4. Inflammation, injury and degeneration are increased in adult *Trim24*^{-/-} mice.

Key components of NASH in humans are aberrant plasma and intrahepatic lipid levels with accumulation of lipids, mainly triglycerides (TG), and increased hepatocellular inflammation and steatosis, with subsequent injury and degeneration [90]. I quantified indicators of liver damage and NASH in plasma from *Trim24*^{+/+} and *Trim24*^{-/-} mice (7 each). Both alanine aminotransferase (ALT) and aspartate aminotransferase (AST) levels were significantly increased in *Trim24*^{-/-}, suggesting liver damage (Fig. 16). In human NASH, there is dysfunction in the normal lipase-mediated hydrolysis of TG in the liver to yield fatty acid and glycerol. Human patients have elevated plasma and hepatic TG levels, often associated with obesity [90]. In contrast, *Trim24*^{-/-} mice are not obese: visceral fat and hepatic TG levels decreased (Fig. 16,17). Although plasma cholesterol and lipoprotein levels decreased, plasma TG and hepatic lipids increased (Fig. 16).

In further assessment of potential NASH, we performed histological analyses and quantified expression of genes associated with hepatocellular steatosis, injury and degeneration. Histological analysis of young adult *Trim24*^{-/-} liver (10 weeks) revealed degenerated or damaged hepatocytes throughout (Fig. 18). Swollen, vacuolated cells (Fig. 18C; b, arrows), Mallory bodies (Fig. 18C; c, arrow), and nuclear inclusion bodies (Fig. 18C; d, arrow and insert) are characteristic of *Trim24*^{-/-}, unlike *Trim24*^{+/+} liver at 10 weeks (Fig. 18). An increase in cleaved-Caspase-3-positive hepatocytes suggested hepatocellular damage induced cell death in the *Trim24*^{-/-} liver by 10 weeks (Fig. 18C; e, f, arrow; quantified in Fig. 18D). Consistent

with these observations, expression of pro-apoptotic genes *Bax* and *Caspase12* and ER stress gene *Ddit3* (DNA-damage inducible transcript 3) are significantly increased in 10-week *Trim24*^{-/-} liver (Fig. 19A). These signs of serious liver damage accompanied significant changes in specific pro-inflammatory gene expression (Fig. 19B). Taken together, lack of *Trim24* in mice recapitulates many of the parameters of human NAFLD and a majority of NASH symptoms with age, although obesity did not occur (Fig. 16,17).

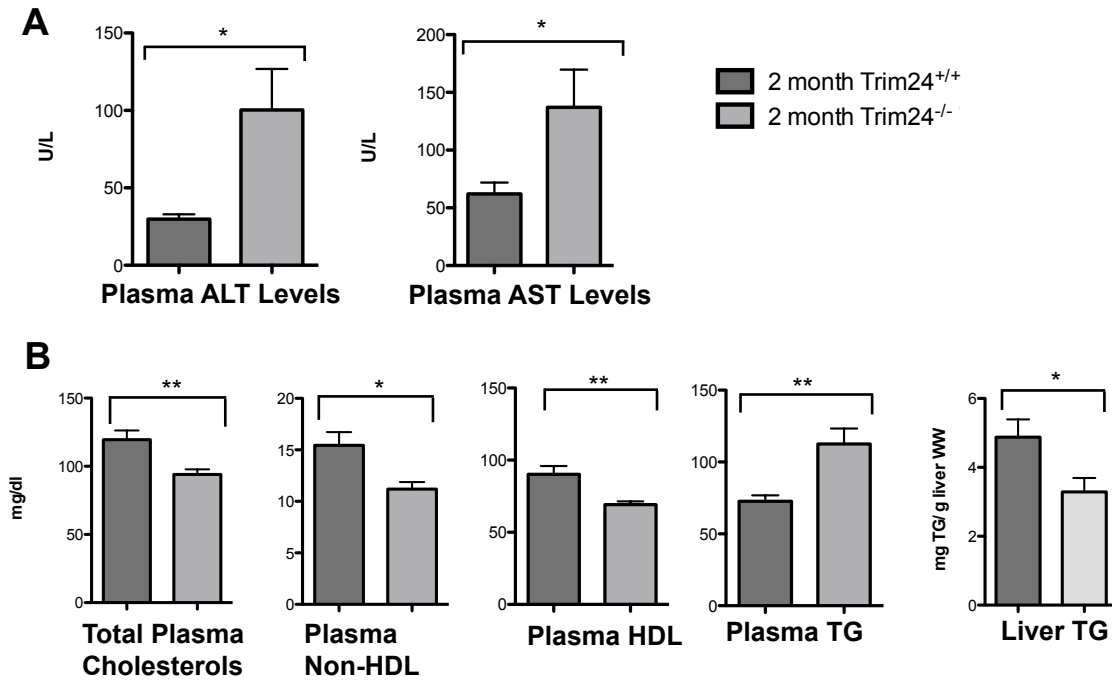


Figure 16. Hepatocellular damage and dysfunction in 2 month *Trim24*^{-/-}. (A) ALT/AST: *Trim24*^{-/-} (n=7), *Trim24*^{+/+} (n=6). (B) Lipoprotein, TG: *Trim24*^{-/-} (n=7), *Trim24*^{+/+} (n=7; except TG n=6). Mean ± SD. * p<0.05, **p<0.01.

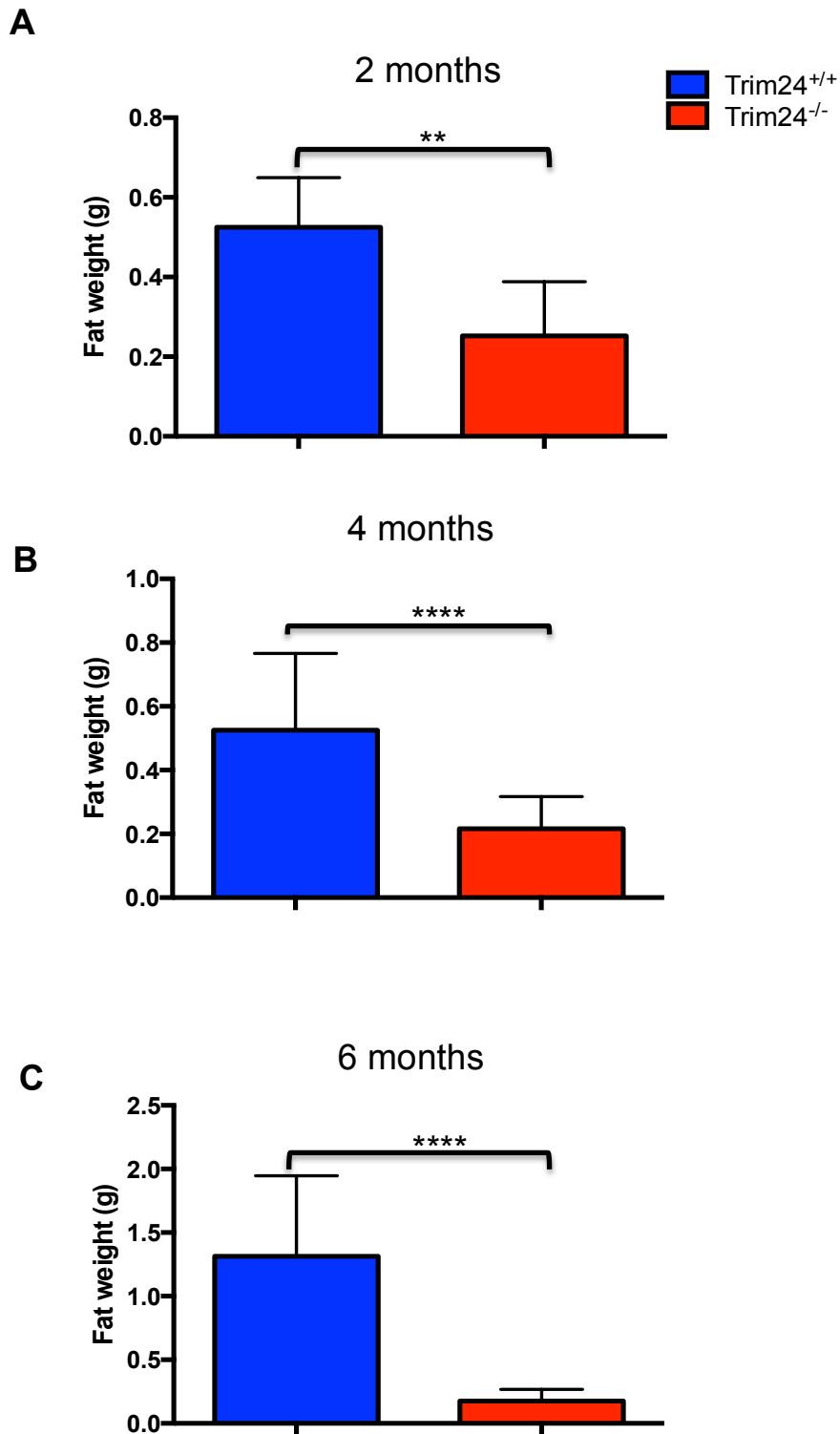


Figure 17. Abdominal peripheral fat is decreased in *Trim24*^{-/-} mice. (A-C) Abdominal peripheral fat weights from 2, 4, and 6 month old *Trim24*^{+/+}, *Trim24*^{+/-}, and *Trim24*^{-/-} male and female mice (n>5).

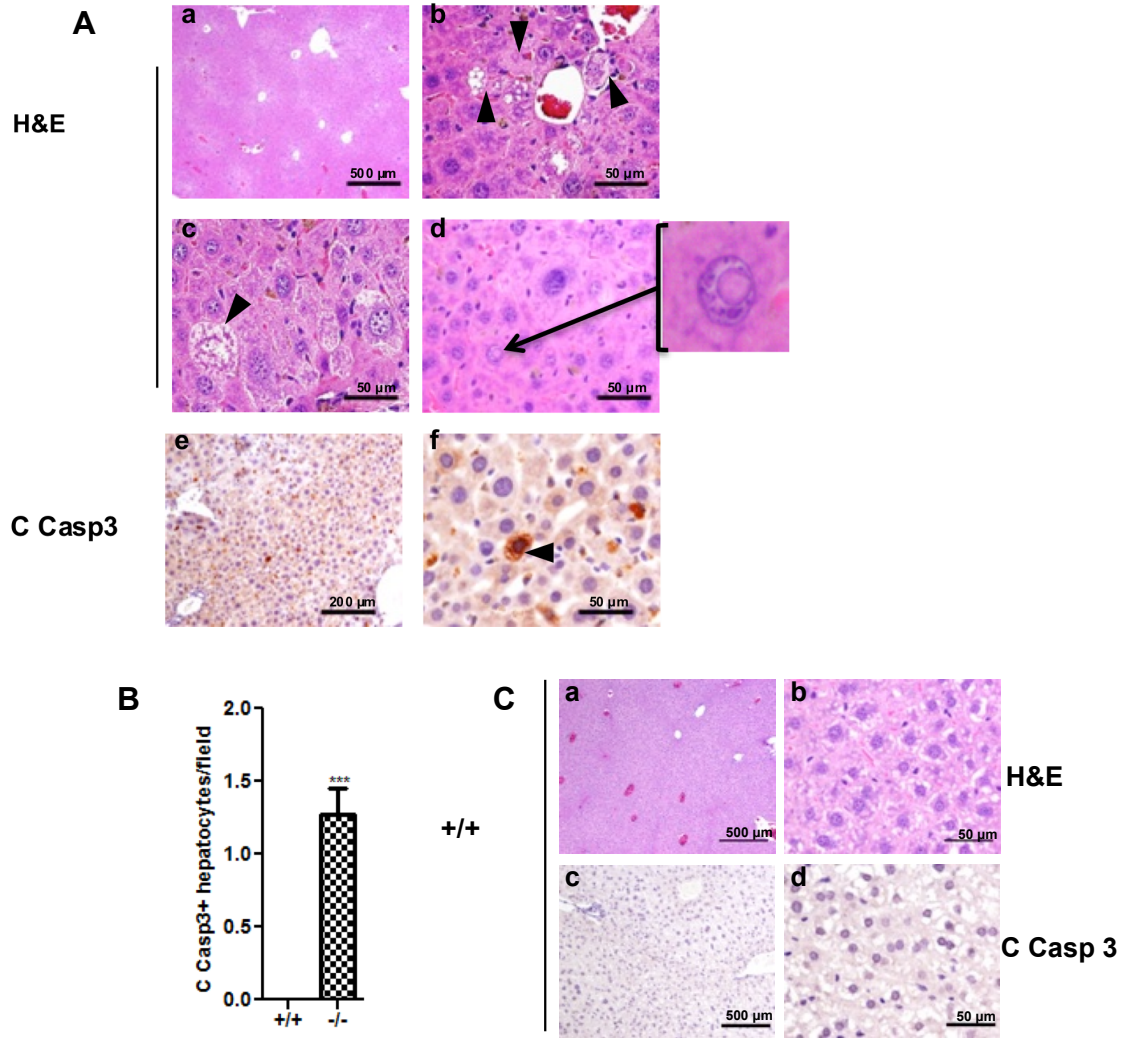
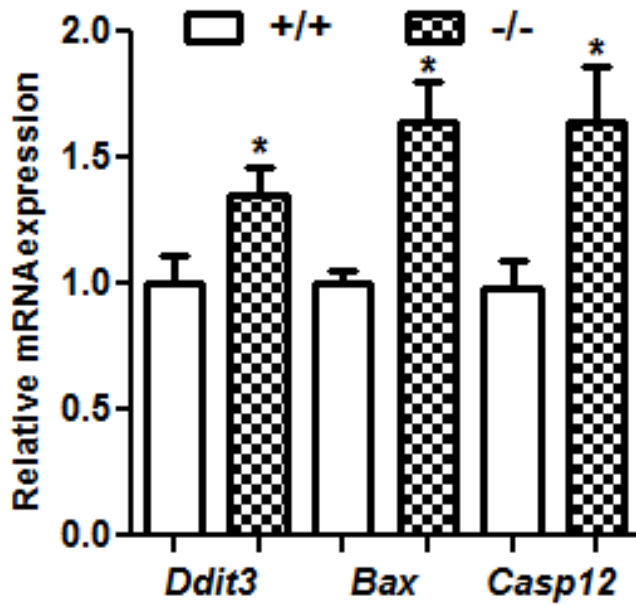


Figure 18. *Trim24*^{-/-} livers show evidence of increased hepatocellular damage. **A)** a-d) Abnormal cells: *Trim24*^{-/-} liver (H&E). (b, arrows) Damaged/vacuolated hepatocytes. (c, arrow) Mallory, (d, arrow and inset) Nuclear inclusion bodies. (e, f, arrow) Apoptotic hepatocytes (IHC: cleaved Caspase 3). Bar: 500 μm (4X); 200 μm (10X); 50 μm (40X). **B)** Cleaved Caspase 3 positive hepatocytes, *Trim24*^{-/-} (20X field). **C)** Histological analysis (H&E staining) shows (a) normal morphology of *Trim24*^{+/+} liver at 4X and (b) 40X and (c) cleaved CASPASE 3 IHC negative staining at 4X and (d) 40X. Bar: 4x: 500 μm; 40x: 50 μm.

A



B

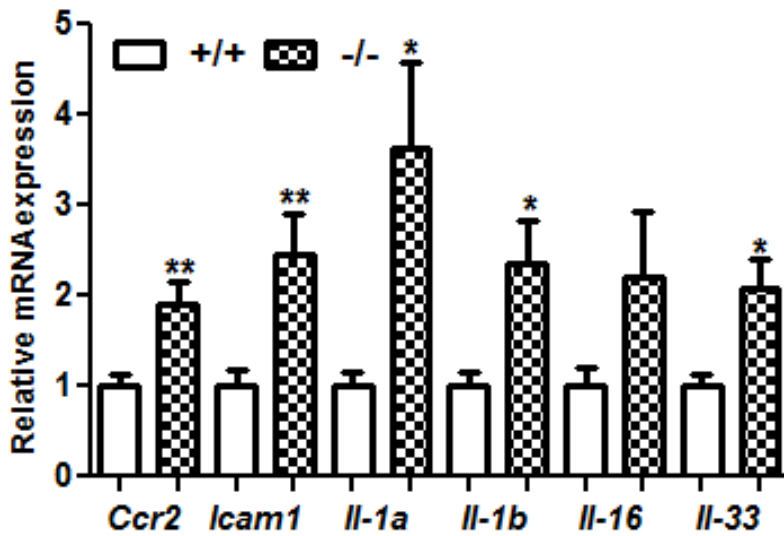


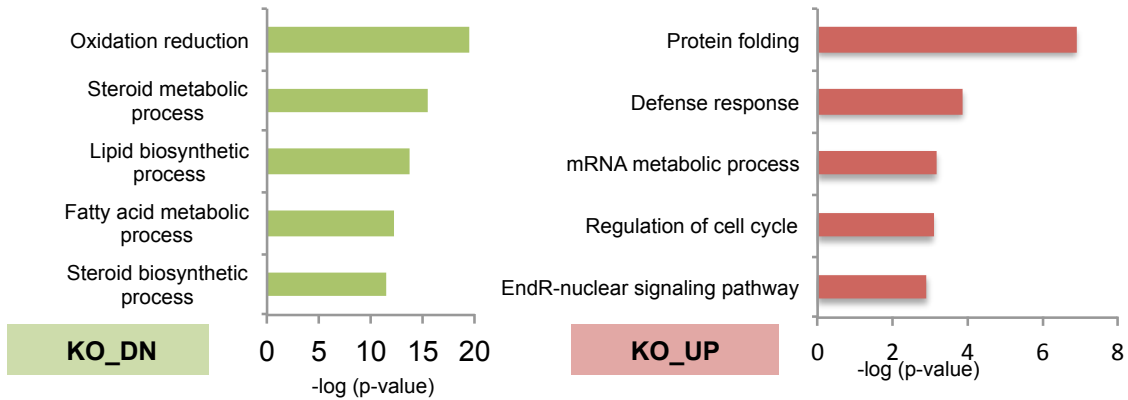
Figure 19. Apoptosis and fibrosis related genes are upregulated in *Trim24*^{-/-} liver. A) Apoptosis-related genes, B) Fibrosis-related genes, n=6 liver samples (mean ± SD), 10 weeks. p value: *p<0.05; **p<0.01; *p<0.005.**

3.5. Genome-wide analysis of RNA expression in *Trim24*^{-/-} liver

To assess the global impact of TRIM24 on gene expression, we performed deep sequencing of RNA (RNA-seq). Three biological RNA replicates were isolated from male *Trim24*^{+/+} and *Trim24*^{-/-} liver at 10 weeks of age and sequenced (Fig. 4). A total of 763 genes showed statistically significant changes and differential expression at a false discovery rate (FDR) adjusted p-value (q-value) of 1%, calculated by EdgeR RNA-Seq analysis [91]. An approximately equal number of genes were activated or repressed in *Trim24*^{-/-} (Table 6), consistent with TRIM24 functions as a co-repressor or -activator of transcription [92-95].

The top five biological functions identified by DAVID analysis [96] of up-regulated genes in *Trim24*^{-/-}, reflecting loss of TRIM24 function as a co-repressor, are protein folding, defense response, RNA metabolism, cell cycle regulation and ER-nuclear signaling (Fig. 20) (Table 6). Genes with decreased expression in *Trim24*^{-/-}, reflecting loss of TRIM24 function as a co-activator, were grouped into biological functions of oxidation/reduction, steroid metabolism, lipid biosynthesis, fatty acid metabolism and steroid biosynthesis (Fig. 20). From this analysis, I hypothesized that the dual role of TRIM24 as a co-repressor and co-activator of transcription provided a link between the misregulated metabolic and inflammatory pathways observed in the phenotype of the *Trim24*^{-/-} mouse. These links led me to pursue a more in-depth analysis involving overlap of this RNA-seq dataset and ChIP-seq to determine TRIM24 specific regulatory roles in metabolism, inflammation, and disease progression (see Chapter IV for more details).

A



B

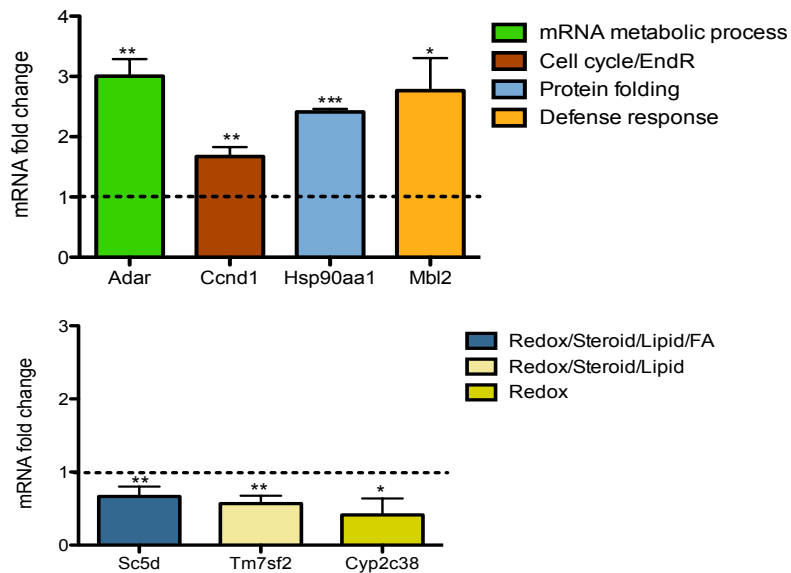


Figure 20. Loss of TRIM24 causes hepatic misregulation of lipid metabolic, stress, and inflammatory related gene expression. **A)** RNA-seq, DAVID Analysis - Top 5 enriched biological functions for up-regulated and down-regulated genes in *Trim24*^{-/-} versus *Trim24*^{+/+} liver at 10 weeks. **B)** Confirmation of misregulated gene from DAVID categories. qRT-PCR fold change with *Trim24*^{+/+}=1 (dashed line), n=3 each (mean ± SD). *p<0.05; **p<0.01; ***p<0.005.

3.6. Lipid metabolism and inflammation are aberrantly regulated in *Trim24*^{-/-} liver.

We assessed key genes associated with biological functions significantly impacted by loss of *Trim24*, as well as aberrantly regulated in human NAFLD and NASH [29, 35]. Hepatic lipases, lipid transport/receptors and pro-inflammatory factor genes were significantly up-regulated, consistent with both the *Trim24*^{-/-} phenotype and human NAFLD to NASH progression (Fig. 21 A,B, Table 7). Inconsistent with human NASH, genes associated with endogenous fatty acid synthesis (i.e. *FASN*, *Scd1* and *Acaca*), were generally and significantly down-regulated (Fig. 21 A,B, Table 7). These inconsistencies between human NAFLD and NASH and the *Trim24*^{-/-} mouse need to be further studied to determine if each model is directly comparable to each other.

Overall, loss of *Trim24* decreased expression of genes involved in a) *de novo* lipid synthesis, b) apolipoproteins and lipid droplet/lipid storage, and c) VLDL transporter and receptors; as well as, increased expression of genes d) encoding lipases and apolipoprotein receptors and e) involved in proinflammation/fibrosis (Fig. 21 A,B). Expression changes and levels of individual genes differ in levels and time of induction, likely reflecting developmental and epigenetic regulation during aging.

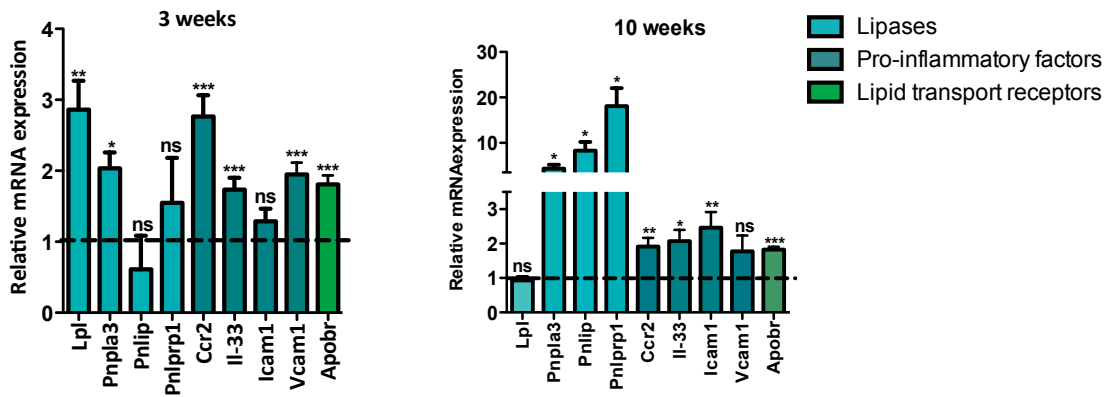
3.7. TRIM24 directly regulates genes in lipid metabolic, inflammation and damage pathways

As a histone reader, TRIM24 does not bind DNA in a sequence-specific manner but rather interacts with specific histone post-translational modifications via a C-terminal PHD/bromodomain [59]. TRIM24 enrichment at chromatin may recruit specific TRIM24-interacting transcription factors, e.g. nuclear receptors RAR α or estrogen receptor, to DNA binding sites [59, 84]. Ingenuity Pathway Analysis [97] of the most significant, differentially expressed, down-regulated gene pathways (by p-value): LPS/IL-1 inhibition of RXR function, FXR/RXR activation, super-pathway of cholesterol biosynthesis, PXR/RXR activation, and maturity onset diabetes of young (MODY) signaling, further supported TRIM24/nuclear receptor regulatory interactions. Thus, we used nuclear receptor DNA binding motifs (GGTCA half-sites) [98, 99] to focus ChIP-PCR analysis (Fig. 22) of TRIM24-chromatin interactions and assess direct regulation of genes altered in *Trim24*^{-/-} liver.

Among the apolipoprotein genes (Fig. 21), we found significant TRIM24 binding at *Apoa1*, *Apoc3* and *Apod1* (Fig. 22). Several *de novo* lipid synthesis genes down-regulated in the *Trim24*^{-/-} liver, such as *Acacb*, were bound by TRIM24 at verified RAR α binding sites [100]. Additionally, TRIM24 bound and directly regulated lipase *Pnpla3*, as well as VLDL transporter *Mttp* and the *Vldlr* gene (Fig. 21). Increased expression of several lipases in *Trim24*^{-/-} liver (Fig. 21) suggests an imbalance in energy use or feedback response to accumulation of lipid [101]. TRIM24 was also enriched at genes, associated with inflammation and liver damage, with significantly altered expression (Figs. 10, 21). Pro-inflammatory factors *Ccr2*, *Icam* and *Il-1a*, as

well as liver damage and apoptosis genes, *Ddit3*, *Bax* and *Casp12*, had TRIM24 enrichment, consistent with changes in gene expression and liver damage in *Trim24*^{-/-}. TRIM24 binding at the RARE/ERE consensus sites of *Apoc3*, at -150, and *Ccr2*, at -100, proved insignificant, reinforcing that not all predicted RARE/ERE sites show TRIM24 recruitment in liver tissue. These studies of TRIM24-chromatin interactions and direct regulation of target gene expression support a significant role for TRIM24 in homeostasis by regulating genes of the lipid metabolic, inflammatory, and apoptotic pathways of the liver.

A



B

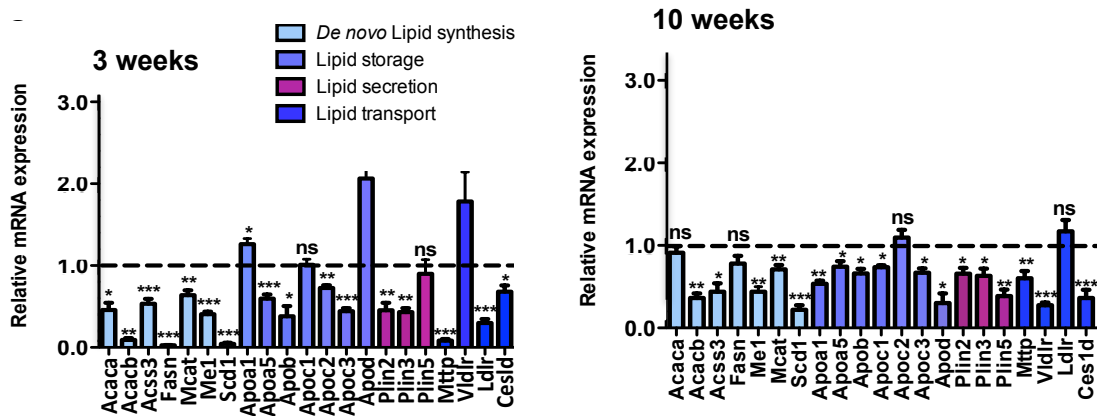


Figure 21. Loss of TRIM24 causes misregulation of inflammatory, stress, and lipid metabolic related gene expression indicative of NAFLD/NASH. A) TG hydrolysis (lipases), pro-inflammation, and lipid transport gene expression at 3 and 10 weeks. B) De novo lipid synthesis, storage, secretion, and transport gene expression at 3 and 10 weeks. (A and B) qRT-PCR fold change with *Trim24*^{+/+}=1 (dashed line), n=3 each (mean ± SD). *p<0.05; **p<0.01; *p<0.005.**

Trim24 ChIP

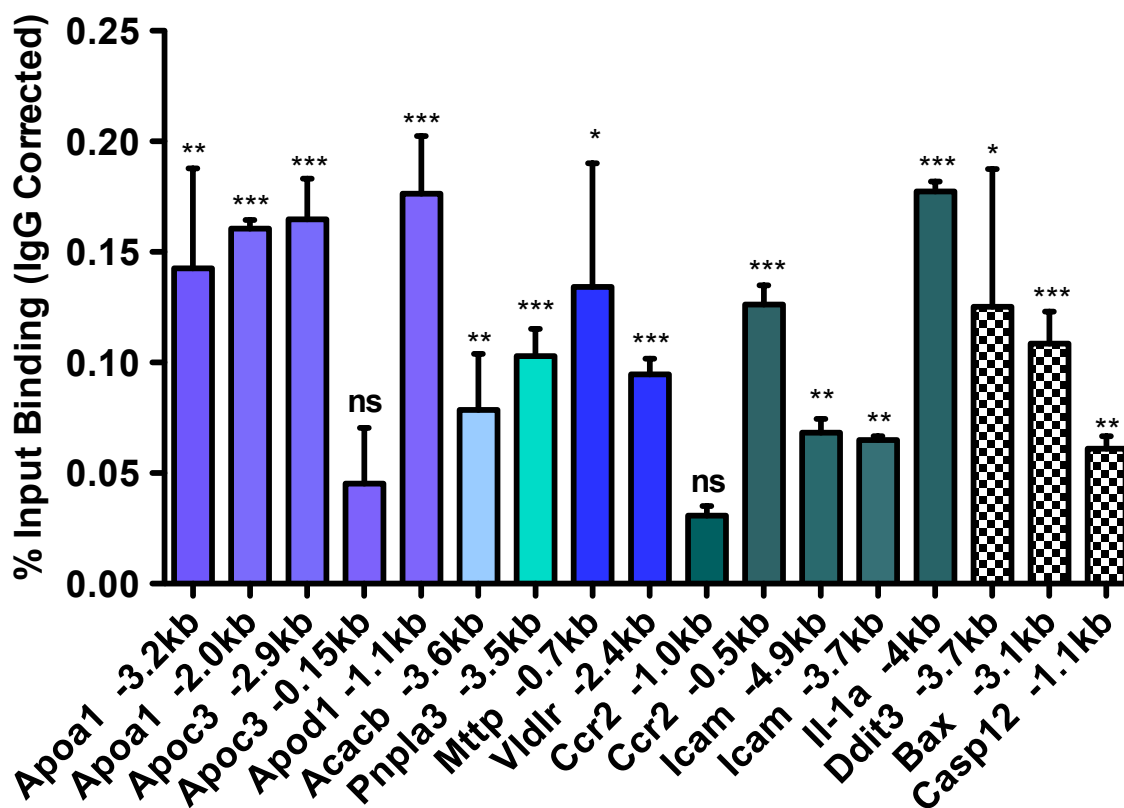


Figure 22. TRIM24 regulates hepatic lipid metabolism, stress and inflammation genes. *Trim24*^{+/+} 2-months liver tissue ChIP: Significant binding by TRIM24: *p<0.05; **p<0.01; ***p<0.001, ****p<0.0001. NS – nonspecific binding. Y-axis: TRIM24 enrichment as % input DNA.

3.8. Discussion.

Altered regulation of hepatic lipid metabolism, accompanied by chronic inflammation, is clearly linked to higher incidence of HCC in humans [85, 102]. Aberrant expression of several key genes in these pathways is associated with progression from NAFLD, where lipid metabolic and regulatory genes are indicated, to NASH, where inflammation is thought to play a major role in driving progression to HCC [103]. Here, we show that histone reader TRIM24 plays a direct role in the regulation of liver fat metabolism and inflammatory processes, prior to tissue damage and fibrosis. Additionally, global expression analyses of the *Trim24*^{-/-} liver unveiled pathways, such as the Unfolded Protein Response and EndR-Nuclear Signaling, closely associated with human NAFLD, inflammatory stress and progression to apoptosis and tissue damage [104]. When *Trim24* expression is completely absent, there is spontaneous development of disease across the spectrum of NAFLD-NASH-HCC, even when *Trim24*^{-/-} mice are fed a normal diet. Mouse models genetically engineered for altered expression of *Sfrp*, *Nemo*, *Pnpla3-Il48M*, *Adiponectin*, *Mttp*, *ApoB* and *ApoC3* genes exhibit this disease progression, but only when stimulated by a high fat diet [101, 103]. Our finding that TRIM24 directly regulates certain of these genes, such as *Pnpla3*, *ApoC3*, and *Mttp*, suggests an epigenetic hierarchy. TRIM24 may be a linchpin in transcription networks that intersect to prevent NAFLD and progression to HCC, due to its ability to serve as either an epigenetic co-repressor or co-activator of nuclear receptors and other transcription regulators [105] [59, 60].

The phenotype of a previous *Trim24* mouse model with an exon 4 (E4) deletion, *Trim24*^{dIE4/dIE4}, suggested that the only significant function of TRIM24 was prevention

of hepatic inflammation, as a co-repressor of retinoid-dependent genes and LTR-driven enhancers [60, 85]. In contrast, although specific inflammatory-associated genes were altered in liver devoid of *Trim24*, we did not see an early or major response of RAR-regulated or retrovirus LTR-regulated genes associated with inflammation (Fig. 23, 24). Rapid development of HCC in the E4-deletion *Trim24*^{dIE4/dIE4} model lacks apparent progression through NAFLD or NASH, and a role for TRIM24 in pathways of lipid/fatty acid/steroid metabolism, oxidation/reduction and ER stress was not apparent, as summarized in Table 8.

Interestingly, alternative start sites of *Trim24* transcription yield native isoforms of *Trim24* lacking E4, as expressed in the *Trim24*^{dIE4/dIE4} mouse [85], and predicted to produce proteins known as TRIM24 variants 1 and 3, which have high similarity to *BRAF* (Variant 1: 84% protein identity, Variant 3: 64% protein identity) (Table 9). Intriguingly, chromosomal translocation and fusion of proto-oncogene *BRAF* and *TRIM24* are reported in specific leukemias [106, 107]. Comparison of the two mouse models of TRIM24 function (Table 8) suggests that inflammation is the major driver that causes liver dysfunction to progress rapidly to HCC but when lipid metabolic pathways are significantly misregulated, prior to inflammation and damage, a more progressive development of HCC occurs. These findings suggest that aggressive limitation of inflammation in human NAFLD patients may subvert or greatly delay development of HCC.

It remains unclear why aberrantly high expression of TRIM24 is associated with multiple human cancers, including HCC [83]; although, in a much smaller cohort of patients, significantly lower than normal levels of TRIM24 is reported [108]. This

discontinuity may be due to TRIM24 functions in hepatic homeostasis with over- or under-expression leading to a regulatory imbalance. Additionally, not all hallmarks of NAFLD and NASH [109] are observed with loss of *Trim24*, although hepatic steatosis, inflammation and fibrosis, with hepatocyte injury and apoptosis, are present. Complete loss of *Trim24* caused a striking decrease in peripheral fat accumulation, along with elevated serum triglycerides and hepatocyte lipid accumulation, characteristics recently associated with NAFLD among nonobese patients [110]. Further study of the *Trim24*^{-/-} mouse and manipulation of diet may offer mechanistic insights as a model of human NAFLD, which may progress to NASH and HCC, among nonobese patients.

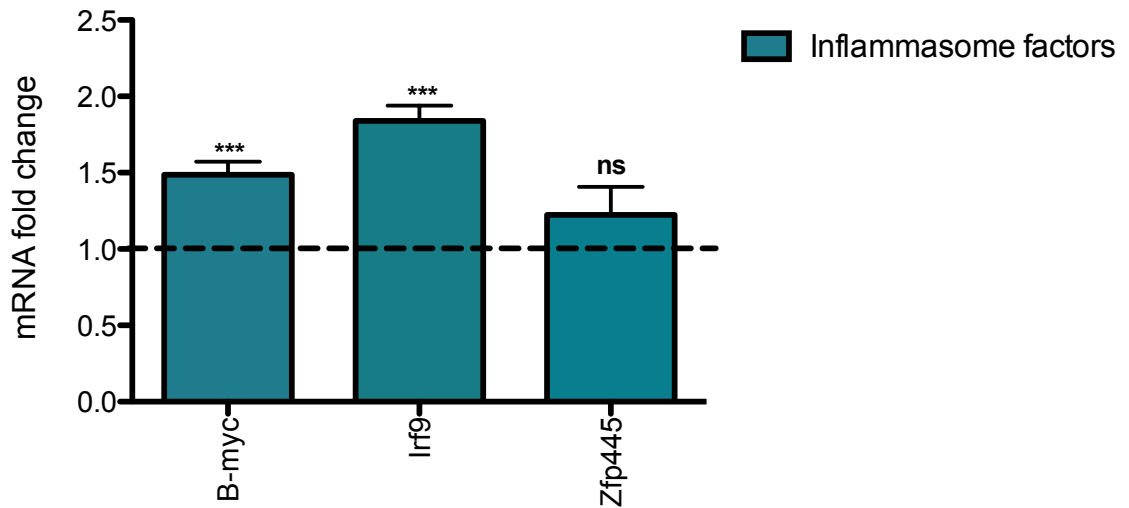


Figure 23. Retro-viral associated gene expression is increased in *Trim24*^{-/-} mice. Genes associated with VL30-retrotransposon viral control show upregulated mRNA expression levels in *Trim24*^{-/-} livers (10 weeks, performed with the same RNA as used in RNA-Seq, all additional samples were age matched) and the data shown represent n=3-5 male liver samples (mean ± SD). Dashed line is *Trim24*^{+/+} gene expression, normalized to 1. mRNA expression levels were normalized to *Hprt*, *p<0.05.

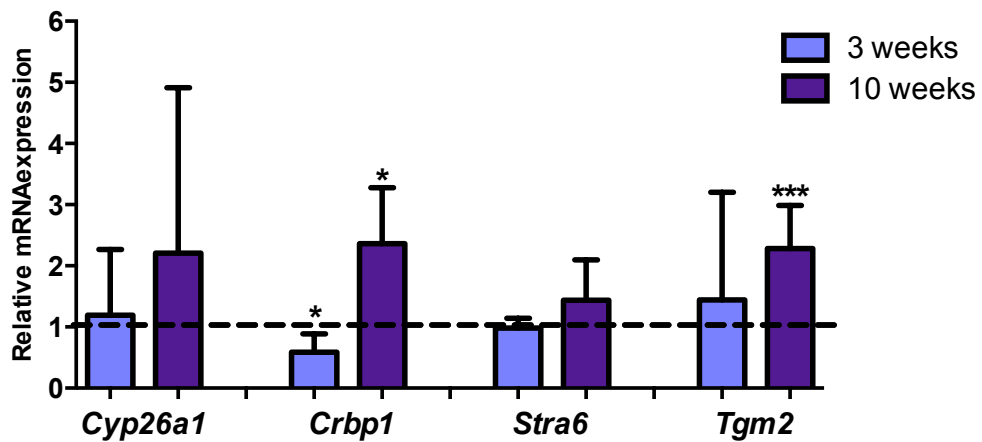


Figure 24. Some retinoid responsive genes are misregulated in *Trim24*^{-/-} livers at 3 and 10 weeks of age. mRNA levels of genes shown to be retinoid responsive show varying levels of differential expression compared to wildtype control. All mRNA expression levels of 3 & 10 week livers were performed represent n=11, n=12 male liver samples, respectively (mean ± SD). All mRNA expression levels were normalized to *Hprt*, *p<0.05; ***p<0.005.

CHAPTER IV

TRIM24 suppresses progressive chronic inflammation and protects from secondary metabolic disorders associated with NASH progression.

4.1. Introduction.

Macrophages throughout the body arise from committed hematopoietic cells in the bone marrow. Macrophage precursors are released from the bone marrow as monocytes and seed into various organs, such as the spleen [111]. As monocytes travel from circulation to specific organs, they differentiate into either macrophages or dendritic cells (DCs), which have a primary function to aid the innate immune response by phagocytosis [112]. Several cell surface markers are available that are positive in macrophages but not DCs, such as F4/80, CD1b, CD18, CD68, and FC receptors. However, it should be kept in mind that since both of these cell types arise from common myeloid progenitor populations, these markers are not completely definitive, but provide the best mode of identification available at present [112]. Based upon location and phenotype, macrophages are divided into sub-populations: osteoclasts (bone), alveolar (lung), histiocytes (connective tissue), and Kupffer cells (liver) [113]. All of these tissue specific macrophages work with DCs to maintain homeostasis. Seminal studies in the 1980's by Mosmann et al. found T helper (Th) cells could be divided into two distinct categories based on their activation and production of either IFN γ (Th1) or IL-4 (Th2) [114]. Mills et al. found that macrophages showed differential activation based upon stimulus with either LPS or IFN γ in mouse models with Th1 or Th2 backgrounds [115]. They found that M1 macrophages produced toxic nitric oxide (NO), while M2 macrophages produced trophic amines. Further studies showed that development of classically activated (M1) and alternatively activated (M2) macrophages was independent of T and B cells and reliant on transforming growth factor-beta (TGF- β) inhibition of induced

nitric oxide synthase (iNOS) [112] [116]. M1 macrophages are activated by the presence of bacteria, protozoa, and viruses and have roles in antitumor immunity. M2 macrophages have anti-inflammatory functions and typically regulate wound healing and fibrosis [117, 118]. Interestingly, M2 macrophages regulate metabolic functions [119] and are induced by peroxisome proliferator activated receptor- γ (PPAR- γ) signaling to maintain adipocyte function, along with glucose and insulin metabolism, in prevention of diabetes and obesity. [119, 120]. In tumorigenesis, M1 macrophages are considered tumor protective, with tumor suppressive roles that antagonize immune-suppressive activities of M2 macrophages. M2 macrophages and other regulatory macrophages (also tumor-associated macrophages) reportedly suppress immune responses to tumor progression and promote tumor growth, invasion, metastasis, and angiogenesis [121-126].

Multiple studies suggest that progression from NAFLD to NASH is accomplished via increased circulating NEFAs, adipokines, hepatocellular damage, oxidative damage, and endoplasmic reticulum stress, all of which are associated with aberrant inflammatory processes [127-129]. The progression of HCC is also known to be associated with these processes, which are dependent upon KCs that are primed to promote tumorigenesis [130]. However, little is known about the causative mechanisms and specific cell populations in the liver underlying progression from NAFLD to NASH and ultimately HCC.

Regulation of glucose metabolism and insulin sensitivity is a key component of healthy metabolic function. The endpoint of glucose and insulin homeostasis is to provide usable energy in the form of sugar and ATP to the brain through a complex,

highly regulated network that manages the influx and efflux of glucose between the pancreas, liver, muscle, and brain [131]. Glucose can be produced from 3 sources (apart from the ingested form): fat, proteins, and glycogen [131]. Adipose tissue serves as the main reserve for glucose and, ultimately, energy in the body. Proteins are the substrates for gluconeogenesis, which is the process by which proteins are broken down into glucose mainly by the liver and the kidneys (only during prolonged fasting and acidosis) [131-133]. More specifically, the liver, along with muscle, is instrumental in converting glucose taken from the bloodstream to glycogen, through glycogen synthesis. Briefly, during intake and digestion of a meal, glucose levels in the blood rise, causing secretion of insulin by beta cells of the pancreas. As glucose enters the liver via the portal vein and into hepatocytes, the secreted insulin activates glycogen synthase. A protein known as glycogenin, the substrate for glycogen synthase, has the ability to bind and produce short chains of glucose. Once there are 10 or more glucose residues in the chain, proglycogen and glycogen synthase elongate the chain and transfer a free glucose to the ends of the chain. Uridine diphosphate (UDP) is needed as the energy source for the reaction and drive the reaction leading to the final product of glycogen [131].

During fasting, the liver converts stores of glycogen to glucose in a process known as glycogenolysis. First, glycogen is converted to glucose-6-phosphate (G6P) by glycogen phosphorylase. Glucose-6-phosphatase then converts G6P to free glucose (Fig. 25). Following extended periods of fasting (>8 hours), the liver gradually reverts to gluconeogenesis to replace glycogenolysis [131]. This turnover is accomplished by a signaling cascade set in motion by a decrease in hepatic

glycogen, which in turn leads to a decrease in blood glucose and insulin levels. The pancreas then increases glucagon secretion, mobilization of gluconeogenesis precursors, free fatty acids (alternative forms of energy), increases intracellular production of cyclic adenosine monophosphate (cAMP) and signals to increase hepatic gluconeogenesis. Conversely, when hepatic glucose levels have reached appropriate levels, insulin is secreted from the pancreas, causing a marked decline in cAMP levels, hepatic glucose output, and inhibition of glucagon secretion [134]. For these processes to occur, glucose, due to its hydrophilic nature, relies on glucose transporters for entry into the cell (Table 10). There are two types of glucose transporters: the sodium-dependent glucose transporter (SGLT) family and the glucose transporter (GLUT) family. SGLT family members transport against the concentration gradient via a sodium electrochemical gradient, while GLUT family members utilize facultative transport [135]. The glucose transporter or solute carrier 2A (SLC2A) proteins are divided as follows: Class I (SCL2A1-4, 14), II (SCL2A 5, 7, 9, 11), III (SCL2A 6,8,10,12,13) based upon their action in various organs and dependence on insulin [136]. Once glucose has entered the cytosol via the glucose transporter, glycolysis must be utilized in order to convert 1 mole of glucose into 2 moles of ATP, 2 moles of NADH, and 2 moles of pyruvate (Fig. 25) (glycolysis and TCA cycle). Under aerobic conditions, pyruvate is then converted to acetyl CoA (substrate of mitochondria to generate ATP) via the tricarboxylic acid (TCA) cycle and nets 36 moles of ATP for every mole of glucose. Anaerobic conditions force the cell to solely rely on glycolysis, where pyruvate is converted to lactate, which in turn produces the factors needed for glycolysis.

It is well established that dramatic shifts in metabolism are associated with cancer incidence [137]. Due to massive increases in energy expenditure by cancer cells, shifts in glucose-dependent metabolic activity toward increased aerobic glycolysis are common in invasive cancers [138]. The ability of cancer cells to alter metabolic activity provides a critical source of increased energy for processes that are hallmarks of cancer progression: uninhibited proliferation through evasion of growth inhibitory signals, migration, angiogenesis and vascularization, and metastasis of cells to distant target organs [139]. While oncogenes, tumor suppressors and metabolic transformation in cancer cells are recognized as key components in potential therapeutic strategies, little is known regarding how these linked processes relate to one another.

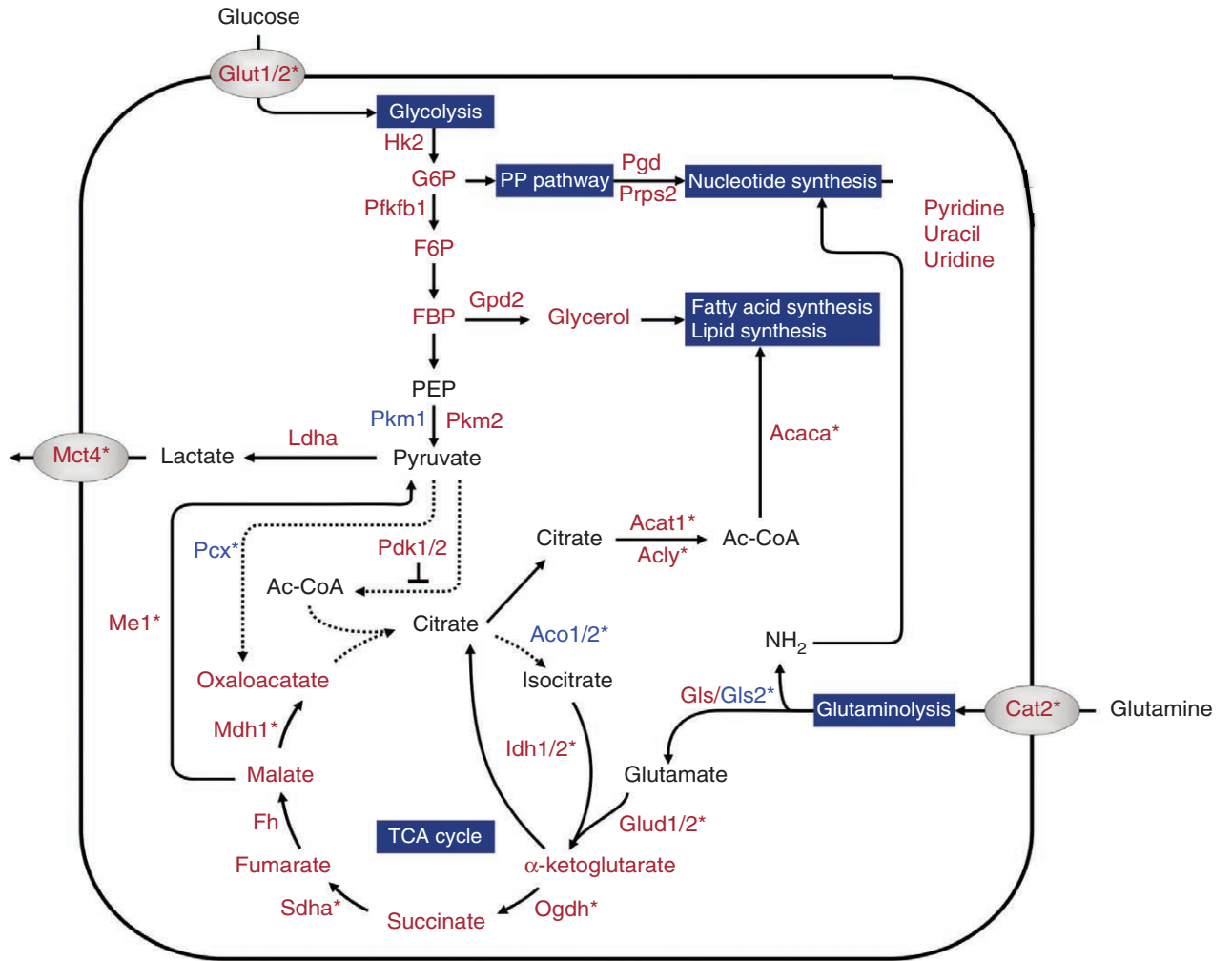


Figure 25. Glycolysis, TCA cycle, and Fatty Acid Regulation.
 Modified from *Nature Genetics* 2014, 46, 24-32 [140]

Class	GLUT isoform	Hepatic expression	Subcellular expression/localisation	Protein/mRNA
Class I	GLUT1	Yes	Sinusoidal membrane of hepatocytes, protein restricted to hepatocytes proximal to the hepatic venule, also expressed on endothelial cells, kupffer cells and cholangiocytes; hepatocyte expression in HCC	Both
	GLUT2	Yes	Hepatocytes	Protein
	GLUT3	Yes	Hepatocytes, bile canalicular membrane more enriched than sinusoidal membrane	Protein
	GLUT4	Yes	Stellate cells	mRNA
	GLUT14	No		
Class II	GLUT5	Yes	Normal liver tissue hepatocytes (cytoplasmic)	Both
	GLUT7	No		
	GLUT9	Yes	Majority of expression in hepatocytes of normal liver and HCC with cytoplasmic expression in pericentral areas	Protein
Class III	GLUT11	Yes		mRNA
	GLUT6	Yes		mRNA
	GLUT8	Yes	Perivenous hepatocytes	Both
	GLUT10	Yes		mRNA
	GLUT12	Yes		mRNA
	GLUT13	No		

Table 10. Glucose transporter genes expressed in the liver. Modified from *World J Gastroenterol.* 2012;18(46):6771-81 [136].

Metabolic syndrome (MS) is a growing problem in the Western world, and is commonly defined by: dyslipidemia manifested as hypertriglycemia, glucose intolerance (fasting hyperglycemia), insulin resistance, and central obesity [141]. The equivalent of MS in the liver is manifested in NAFLD, NASH, and HCC. As discussed in the first chapters of this work, our mouse model of *Trim24* deletion, which completely lacks *Trim24* expression, showed different results from the original deletion of exon 4 of *Trim24* [85, 105]. We discovered a previously unknown role for TRIM24 in hepatic homeostasis, as an epigenetic regulator of oxidation/reduction, lipid, steroid and fatty acid metabolism, as well as unfolded protein response and ER-stress and inflammatory pathways; all without manipulation of dietary fat or chemical induction. This mouse also shows hallmarks and progression of NAFLD, NASH, and HCC by misregulation of key metabolic and inflammatory related genes in the liver. However, key components of secondary metabolic syndrome such as aberrant glucose metabolism and insulin sensitivity, accompanied by central obesity were not defined in this model.

I reasoned that it would be important to not only test the specific immune cell populations that were regulated by TRIM24 in NAFLD and NASH progression, but to also determine if a metabolic link, possibly related to this progression, was “setting the stage” for transformation of normal hepatic cells to cancer. Therefore, in this chapter, I focus on establishing the status of aberrant inflammation and metabolism in the *Trim24*^{-/-} mouse model.

4.2. Germline deletion of TRIM24 causes an increase in hepatic macrophage populations.

Since previous studies detailed in the first portion of this work, showed that germline deletion of *Trim24* causes dysregulation of genes related to NAFLD and NASH progression, I utilized this same model in an effort to understand the effects of TRIM24 loss on specific, hepatic immune populations and their contributions to the disease progression of this mouse model. Utilizing immunohistochemistry for F4/80, I found that hepatic macrophage populations (dark blue staining marked by arrow) were increased in comparison to control at 2 months (10 weeks of age) (Fig. 26). To further determine if this increase in hepatic macrophage populations was significant, I perfused and isolated hepatic immune cells and analyzed by Flow Cytometry using the cell surface markers listed in Table 14. I found that hepatic macrophage (CD45+, F4/80+) populations were significantly increased in *Trim24*^{-/-} liver, suggesting possible macrophage infiltration (Fig. 27). Additionally, though not significant, myeloid lineage (CD45+, CD11b+) populations were increased in *Trim24*^{-/-} liver (Fig. 28). These findings suggest that *Trim24* may have an immuno-protective role in the liver to regulate macrophage and myeloid populations.

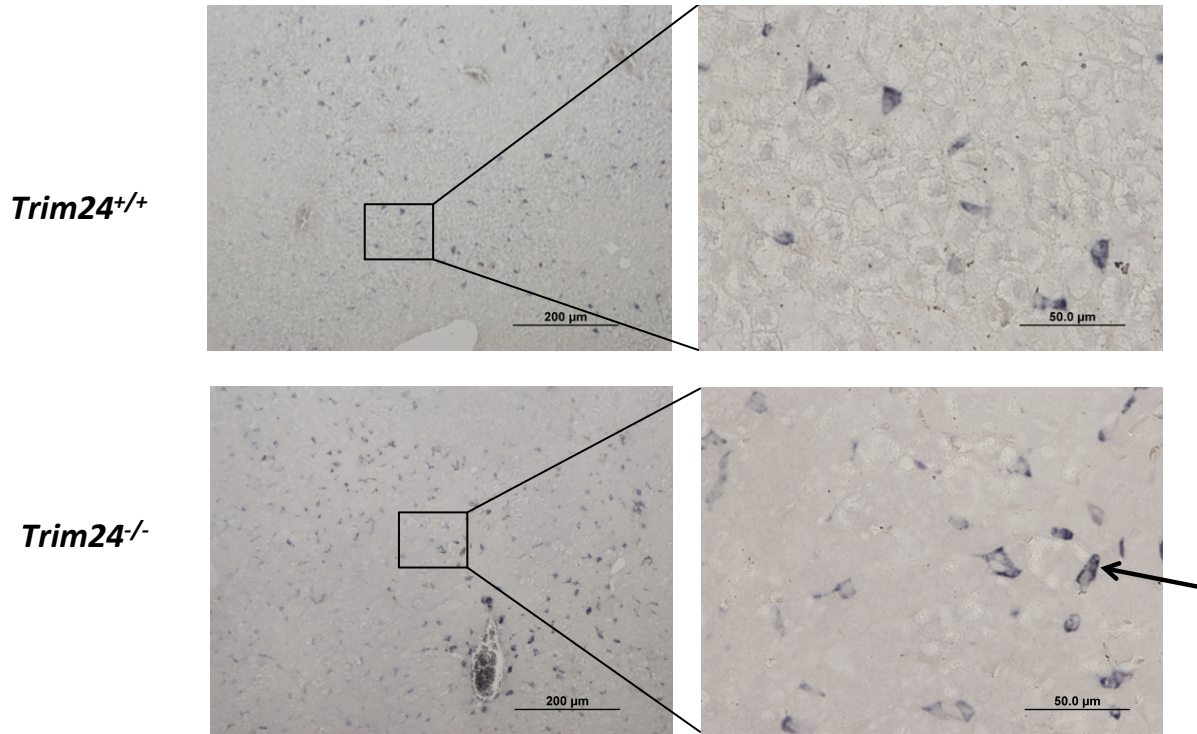


Figure 26. Hepatic macrophages are increased in *Trim24*^{-/-} liver. IHC for F4/80, cell surface marker for macrophages is shown by positive blue staining in liver sections. *Trim24*^{+/+} and *Trim24*^{-/-} liver are shown at 10x: 200 μm; 40x: 50 μm. Arrow indicates positive F4/80 staining for macrophages. N=3 for both genotypes, 10 weeks of age.

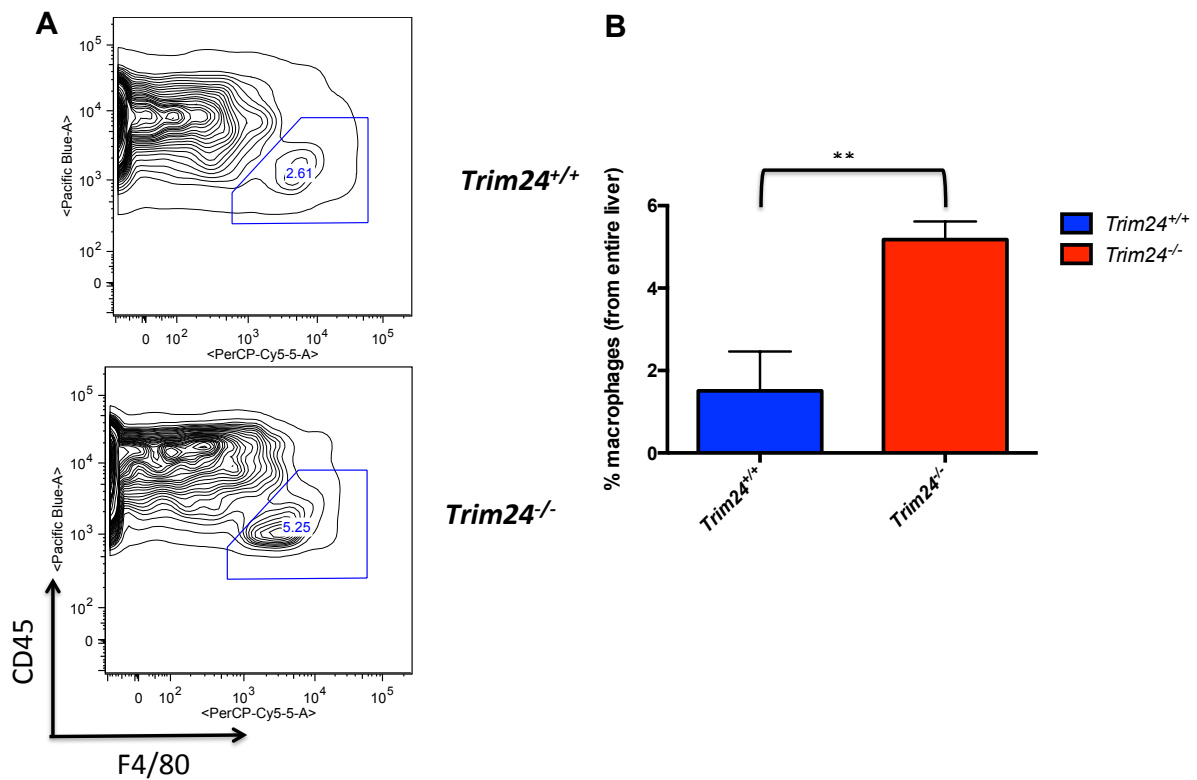


Figure 27. Hepatic macrophages are increased in *Trim24*^{-/-} liver. A) Flow cytometry using cell surface markers for CD45 (Pacific Blue) and F4/80 (PerCP-Cy5-5-A) showed an increase in hepatic macrophages in *Trim24*^{-/-} liver compared to control. **B)** Quantification of the cell populations in A). 10 weeks of age, isolated from whole liver. N=3 per genotype. **p<0.01.

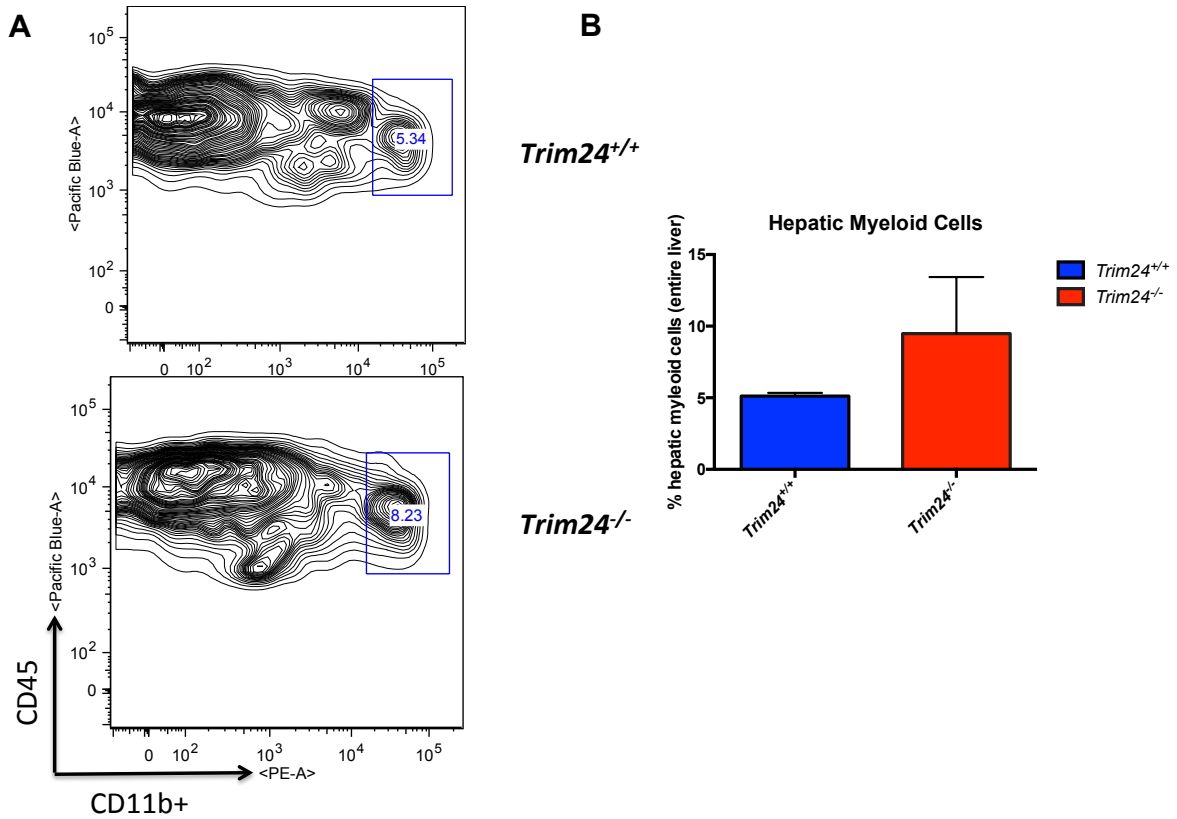


Figure 28. Hepatic myeloid cells are increased in *Trim24^{-/-}* liver. **A) Flow cytometry using cell surface markers for CD45 (Pacific Blue) and Cd11b (PE), showed an increase in hepatic hepatic myeloid populations in *Trim24^{-/-}* liver compared to control. **B)** Quantification of the cell populations in A). 10 weeks of age, isolated from whole liver. N=3 per genotype.**

4.3. Intersection of RNA-seq and ChIP-seq analysis reveals differentially expressed TRIM24 bound metabolic and inflammatory target genes

While the results of the phenotypic analysis of both the germline and liver-specific deletion pointed to TRIM24 as a potential regulator of both metabolic and inflammatory processes, I needed further evidence of a direct regulatory function of TRIM24. Thus, I mined unpublished liver RNA-seq (male and female, 10 weeks, *Trim24*^{+/+} and *Trim24*^{-/-}) and TRIM24-ChIP-seq (liver; pooled genders, 10 weeks, *Trim24*^{+/+}) to determine the transcriptional activity of TRIM24 in early disease development (2 months of age). I chose this timepoint due to the fact that early changes in the liver are likely critical catalysts for disease progression. Intersection of the RNA-seq and TRIM24-ChIP-seq datasets revealed direct TRIM24 gene targets that could be divided into categories of repressed or activated by TRIM24. Functional annotation analyses revealed that TRIM24-repressed genes are primarily involved in inflammatory and oxidative stress response, whereas genes activated by TRIM24 are involved in lipid and glucose metabolism (these categories will be discussed later in the chapter) (Figs. 29-30, Table 11). The first category of TRIM24 repressed genes, NRF2-mediated Oxidative Stress Response, includes genes such as *Jun*, *JunD*, *JunB*, and *Nrf2* (*Nfe2l2*). The oxidative stress response causes not only activation of genes associated with acute phase inflammatory response (such as *Nrf2*) as well as proto-oncogenic families such as the Jun family. Upon loss of *Trim24*, loss of repression of these genes has been shown to be integral to the progression of HCC [142] [143].

The Aryl Hydrocarbon Receptor (AHR) Signaling/ATM Signaling categories include genes such as *Jun*, *Cdkn1a*, and *Nrf2*. AHRs have been shown to be integral in protection against toxins, immune system defects and homeostasis of hematopoiesis in AHR knockout mouse models [144]. Additionally, ATM signaling, especially in the case of *Cdkn1a* (*p21*) is implicated in misregulation of cell cycle homeostasis, leading to genomic instability, cell damage, and in the case of the liver, chronic damage if not tightly regulated [145]. The Acute Phase Response Signaling category includes genes such as *Jun*, *Saa1*, and *Saa2*. The first mounted response of the immune system is the acute phase response, which includes phagocytosis of foreign material by macrophages [146]. *Saa1/2* (serum amyloid A) are associated with inflammatory acute phase response and secreted primarily by hepatocytes [147]. Additional studies have linked SAA proteins to stimulation of monocytes and macrophage misregulated lipid metabolism [147, 148]. Finally, the UVA-Induced MAPK Signaling category includes genes such as *Jun* and *Parp12*. *Parp12* has been shown to be associated with increase cellular damage and DNA injury [149]. Taken together, these changes are consistent with increased inflammation and damage observed in NAFLD, NASH, and HCC progression.

The genes that are most significantly misregulated and bound by TRIM24 are involved in inflammatory/oxidative stress response pathways, I found that *Nrf2* and *Saa1* were significantly bound by TRIM24 and up-regulated upon loss of TRIM24. TRIM24 enrichment at these gene promoters was validated by ChIP-qPCR, thus providing evidence of direct regulation of these genes by TRIM24 (Fig. 31). While both binding levels were significant, *Nrf2* is the most significantly regulated gene by

TRIM24, suggesting that misregulation of *Nrf2* expression is the most likely contributing to a combination effect that leads to the phenotype evident in the *Trim24*^{-/-} mouse liver. Thus, while *Nrf2* misregulation is a key factor in disease progression, loss of *Trim24* is the overall driver of the changes that are occurring in the mouse model, as evident by both RNA- and CHIP-seq analyses.

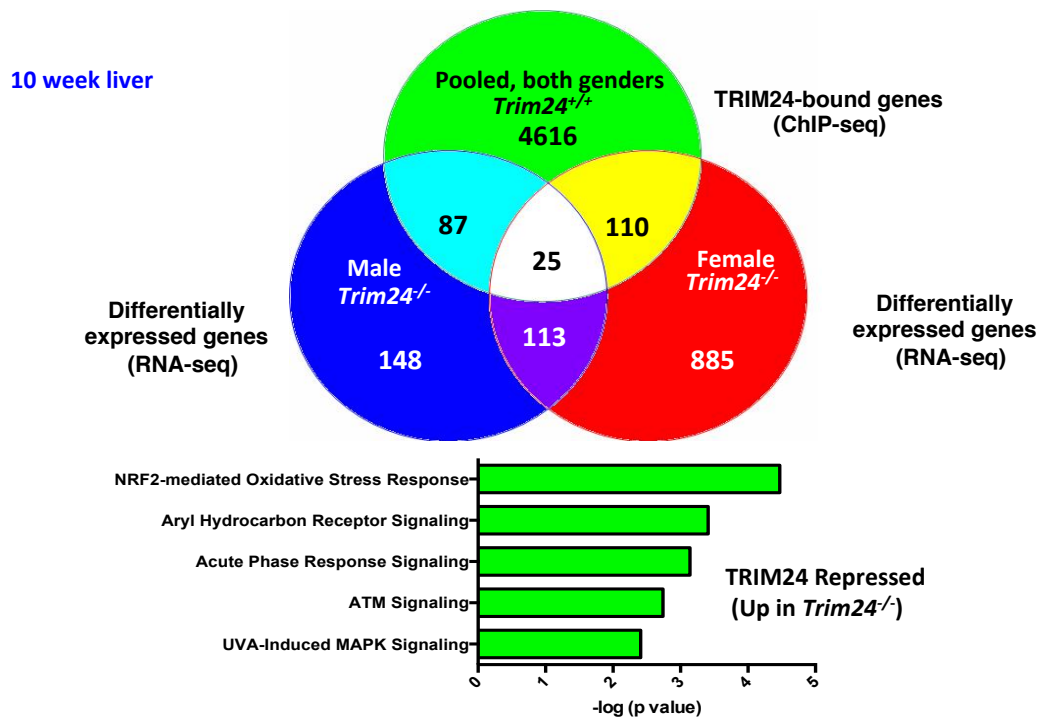


Figure 29. Integrated RNA- and ChIP-seq and identification of TRIM24 bound, differentially expressed gene targets that are repressed by TRIM24. A) Venn diagram of overlapping 10 week male and female *Trim24*^{-/-} liver RNA-seqs with *Trim24*^{+/+} liver pooled gender ChIP-seq. **B)** IPA analysis of top differentially expressed TRIM24 bound gene pathways.

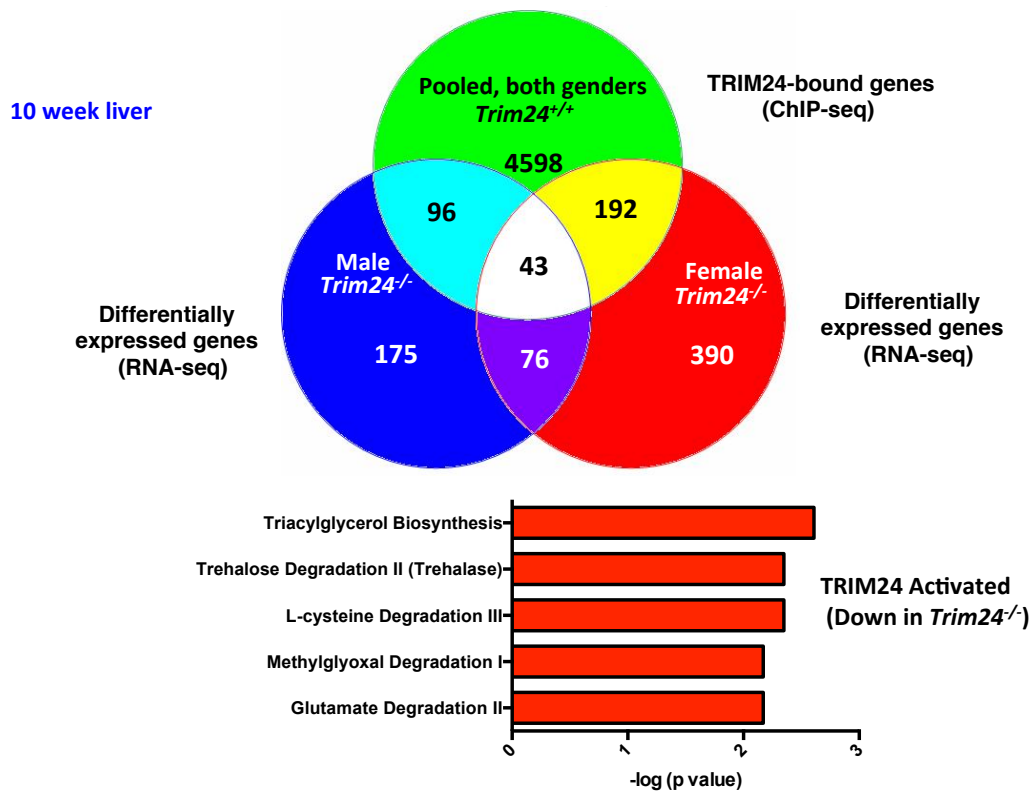


Figure 30. Integrated RNA- and ChIP-seq and identification of TRIM24 bound, differentially expressed gene targets that are activated by TRIM24. A) Venn diagram of overlapping 10 week male and female *Trim24^{-/-}* liver RNA-seqs with *Trim24^{+/+}* liver pooled gender ChIP-seq. **B)** IPA analysis of top differentially expressed TRIM24 bound gene pathways.

IPA Pathway – TRIM24 repressed genes	Genes
NRF2-mediated Oxidative Stress Response	<i>Jun, JunD, JunB, Nfe2l2</i>
Aryl Hydrocarbon Receptor Signaling	<i>Jun, Cdkn1a, Nfe2l2</i>
Acute Phase Response Signaling	<i>Jun, Saa1, Saa2</i>
ATM Signaling	<i>Jun, Cdkn1a</i>
UVA-Induced MAPK Signaling	<i>Jun, Parp12</i>

IPA Pathway – TRIM24 activated genes	Genes
Triacylglycerol Biosynthesis	<i>Lpin1, Lpin2</i>
Trehalose Degradation II (Trehalase)	<i>Gck</i>
L-cysteine Degradation III	<i>Got1</i>
Methylglyoxal Degradation I	<i>Glo1</i>
Glutamate Degradation II	<i>Got1</i>

Table 11. Top 5 IPA categories and gene targets from integration of RNA- and CHIP-seq in mouse liver. A) TRIM24 activated pathways are mainly concentrated in oxidative stress and inflammatory related (acute phase response) pathways. **B)** TRIM24 repressed pathways are mainly concentrated in lipid and glucose metabolic pathways. 10 week male and female *Trim24*^{-/-} liver RNA-seqs with *Trim24*^{+/+} liver pooled gender CHIP-seq.

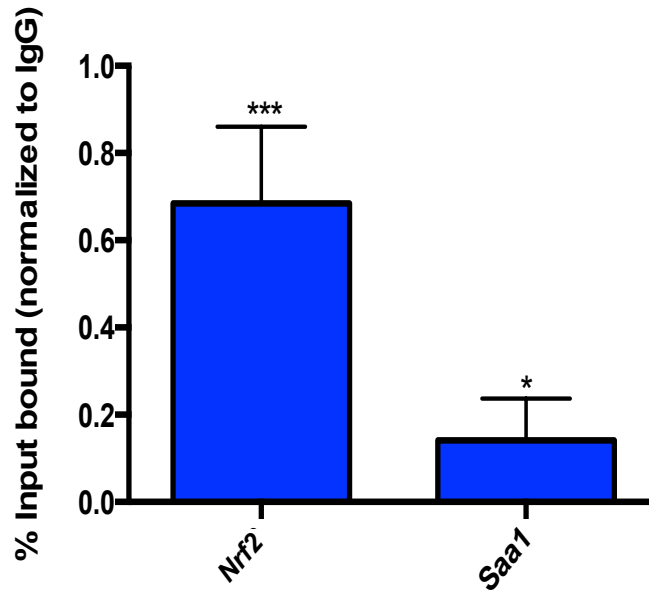


Figure 31. TRIM24 binds oxidative stress response and inflammatory related genes in the liver. *Trim24*^{+/+} 2-month liver tissue ChIP: Significant binding by TRIM24: N>4 *p<0.05; ***p<0.001. Significance is based upon comparison to non-specific binding control. Male and female liver samples were pooled for this analysis. Y-axis: TRIM24 enrichment as % input DNA.

4.4. *Trim24*^{-/-} mice exhibit increased glucose metabolism and insulin sensitivity

As mentioned previously, secondary metabolic disorders, such as insulin resistance and diabetes, frequently accompany human NAFLD and NASH progression. In order to determine if loss of *Trim24* recapitulates this phenotype, I performed glucose tolerance (GTT) and insulin tolerance (ITT) tests on 2, 4, and 6 month old mice (Fig 32). Interestingly, while mice exhibit misregulation of hepatic lipid metabolic genes as early as 10 weeks (2 months) of age, they do not exhibit signs of diabetes. In fact, GTT and ITT test results show that both male and female *Trim24*^{-/-} mice metabolize glucose at a faster rate and are more sensitive to insulin than their wild-type counterparts over a time-course of age, which becomes more significant as the disease progresses (Figs. 33-34). Gene expression of glucose transporters and insulin receptor substrates that are typically misregulated in metabolic disease (*Irs* 1/2 levels are decreased, glucose transporter levels are increased) showed an increase in expression of *Irs1* (not significant), but no changes in *Irs2* or *Glut2* expression (data not shown). Gene expression levels of specific, key components of hepatic glycolysis were decreased in *Trim24*^{-/-} liver compared to control (Fig. 35). I further tested the livers collected from fasting *Trim24*^{+/+} and *Trim24*^{-/-} mice that were tested in GTT and ITT experiments for metabolism of glycogen by Periodic Acid Schiff (PAS) staining. PAS staining detects polysaccharides such as glycogen by breaking down the components of the sugars to produce aldehydes that react with Schiff's reagent to produce a purple-magenta color. Upon staining, I found that as the disease progressed, *Trim24*^{-/-} liver showed

less hepatic glycogen compared to control (arrows, Fig. 36). These results suggest that *Trim24* expression may be instrumental in keeping hepatic glycogen storage levels stable as a source of easily convertible energy for the body. Taken together, these metabolic and gene expression studies confirm that while glucose metabolism, insulin sensitivity, and glycogen storage are aberrant upon loss of *Trim24*, diabetes does not occur.

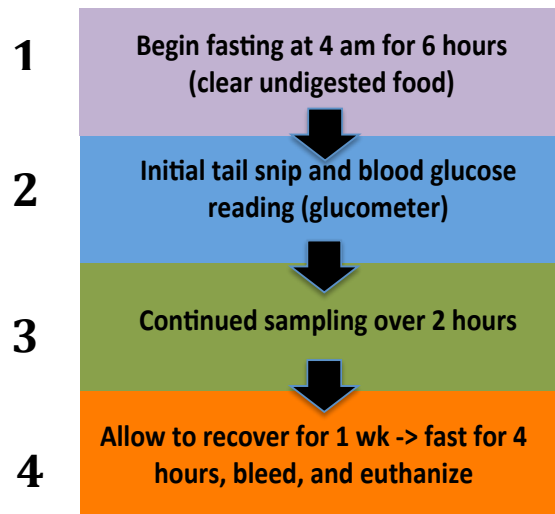
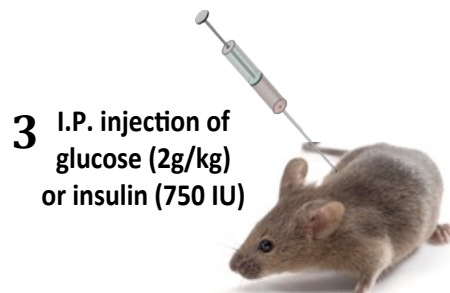


Figure 32. Workflow of glucose and insulin tolerance tests (GTT/ITT). **1)** Mice were fasted for 6 hours from 4 a.m. – 10 a.m. to clear undigested food. Weight was recorded and glucose/insulin was calculated based upon body weight just prior to beginning the testing period. **2)** An initial tail snip and blood glucose reading were taken to establish a baseline reading. **3)** Mice were injected interperitoneally (I.P.) with either glucose or insulin and sampled at 15, 30, 60, and 120 minutes following injection. **4)** After the final reading, mice were allowed to recover for a week before the reciprocal test was performed. Another week of recovery was allowed prior to serum/plasma collection, euthanasia and harvesting.

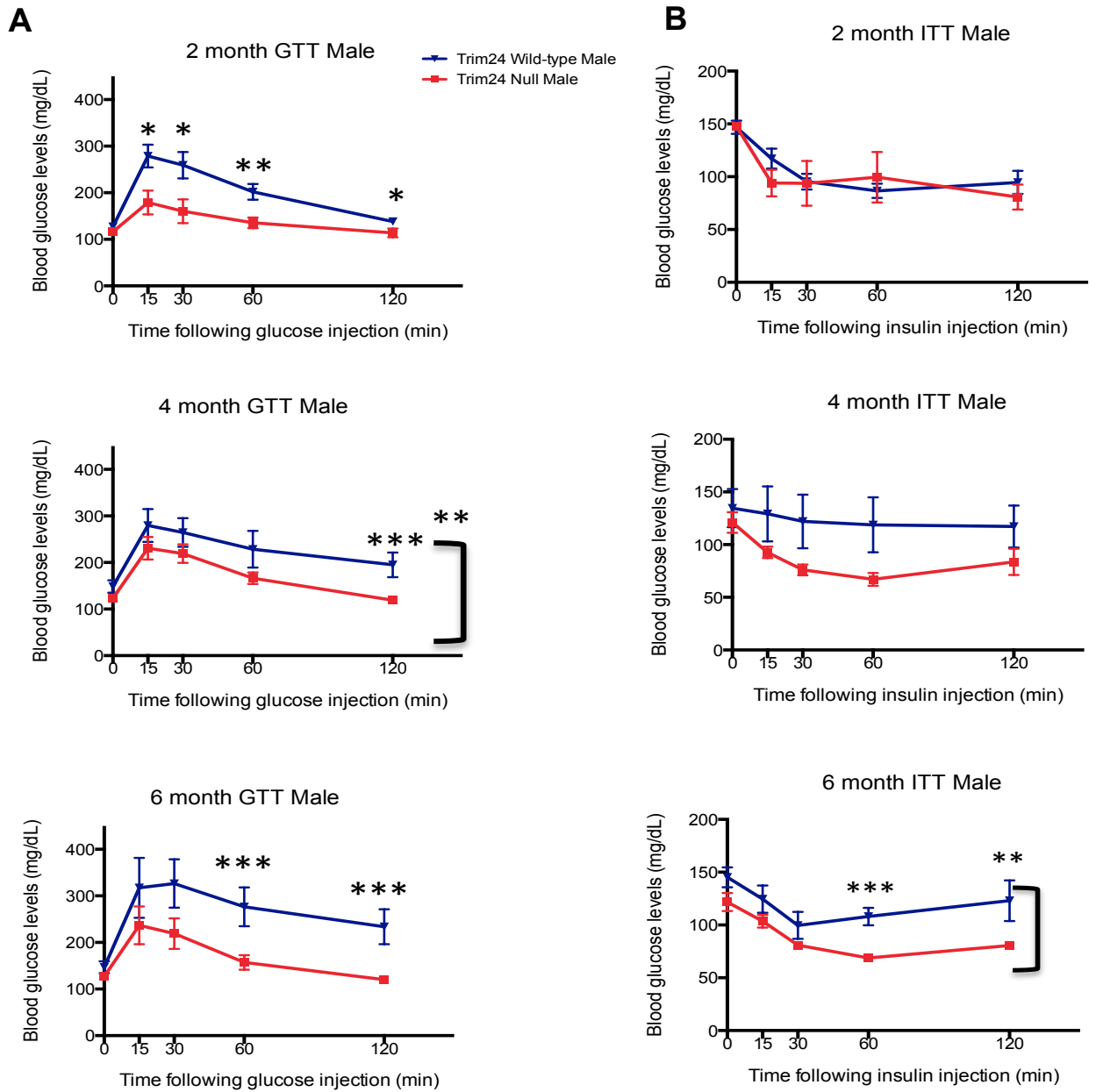


Figure 33. Glucose metabolism and insulin sensitivity increases in male 2, 4, and 6 month *Trim24*^{-/-} mice. **A)** Glucose tolerance tests were performed over a two hour time period, following six hours of fasting. The Y-axis represents blood glucose levels following glucose injection (mg/dL) and the X-axis represents time following glucose injection (min). **B)** Insulin tolerance tests were performed over a two hour time period, following six hours of fasting. The Y-axis represents blood glucose levels following insulin injection (mg/dL) and the X-axis represents time following insulin injection (min). N>10. Mean \pm SD. *p<0.05, **p<0.01, ***p<0.001.

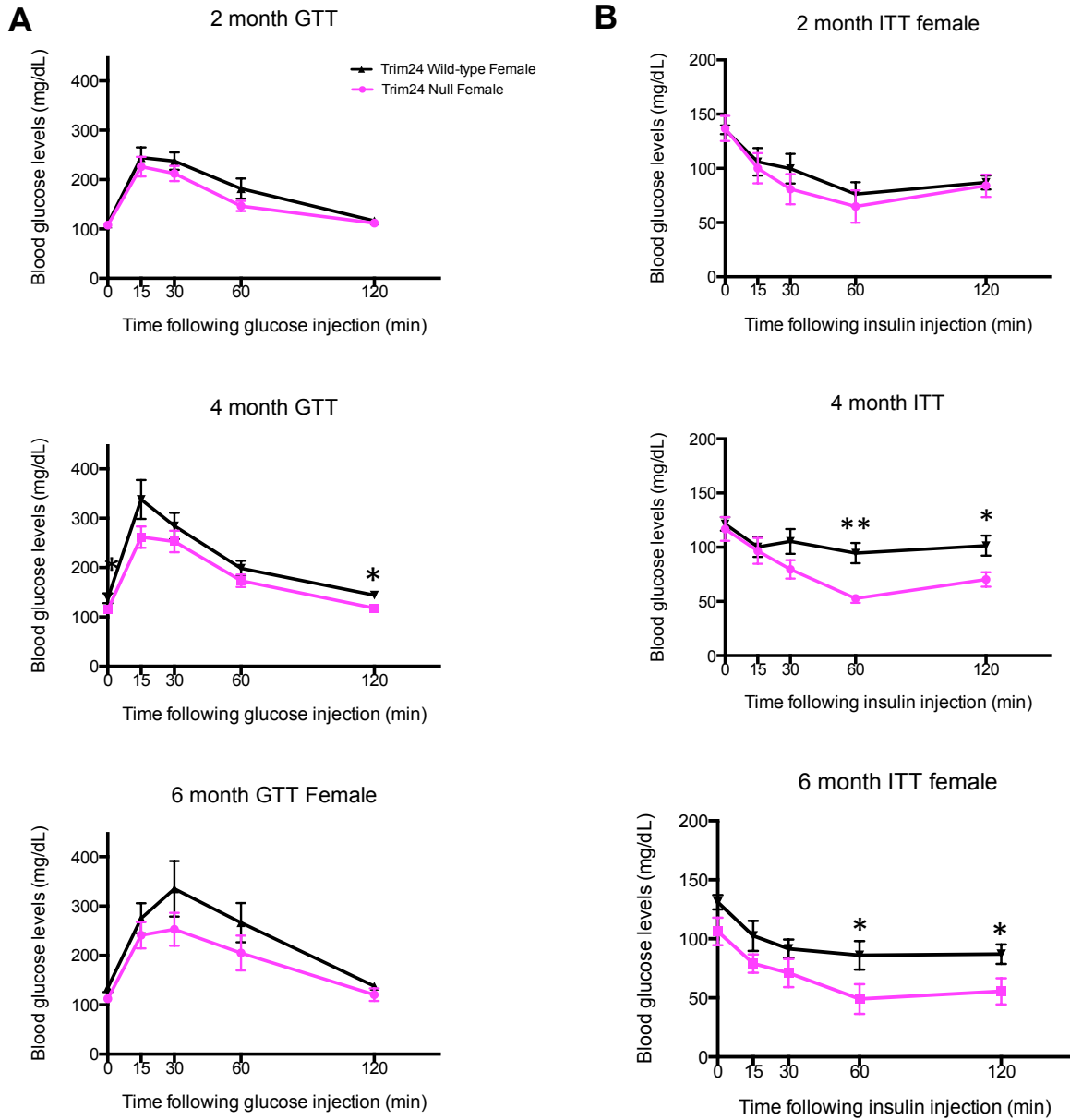


Figure 34. Glucose metabolism is relatively unchanged and insulin sensitivity increases in female 2, 4, and 6 month *Trim24^{-/-}* mice. A) Glucose tolerance tests were performed over a two hour time period, following six hours of fasting. The Y-axis represents blood glucose levels following glucose injection (mg/dL) and the X-axis represents time following glucose injection (min). N>10. Mean \pm SD. * p <0.05. B) Insulin tolerance tests were performed over a two hour time period, following six hours of fasting. The Y-axis represents blood glucose levels following insulin injection (mg/dL) and the X-axis represents time following insulin injection (min). N>10. Mean \pm SD. * p <0.05, ** p <0.01.

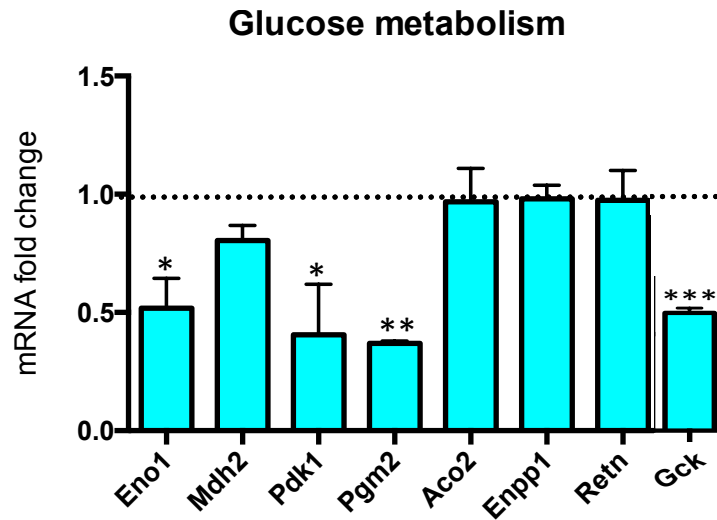


Figure 35. Hepatic gene expression levels of glycolysis related factors are decreased upon loss of *Trim24* (2 months of age). mRNA levels of glucose metabolism genes show varying levels of differential expression compared to wildtype control (dotted line). All mRNA expression levels of 10 week livers were performed represent n=3 liver samples, respectively (mean \pm SD). All mRNA expression levels were normalized to *Hprt*, *p<0.05; **p<0.01, ***0.001.

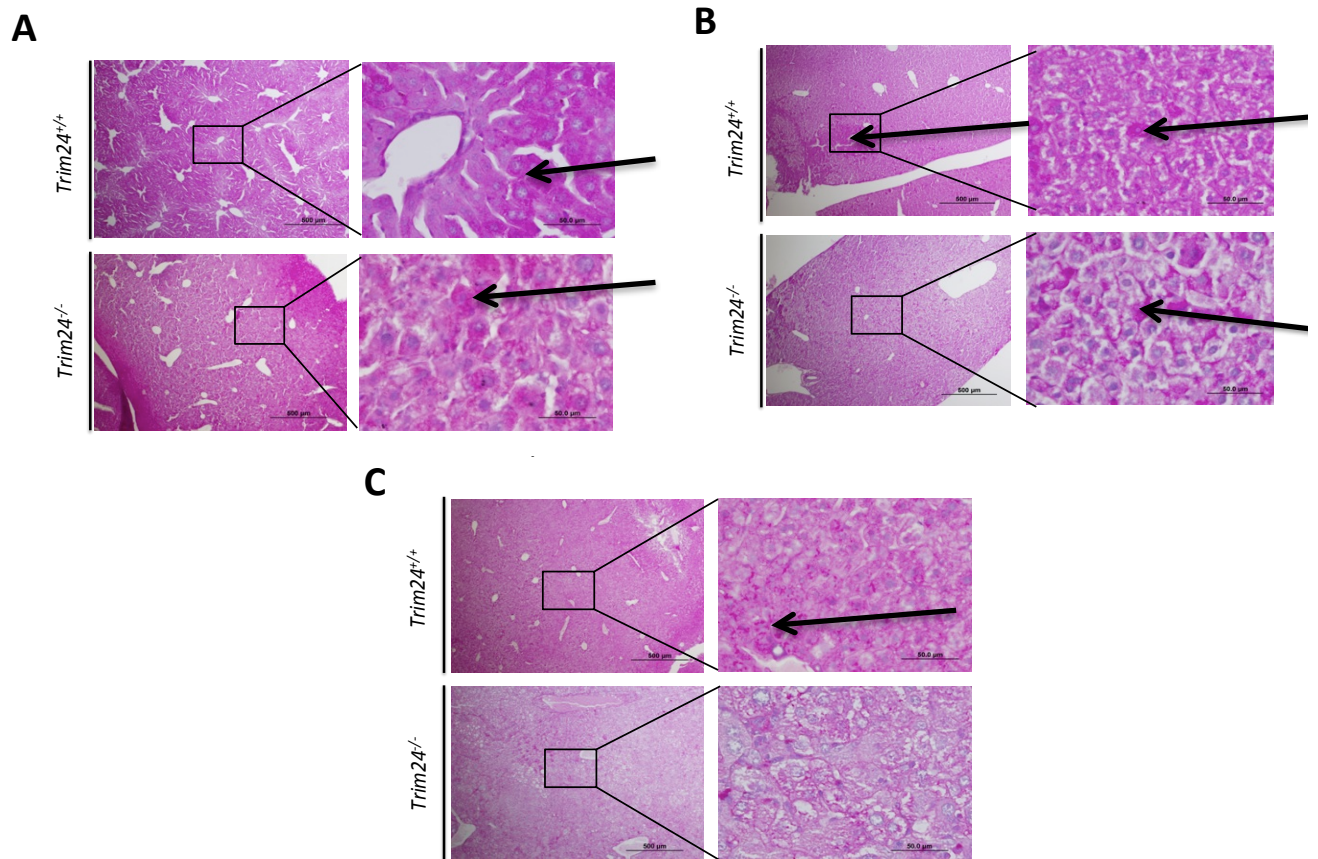


Figure 36. Loss of TRIM24 leads to decreased glycogen metabolism during aging. PAS staining of aging *Trim24*^{-/-} compared to *Trim24*^{+/+} liver at **A)** 10 weeks, **B)** 4 months, **and C)** Aging (>7 months). Bar: 4x: 500 μm; 40x: 50 μm. Arrows indicate dark pink staining = positive glycogen staining.

4.5. Loss of TRIM24 causes a decrease in visceral body fat

The storage of lipid is necessary to serve as an alternative energy source, but excess stores of lipid can cause a myriad of disorders such as metabolic syndrome and NAFLD. The majority of patients that present with NAFLD or NASH are obese and diabetic, however a subset of patients is lean and otherwise healthy [38]. Given the results obtained by testing glucose, insulin, and glycogen metabolism, I reasoned that *Trim24*^{-/-} mice are likely to be lean. To measure the amount of visceral white fat in our mice (as a comparison to human disease), I weighed the mice and recorded total body and visceral abdominal white fat weights. From these analyses, I found that *Trim24*^{-/-} mice have lower overall body weight and visceral fat weights in both genders at 2, 4, and 6 months of age (Fig. 37-38). There were no appreciable differences in liver index at these timepoints, which are prior to HCC progression (Fig. 39). Thus, *Trim24*^{-/-} mice are non-obese and non-diabetic.

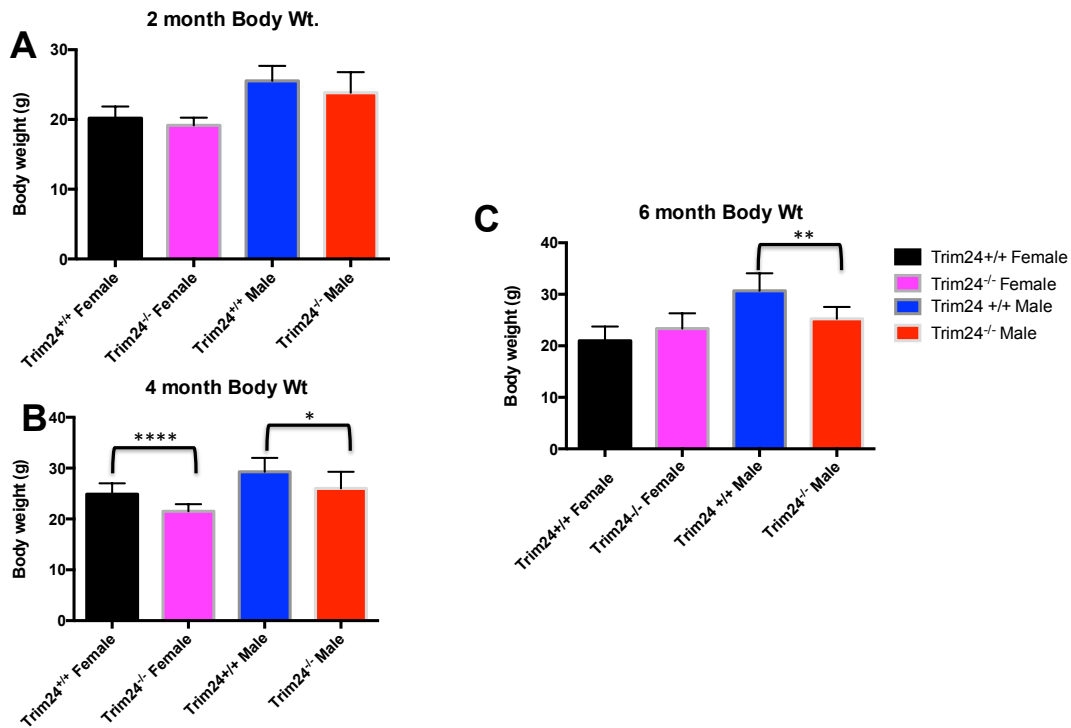


Figure 37. Loss of TRIM24 causes a decrease in total body weight during aging. Body weights are expressed in grams. **A)** 2, **B)** 4, **C)** 6 month male and female mice n>5. Mean \pm SD. * p<0.05, **p<0.01, ****p<0.0001.

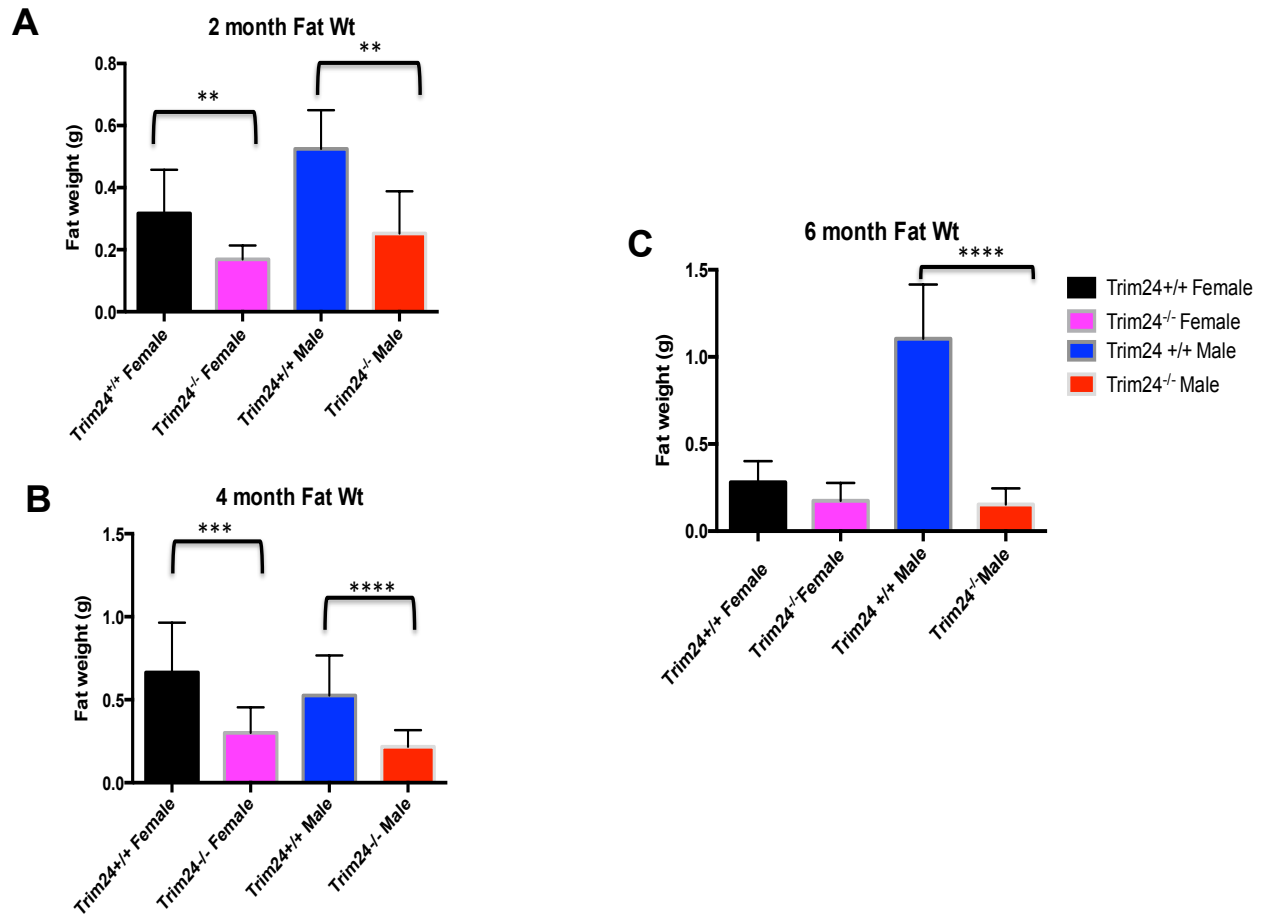


Figure 38. Loss of TRIM24 causes a decrease in visceral white fat weight during aging. Visceral white fat weights are expressed in grams. . **A)** 2, **B)** 4, **C)** 6 month male and female mice n>5. Mean \pm SD. * p<0.05, **p<0.01, ***p<0.001, ****p<0.0001.

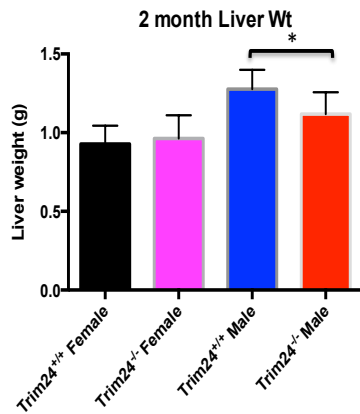
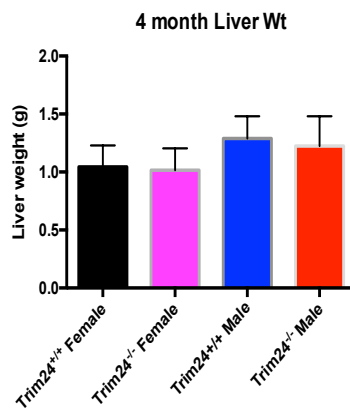
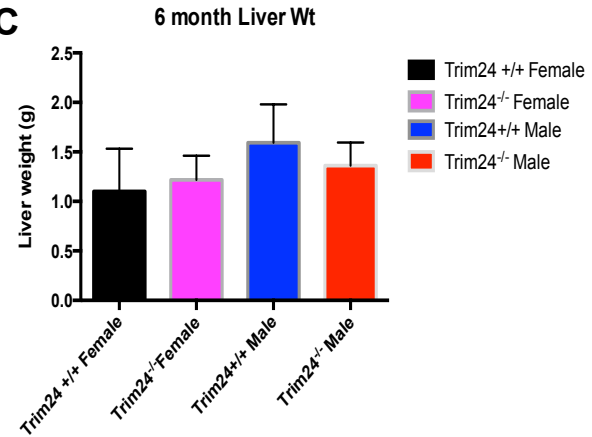
A**B****C**

Figure 39. Loss of TRIM24 has no effect on liver index prior to HCC progression. Liver indexes are expressed in grams and calculated by divided body weight by liver weight. **A)** 2, **B)** 4, **C)** 6 month male and female mice n>5. Mean \pm SD. * p<0.05.

4.6. Overlap of RNA-seq and ChIP-seq analysis reveals differentially expressed TRIM24 bound lipid and glucose metabolic target genes

Based on the analysis of genome-wide expression (see Section 4.3), TRIM24 activated gene targets are primarily involved in lipid and glucose metabolic pathways. The Triacylglycerol Biosynthesis category includes the genes: *Lpin1/2*. *Lpin1/2*, which are key genes associated with lipid storage. The Trehalose Degradation II (Trehalase) category includes the *Gck* gene, which is a key enzyme involved in the first step of glycolysis. The next categories, L-cysteine Degradation III and Glutamate Degradation II include the *Got1* gene. *Got1* (glutamic-oxaloacetic transaminase 1) is a gene that is induced by p53 and is responsible for amino acid metabolism as well as urea and TCA cycles [150]. The final category, Methylglyoxal Degradation I, includes the gene, *Glo1* (glyoxalase I). *Glo1* functions to detoxify reactive metabolites that are a byproduct of hyperglycemic metabolism [151]. Upon ChIP-qPCR validation, I found that *Lpin1* and *Gck* were significantly bound by TRIM24. (Fig. 40) While these mice are not obese and do not develop diabetes, hepatic metabolism of lipid and glucose are severely misregulated.

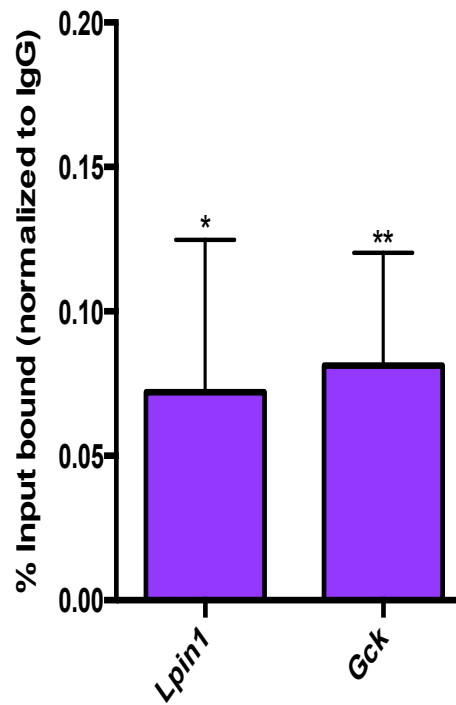


Figure 40. TRIM24 binds lipid and glucose genes in the liver. *Trim24*^{+/+} 2-month liver tissue ChIP: Significant binding by TRIM24: * $p < 0.05$; ** $p < 0.01$, *** $p < 0.001$. Significance is based upon comparison to non-specific binding control. Male and female liver samples were pooled for this analysis. Y-axis: TRIM24 enrichment as % input DNA.

4.7. Discussion.

Taken together, these results suggest that our *Trim24*^{-/-} mouse model recapitulates disease progression that is similar to non-obese NAFLD patients. The TRIM24-repressed genes, *Nrf2* and *Saa1*, are indicative of aberrant hepatic and systemic inflammatory changes. More specifically, Nuclear factor erythroid-derived 2, like 2 (*Nrf2* or *Nfe2l2*) encodes a transcription factor that regulates the expression of genes that encode anti-oxidant and ROS-detoxifying proteins [152]. RXRs can form homo- and hetero-dimers with other nuclear receptors such as those for retinoid receptor α (RAR α) or peroxisome proliferator-activated receptors (PPARs) [142]. In a study of rat macrophages, PPAR γ was shown to directly interact with NRF2 and repress its transactivation [153]. Additionally, overexpression of PPAR γ was shown to inhibit *Nrf2* transcription [153].

As previously discussed, TRIM24 is a co-regulator of RAR α , RXR, and ER α , and possibly PPAR γ . Thus, though further studies must be done, it is possible that TRIM24's co-regulation of these nuclear receptors that bind to *Nrf2* are keeping the progression of NAFLD and NASH in check in normal mice. Activated *Nrf2* has been shown to both delay proliferation and cause apoptosis in the regenerating liver [152]. Additionally, activated *Nrf2* is implicated during tumor initiation and progression [154]. *Nrf2* redirects of glucose and glutamine into anabolic pathways, allowing enhancement of metabolic activity, growth, tumor cell proliferation in both human cancer cell lines and mice [155]. Additionally, NRF2 also upregulates expression of anti-apoptotic proteins, such as Bcl-2 and Bcl-xL, increasing drug resistance and survival in cancer cells [156, 157]. With loss of *Trim24* expression, *Nrf2* expression

is upregulated, leading to increased oxidative stress and misregulated metabolism, aberrant processes in the disease progression of NAFLD and NASH.

The TRIM24 activated genes, *Lpin1* and *Gck*, indicate a pivotal regulatory role of TRIM24 hepatic lipid and glucose metabolic changes observed in the mouse model. *Lpin1* is a transcriptional co-regulator of fatty acid oxidation and inflammatory genes [158]. In the liver, *Gck* is a key gene that controls glucose uptake and glycogen synthesis [159, 160]. As TRIM24 directly binds these genes, their downregulation in *Trim24^{-/-}* liver is indicative of the metabolic phenotype observed in these mice.

When compared to the predictive factors for non-obese NAFLD patients, some interesting observations can be made. A comparison of lean to overweight-obese NAFLD patients shows that lean NAFLD patients are younger (65% less than 45 years of age), male, and less likely to present with hypercholesterolemia and insulin resistance (diabetes) [40] (Table 12). While the causes of this dichotomy have not been determined, it is postulated that underlying causes could include genetic predisposition, intestinal dysmotility, and other metabolic abnormalities not associated with obesity [40]. Thus, the findings in our *Trim24^{-/-}* mice offer a promising model to further dissect the mechanism underlying disease in non-obese NAFLD patients and offers an opportunity to expand the knowledge about both TRIM24 and an understudied area of the disease spectrum.

Predictor	OR (95% CI)	P
Factors associated with lean NAFLD compared to overweight-obese NAFLD		
Age	0.98 (0.97–0.99)	0.0008
Male sex	0.60 (0.41–0.87)	0.008
Insulin resistance	0.10 (0.07–0.16)	<0.0001
Hypercholesterolemia	0.34 (0.22–0.51)	<0.0001

Abbreviations: NAFLD = nonalcoholic fatty liver disease, OR = odds ratio, 95% CI = 95% confidence interval.

Table 12. Predictive factors of NAFLD in lean compared to obese patients.
Modified from *Medicine*. 2012;91(6):319-327 [40].

CHAPTER V

DISCUSSION

AND

FUTURE

DIRECTIONS

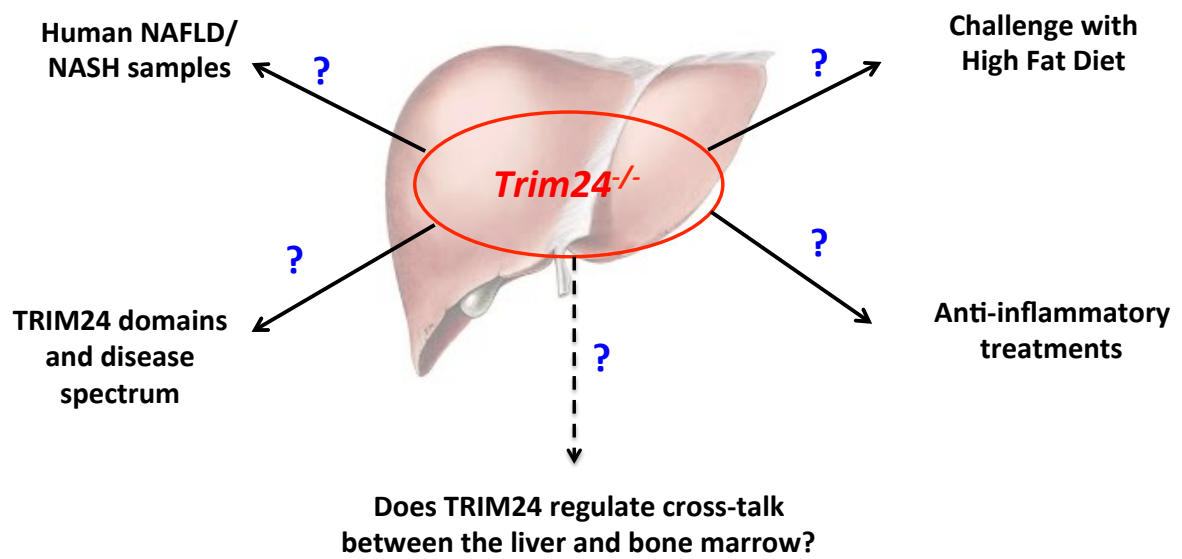


Diagram 7. Future direction studies.

TRIM24 and metabolism...a balancing act? (Refer to Diagram 7.)

This work has established the regulatory functions of TRIM24 in metabolic and inflammatory processes. The germline deletion of *Trim24* recapitulates the hallmarks of NAFLD, non-obese NASH and progression to HCC without a change in diet. Further studies are needed to see if *Trim24*^{-/-} mice will develop secondary metabolic effects when they are fed a high fat or “Western diet” (42 kcal from fat) that generally leads to development of obesity. Further dissection of this question with mouse models of both germline and liver-specific deletion of *Trim24* is needed to better understand the complexities of TRIM24’s regulation of metabolism and inflammation under dietary challenge. Comparison of changes in disease progression, spectrum, metabolic parameters, and dysfunction between systemic and intrinsic (hepatic) models will lead to further understanding of the regulatory mechanisms governing metabolism and inflammatory processes that are utilized by TRIM24. By implementation of this diet and our genetically altered model system, we will be able to better establish the altered pathways kept in check by TRIM24 that protect against HCC progression.

Our *Trim24*^{-/-} mice exhibit misregulated lipid and glucose metabolic gene expression leading to changes in glucose/insulin tolerance and visceral fat accumulation at 2, 4, and 6 months of age. Due to the fact that HCC does not develop until later timepoints in these mice, further studies should be performed in order to study glucose metabolic gene expression that could be misregulated due to cancer progression. It is well established that changes in cellular metabolism are occur due to aberrant expression of various key components of glucose metabolism,

such as glucose transporters, upon progression of cancer. In fact, in mouse models of NAFLD progression, it has been reported that there is a switch to the Warburg effect, which involves aberrant glucose metabolism via misregulation of glucose transporters and enzymes that are key to glycolysis, which is associated with cancer progression [161]. Overexpression of GLUT1 (both protein and RNA) is linked to multiple cancers such as: hepatic, pancreatic, breast, esophageal, brain, renal, lung, cutaneous, colorectal, endometrial, ovarian, and cervical cancers [162]. GLUT2 (protein and RNA) is normally expressed in the liver, pancreatic islet cells, and retina, with over expression observed in breast, colon, and liver carcinoma [163]. GLUT5 (both protein and RNA) is over expressed in liver metastasis compared to primary lung cancer [57] [164].

Further analysis of the role of *Trim24* in protection from aberrant glucose metabolism, associated with cancer progression (Warburg effect) should be addressed. Experiments utilizing liver and primary hepatocytes from aging *Trim24*^{-/-} mice should be performed to analyze glucose enzyme gene and protein *in vitro* and *in vivo* to determine if the Warburg effect is indeed a factor in disease progression. Further measurement of changes in hepatic metabolism could also be analyzed by mass spectrometry of metabolic output. RNA- and CHIP-sequencing of aging mice from *Trim24*^{-/-} liver would aid in further dissection of the regulatory role of TRIM24 in transformed cancer cell metabolism due to HCC progression.

This point leads us to the dichotomy of TRIM24, where in some instances it is an oncogene and others a tumor suppressor. While our germline deletion mouse models support the role of TRIM24 as a tumor suppressor, recent human HCC studies show over expression of TRIM24 [83]. Furthermore, TRIM24 is implicated in a regulatory capacity in oxidation/reduction and metabolism by studies in our laboratory, using an induced human mammary epithelial cell (iHMEC) culture model [67]. Over expression of *TRIM24* in HMECs led to an increased glycolytic and tricarboxylic acid (TCA) cycle gene signature, increased activation of glucose metabolic pathways and transformation of these HMECs. Xenografts of TRIM24 over expressing HMECs led to development of mid-to high-grade TRIM24-dependent tumors [67]. Mouse models of both over expression and deletion of TRIM24 are available to address this dichotomy (Table 13). To better understand this balance in expression, we have mice that overexpress full length *Trim24* that have been crossed to mice expressing the liver specific promoter (Tg Alb/Afp-Cre; *Trim24* FL). Further characterization of these mice in comparison to the liver specific deletion mouse (*Alb-Cre;Trim24^{flox/flox}*) and germline deletion (*Trim24^{-/-}*) will clarify the balance of *Trim24* expression in disease progression in the liver. More specifically, RNA- and ChIP-sequencing in the liver of each of these models in comparison to the sequencing data from the *Trim24* germline deletion will reveal gene targets that are both unique and shared between the models to determine the impact of varying levels of *Trim24* expression on disease progression in the liver. Furthermore, to address the tissue specific dichotomy of *Trim24* as an oncogene in breast cancer and a tumor suppressor in the liver, our laboratory has crossed mice

Mouse lines
Floxed <i>Trim24</i> ^{LoxP/LoxP}
Global deletion null: <i>Trim24</i> ^{-/-}
Hepatocyte-specific Cre: <i>Alb/Afp-cre</i>
Hepatocyte-specific deletion: <i>Alb/Afp-Cre;Trim24</i> ^{flox/flox}
Global p53 deletion: <i>Trp53</i> ^{-/-}
Transgenic (Tg) Flox-Stop-Trim24FL
Tg Flox-Stop-Trim24ΔRING
Tg Flox-Stop-Trim24ΔPHD/Bromo
Tg Flox-Stop-Trim24LXXLLmut
Tg Alb/Afp- driven Trim24FL
Tg Alb/Afp-Trim24N980A (Bromo mut)

Table 13. Current mouse models available in the Barton laboratory for further studies.

expressing a breast specific (MMTV-Cre) promoter to *Trim24* overexpression (Tg MMTV-Cre; *Trim24* FL) and deletion (MMTV-Cre; *Trim24*^{flox/flox}). Characterization of these models along with comparison of sequencing (RNA- and ChIP-) to liver specific models will provide insight to the dual nature of *Trim24*.

This study could be further expanded to dissect the alterations of TRIM24 levels that are responsible for hepatic metabolic disease that sets the stage for progression to HCC. TRIM24 is a histone reader and helps recruit transcription factors to work with chromatin and regulate gene expression. Since it interacts with and can co-regulate several different transcription factors, in addition to its ability to also regulate p53 by ubiquitination, loss or delay of timely and ordered TRIM24 interactions (too low) or gain (too high) impacts gene networks or cellular machines that interconnect and must be precisely regulated. In the liver, metabolic imbalance leads to lipid accumulation and inflammatory signaling, which progresses to tissue damage, fibrosis and HCC. Molecular and metabolic analyses methods that have been implemented in this work could also be employed to determine regulatory mechanisms that are dependent on TRIM24 and how they respond to altered levels.

Do specific domains of TRIM24 regulate inflammatory and lipid metabolic processes in the liver?

TRIM24 is a multi-functional protein that negatively regulates p53, co-regulates nuclear receptors and binds to a specific histone modification signature. While this dissertation did not focus on the roles of specific domains of TRIM24 in the mouse models discussed, the Barton laboratory has several key mouse models that can be

implemented to determine which of these functions is critical in development of NAFLD and progression to HCC. These models utilize genetic rescue with transgenic expression of specific forms of TRIM24 (full-length, RING mutant, LXXLL mutant and PHD/Bromo mutant) and could be implemented in a background of *Trim24* loss in the liver, in hematopoietic organs or globally (Table 13).

I propose that TRIM24 levels must be kept in balance to maintain homeostasis, and it is loss of homeostasis that leads to metabolic disruption. First, to establish cause-and-effect at a molecular level, we could determine the specific domain or domains of TRIM24 that can complement loss-of-function and protect the liver from metabolic imbalance and progression of disease through mouse models that are available in the lab. A liver specific deletion model of the bromo-domain of *Trim24* is being characterized in the laboratory (Tg *Alb/Afp-Cre*; *Trim24N980A*). The results from this model are particularly important in light of a bromo-specific *Trim24* inhibitor that is under development in collaboration with the Institute of Applied Cancer Sciences (IACS) at MD Anderson Cancer Center, based upon studies of inhibition in breast cancer cells. If mutation of the bromo-domain inhibits disease progression (rescues the phenotype) in the liver, this inhibitor will prove a potentially excellent therapeutic option for multiple cancers. Additionally, we have transgenic models with mutations of each domain of *Trim24* (Table 13) readily available for further studies in both the liver and breast in the lab as well. Studies in these mice will reveal the extent to which p53-signaling (RING), nuclear receptor interactions (LXXLL) or histone reader functions (PHD and Bromo) partially or wholly rescue hepatic loss of TRIM24 functions in preventing chronic liver disease and metabolic

syndromes. We will use blood collection and analyses of ALT/AST, total plasma cholesterol (TPC), plasma TG, non-HDL-C, and HDL-C, as early indicators of potential metabolic imbalance without sacrifice of the mice. These indicators will prioritize molecular analyses in an ordered manner. Thus, the tools are ready to further analyze important remaining questions regarding the balance, function of domains, and links to p53 expression and *Trim24* in liver and breast cancer.

Does TRIM24 impact crosstalk between hepatocytes and immune cells in liver disease?

To determine if loss of *Trim24* causes systemic and/or hepatic-specific inflammation, we conditionally deleted *Trim24* in the liver, by crossing *Alb-Cre* and *Trim24^{LoxP/LoxP}* mice. I initiated such experiments in our laboratory by testing whether changes in immune cell populations upon loss of *Trim24* were exclusive to the liver. Previous data on germline deleted mice showed that there was a significant increase in M2 macrophage gene expression (*Arg1*, *Mgl2*, *IL4RA*, *Fiz*) in bone marrow-derived macrophages (Fig. 41). These changes led me to hypothesize that TRIM24 regulates immune populations in both the liver and bone marrow and when removed, causes aberrant M2 macrophage activation, leading to progression of NAFLD and NASH to HCC.

In order to understand if hepatic-specific deletion of *Trim24* is sufficient to cause changes in bone marrow macrophage precursor populations, I utilized Cytometry Time of Flight Mass Spectrometry (CyTOF). CyTOF is a variation of flow cytometry that using antibodies labeled with heavy metal ion tags in the placed of

fluorochromes. Readout by time-of-flight mass spectrometry allows for combination up to 40 antibodies, for both extra- and intra-cellular signaling in a single sample. I applied this method to analysis of bone marrow collected from Floxed *Trim24*^{Loxp/Loxp} and hepatic-specific *Trim24* knockout mice (*Alb-Cre; Trim24*^{Loxp/Loxp}). I reasoned that by using a mouse model that possessed liver specific deletion of *Trim24* and normal bone marrow, I could determine if *Trim24*'s regulation of immune populations was cell autonomous (hepatic specific) or extended to systemic immune regulation (non-autonomous). The *Alb-Cre; Trim24*^{Loxp/Loxp} mice were generated in our lab (unpublished results) and were verified for Cre expression and Floxed *Trim24*^{Loxp/Loxp} status by genotyping for Cre expression and analysis of hepatic Cre gene expression (Fig. 42 A-B). Analysis of TRIM24 expression in the liver specific deletion mice as compared to germline deletion liver samples showed that while TRIM24 expression was negative in parenchymal cells (hepatocytes), non-parenchymal cells exhibited positive staining (Fig. 42C, Arrow). This raises the possibility that expression of TRIM24 in non-parenchymal cells in the *Alb-Cre; Trim24*^{Loxp/Loxp} liver may be involved in changes in disease progression when compared to the germline deletion mouse. To this end, although not fully characterized, preliminary data from these mice show that they develop the hallmarks of disease progression, but at a different rate (Fig. 43) when compared to germline deletion of *Trim24*. Thus, in order to determine if liver damage had occurred at the same age as the germline deletion model, I measured ALT/AST in the circulating serum of 2 months (10 week) old mice (Fig. 44). The liver damage enzyme levels were significantly increased compared to control, and closely recapitulated the results from the germline deletion model, thus

indicating early hepatic damage events associated with NAFLD and NASH progression.

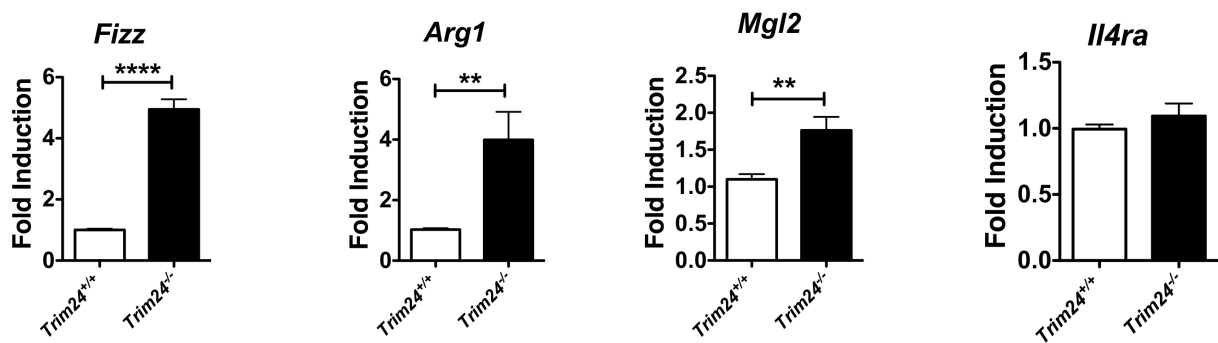


Figure 41. Bone marrow derived macrophages have increased M2 macrophage associated gene expression in *Trim24*^{-/-}. Genes associated with M2 macrophages show upregulated mRNA expression levels in *Trim24*^{-/-} bone marrow derived macrophages (cultured from bone marrow using GM-CSF treatment to isolate) by qPCR analysis. N>3, *p<0.05., **p<0.01, ****p<0.0001.

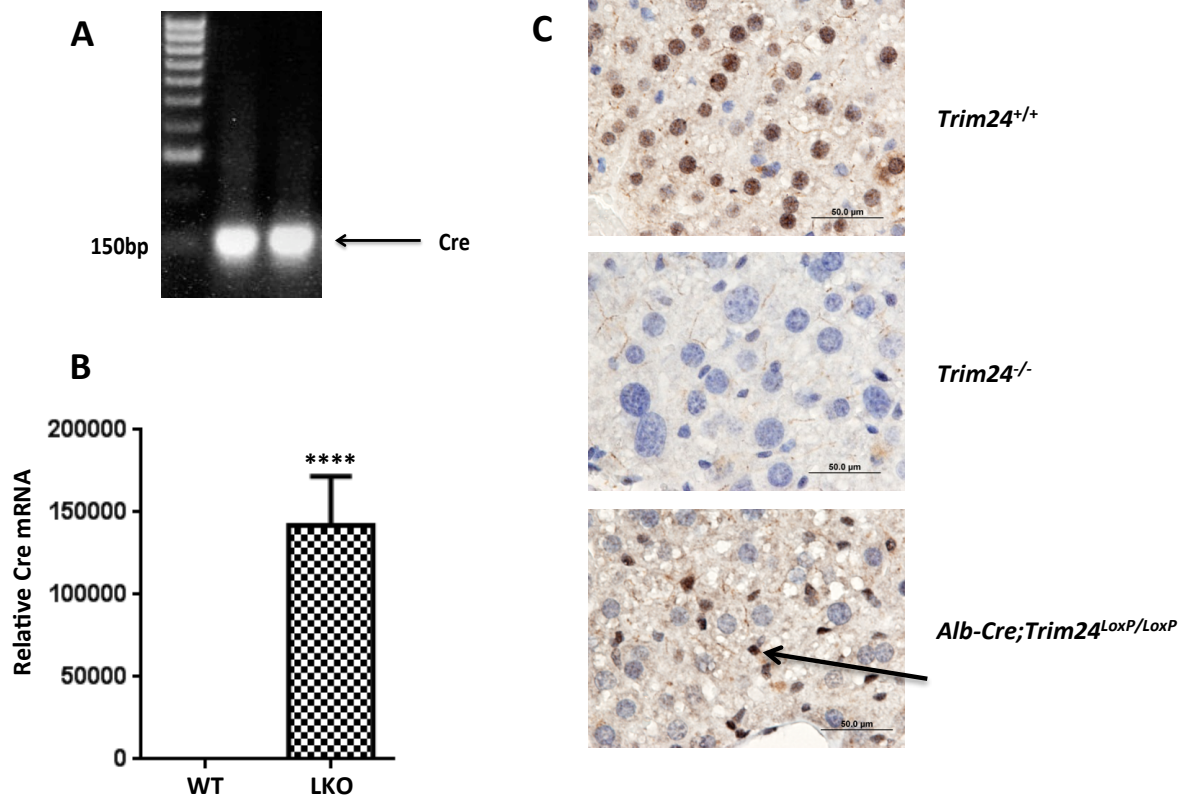


Figure 42. Analysis (PCR, qPCR, and IHC) confirming Cre expression and localization in *Albumin-Cre; Trim24^{LoxP/LoxP}* liver. A) Genotyping showing positive expression of Cre. Samples were obtained from ear punch. + = Cre. B) Gene expression analysis of Cre expression by qPCR shows significant increase in *Albumin-Cre; Trim24^{LoxP/LoxP}* liver compared to control. 3 weeks of age, N>3, **p<0.0001. C) Immunohistochemistry (IHC) for TRIM24 in *Trim24^{+/+}*, *Trim24^{-/-}*, and *Alb-Cre; Trim24^{LoxP/LoxP}* liver sections shows hepatocyte specific loss of TRIM24 expression in germline and liver specific deletion mice. However, positive TRIM24 staining is still apparent in non-parenchymal cells in the liver specific deletion sample (Arrow = positive, dark brown staining).**

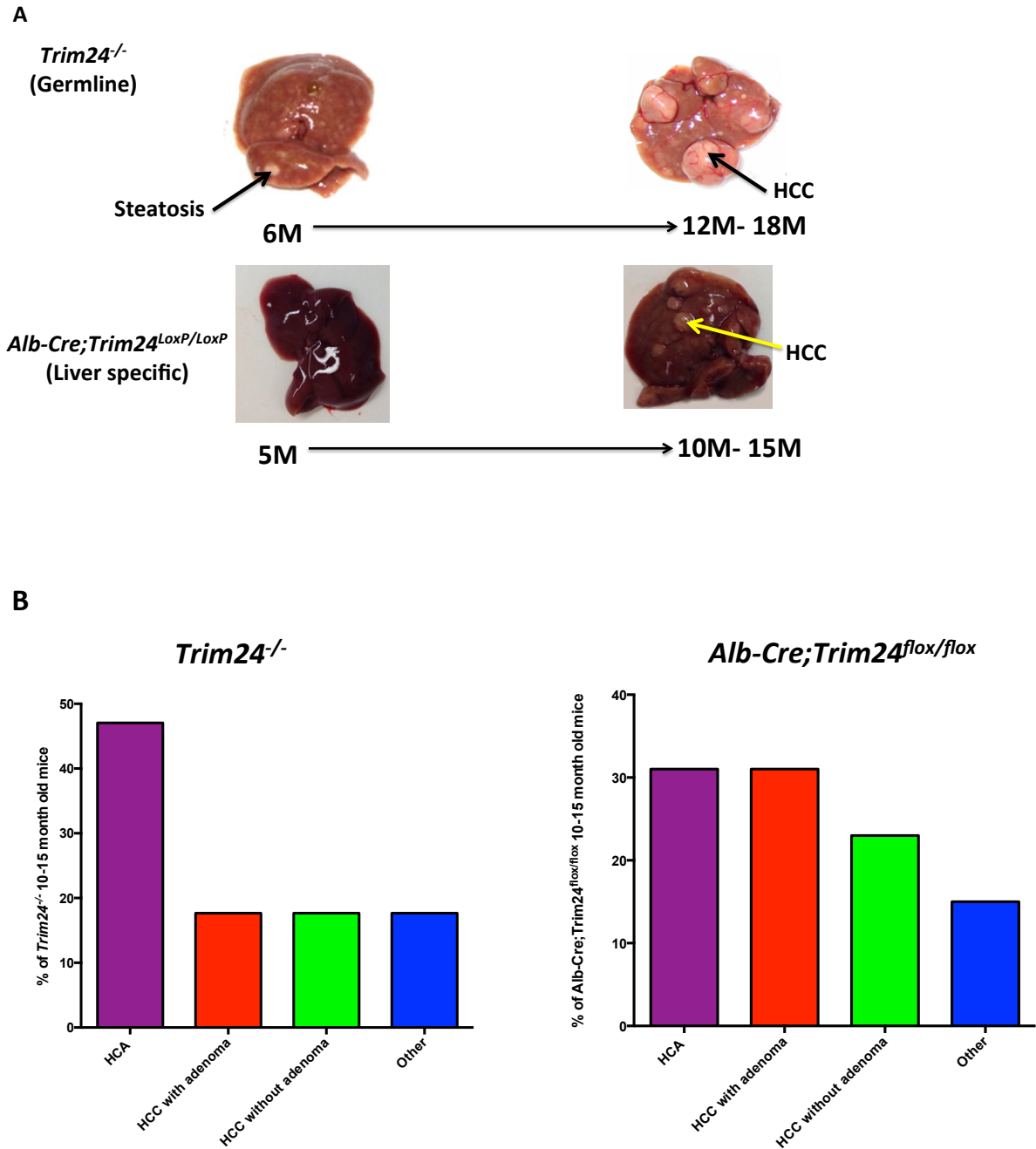


Figure 43. Timeline of disease progression and incidence of HCA and HCC in *Trim24*^{-/-} versus *Albumin-Cre; Trim24*^{LoxP/LoxP}. A) *Trim24*^{-/-} liver morphology showing lipid filled lesions present at 6 months compared to no visible lesions in *Albumin-Cre; Trim24*^{LoxP/LoxP} at 5 months. At 12-18 months of age, *Trim24*^{-/-} liver retain lipid filled lesions and develop HCC. HCC also develops in *Albumin-Cre; Trim24*^{LoxP/LoxP} at 10-15 months. B) Quantification of HCA and HCC incidence in 10-15 month old *Trim24*^{-/-} and *Albumin-Cre; Trim24*^{LoxP/LoxP} mice. M=Months.

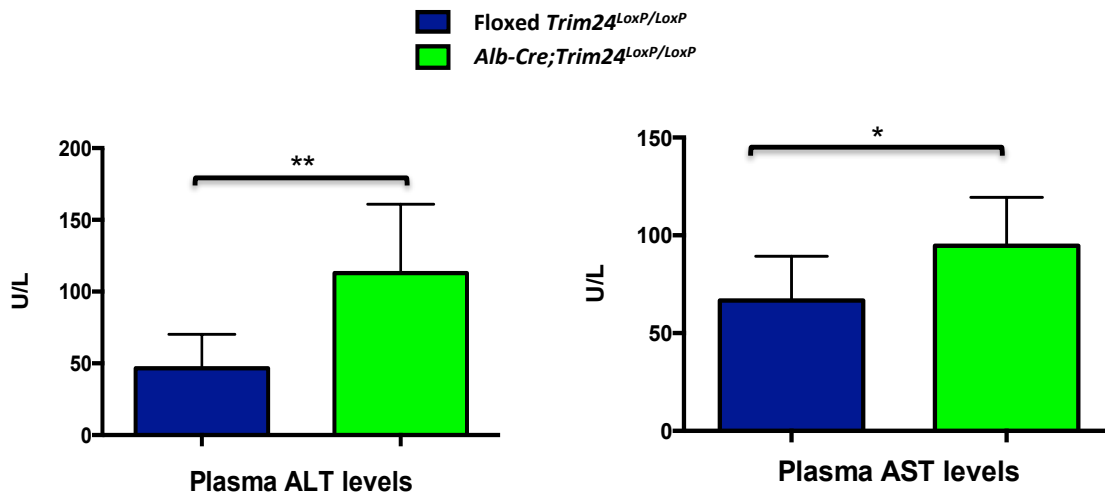


Figure 44. Hepatocellular damage and dysfunction in 2 month *Albumin-Cre; Trim24*^{LoxP/LoxP} mice. ALT/AST: *Albumin-Cre; Trim24*^{LoxP/LoxP} (n>5), Floxed *Trim24*^{LoxP/LoxP} (N>5). Mean ± SD. * p<0.05, **p<0.01

Upon collection of bone marrow from these mice, to quantify CyTOF analysis, I utilized markers (including CD34, CD19, CD45, CD45RA, CD117 and CD11b, Table 15) and distinguished hematopoietic cell types and lineages including hematopoietic stem cells (HSCs), common myeloid progenitors (CMPs), as well as cell types comprising the lymphoid, erythroid and myeloid lineages. The Visual Stochastic Neighbor Embedding (viSNE) algorithm was used to condense 13 parameters or dimensions of data into 2 dimensions of data to allow for visualization of single cell changes based upon the markers from our analysis (Table 15). Comparison of bone marrow cellularity between samples revealed a significant decrease ($p < 0.02$) in the percent populations of non-activated neutrophils (Ly-6g+, CD11b-) and a significant increase ($p < 0.002$) in activated neutrophils (Ly-6g+, CD11b+, IFN γ +) in the *Alb-Cre; Trim24^{Loxp/Loxp}* bone marrow indicating an increase in the inflammatory response (Figs. 45-46). Additionally the promyelocyte population (Ly-6g-, CD11b+) was significantly increased ($p < 0.02$) in the *Alb-Cre; Trim24^{Loxp/Loxp}* mice. (Figs. 45-46) The promyelocyte lineage gives rise to macrophage populations in the bone marrow. While preliminary data suggest that the inflammatory response is diminished in the liver-specific knockout, it is clear that the *Trim24^{-/-}* liver signals to bone marrow, as indicated by increased activated neutrophil and induced pro-myelocytes levels (Figs. 45-46).

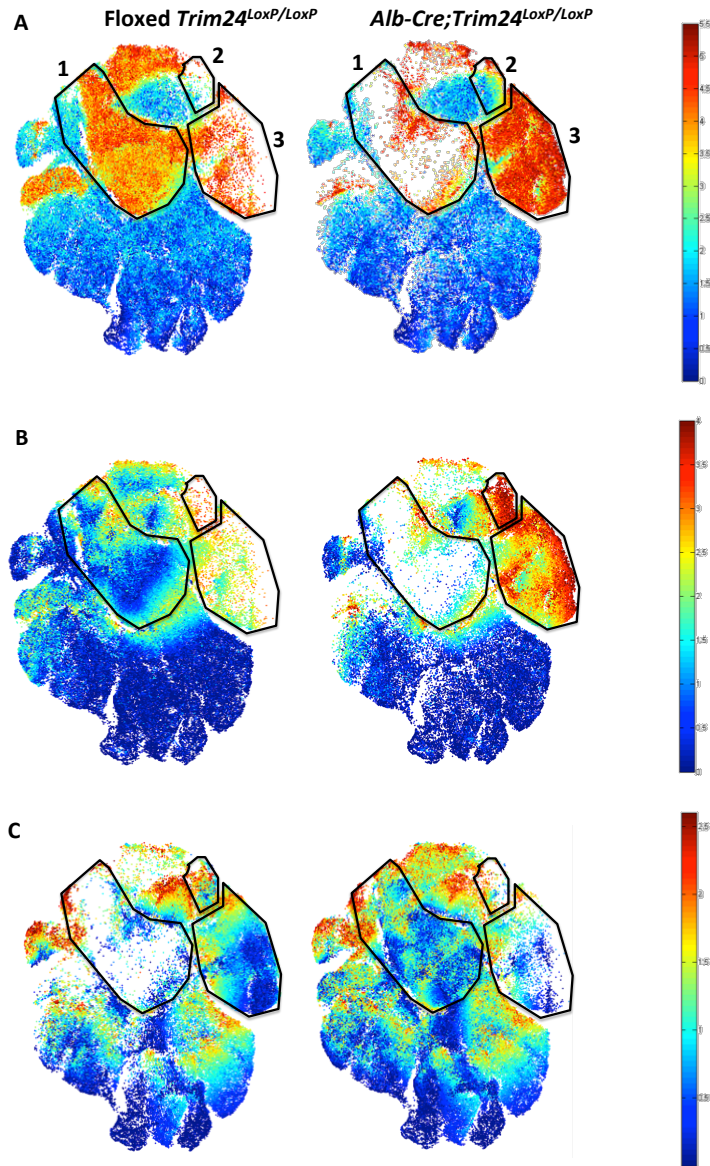


Figure 45. Liver-specific deletion of *Trim24* increases the abundance of myeloid lineage precursor cells in the bone marrow. viSNE analysis was performed to quantify cellularity and construct a map of hematopoiesis based upon the measured parameters; representative viSNE analysis for A) Ly-6g signalling B) CD11b and C) CD34 signaling are shown. Comparison of bone marrow cellularity between samples revealed significant decrease in the percent populations of non-activated neutrophils (Ly-6g+, CD11b-) (Region 1 – all maps) and a significant increase in activated neutrophils (Ly-6g+, CD11b+, IFNg+) (Region 3 – all maps) in the *Alb-Cre;Trim24*^{LoxP/LoxP} bone marrow indicating an increase in the inflammatory response. Additionally the promyelocyte population (Ly-6g-, CD11b+) (Region 2 – all maps) was significantly increased in the *Alb-Cre;Trim24*^{LoxP/LoxP} mice compared to Floxed *Trim24*^{LoxP/LoxP} bone marrow. (N=4, 10 weeks, *p<0.02, **p<0.002) Intensity of signaling is quantified using log2 scale as represented by the color scale bar, Red=High intensity, blue=low intensity.

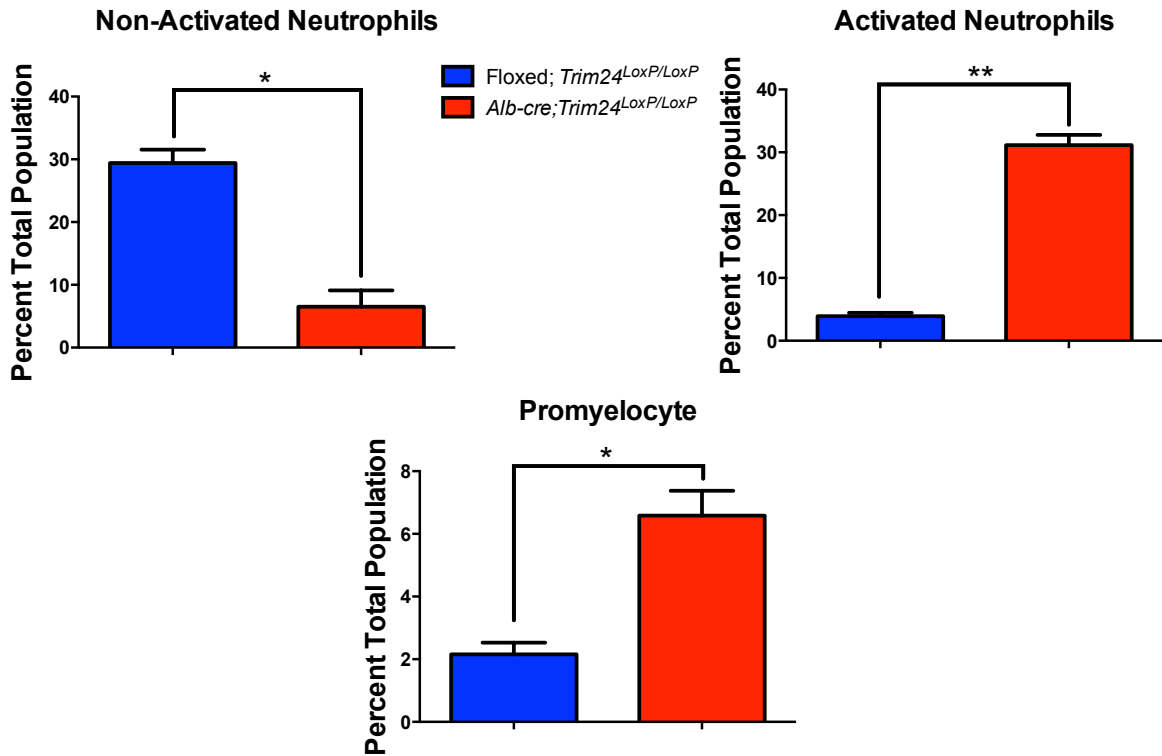


Figure 46. Liver-specific TRIM24 knockout induces an inflammatory response in the bone marrow and increases the abundance of myeloid lineage precursor cells. Comparison of bone marrow cellularity between samples revealed significant decrease in the percent populations of non-activated neutrophils (Ly-6g+, CD11b-) and a significant increase in activated neutrophils (Ly-6g+, CD11b+, IFNg+) in the *Alb-Cre; Trim24*^{LoxP/LoxP} bone marrow. The promyelocyte population (Ly-6g-, CD11b+) was significantly increased in the *Alb-Cre; Trim24*^{LoxP/LoxP} mice compared to Flox *Trim24*^{LoxP/LoxP} bone marrow. (N=4, *p<0.02, **p<0.002).

As discussed in this work, progression of NAFLD to more serious liver disease is complex and poorly understood, marked by changes in lipid metabolism, as well as systemic and hepatic inflammation. Experiments with isolated liver and bone marrow immune cells clearly show that loss of TRIM24 causes an increase in macrophage, neutrophils, and myeloid progenitor populations in both locations. Further analysis indicates that metabolism, inflammatory processes, and oxidative stress genes are directly regulated by TRIM24. These findings suggest that not only are metabolic and inflammatory processes regulated by TRIM24, but specific immune cell populations are as well.

Remaining questions center upon the difference between the inflammation that we observe in germline deletion of *Trim24* as compared to the liver specific deletion model. Experiments testing serum levels of circulating cytokines such as IL-6 and TNF- α by, which are both misregulated in NAFLD and NASH progression and key markers of macrophage activity, should be implemented [112]. Changes in circulating levels in serum (measured by ELISA) would be an indication of NASH development. Continued studies should also be performed to determine if cytokines levels are misregulated in the liver. To determine when changes in inflammatory processes occur, an extensive study beginning with embryonic development through aging should be performed to determine the nature of inflammation (acute, chronic, etc) and age of onset, if it occurs. This study should not only be performed in the germline deletion, but also the liver specific deletion of *Trim24*. By performing the study in both mouse models, the timing, by study of when lipid metabolic versus inflammatory genes were misregulated, could be ascertained. Additionally, since the

liver specific deletion of *Trim24* possesses normal *Trim24* expression in the bone marrow, this model could be used to determine the role of *Trim24* in metabolism and inflammation in the liver versus bone marrow (compared to *Trim24*^{-/-}). Once this is established, a pivotal study utilizing commercially available cytokine inhibitors, such as Tocilizumab (IL-6 inhibitor), should be performed at the onset of inflammation to determine if the phenotype can be rescued by inhibition of misregulated inflammatory processes. As a cautionary note, inhibitors should be chosen based upon action on affected cytokines that found to be misregulated (i.e. IL-6) and special care should be taken to avoid inhibitors that have high rates of liver damage as a side effect.

This same strategy could be further extended to hematopoietic organs (such as bone marrow, spleen, lymph nodes), by crossing *Tie2-Cre* and *Trim24*^{LoxP/LoxP} mice. By segregating liver-specific and hematopoietic-specific functions of *Trim24*, several important questions would be addressed: broadly, how immune cells influence liver disease progression to HCC and, specifically, the regulatory impact of TRIM24 in each tissue compartment. Previous studies have shown that recruited hepatic macrophages, arising from the hematopoietic stem cell niche, home to the liver due to *Ccr2* signalling [165]. This signaling is significantly increased in *Trim24*^{-/-} liver at an early age (Fig. 19). The majority of individuals with NASH are also obese and suffer from obesity related diabetes. While our *Trim24*^{-/-} mice model a phenotype similar to non-obese NASH patients (without diabetes), we realize that they have not been exposed to environmental factors, such as high fat diet, which is typically implicated in patients. Thus, this condition can be modeled in the *Trim24*^{-/-} mice by introducing

a Western high fat diet (42% kcal from fat) at weaning. By changing this environmental factor, the role of TRIM24 and increased lipid consumption could be potentially linked to the NASH phenotype. We have identified both metabolic and inflammatory gene targets of TRIM24. Additionally, in-depth analysis of histone modifications that are associated with the regulatory elements of key inflammatory and metabolic genes should be analyzed in *Trim24*^{+/+} or *Trim24*^{-/-} liver to understand the epigenetic mechanisms involved in NAFLD, NASH, HCC disease progression.

Links between TRIM24, p53 and HCC?

Recent studies have reported that p53-expressing, senescent stellate cells release factors increase production of tumor-inhibiting, M1-state macrophages capable of attacking senescent cells in culture [166]. Conversely, they report that proliferating, p53-deficient stellate cells secrete factors that stimulate production of tumor-promoting, M2-state macrophages and enhance the proliferation of premalignant cells leading to HCC [166]. Macrophages cultured from the bone marrow of *Trim24*^{-/-} mice and stimulated with *Il-6* show activation of phosphorylated STAT, a gene associated with M2 macrophage induction and activation of p53 (data not shown). A determination of whether this phenotype is evident in our model, as an important and previously unknown regulatory capacity of *Trim24* or the regulatory relationship between p53 and TRIM24, is critical.

Implications for inflammasome-directed crosstalk between bone marrow and liver leading to progression of the NAFLD, NASH, HCC spectrum.

While our studies have highlighted the importance of cell- and lineage-specific contributions to the NAFLD, NASH, and HCC disease spectrum, additional studies should be undertaken to address the contribution of the inflammasome within these cell populations. In short, the inflammasome represents a complex of intracellular proteins in both parenchymal and nonparenchymal liver cells that respond to damage or danger signals, usually the result of pro-inflammatory cytokine signaling (IL-1 α , IL-1 β , TNF- α) [167]. The inflammasome then signals to activate caspase-1, IL-1 β , and IL-18 [167]. Recent studies have shown that knock-down of IL-1 α or IL-1 β in liver parenchyma, but not bone marrow, protected mice from diet-induced liver damage due to steatohepatitis and fibrosis [168, 169]. It is important to fully characterize the molecular pathways involved, and more importantly to establish early, potentially sentinel events for better diagnoses and potential therapeutic avenues. Our previous RNA- and ChIP-seq were done with whole liver, but this current work has established a method to isolate specific cell types from the liver: hepatocytes and HSC-derived cells, using the modified protocols from [170]. Therefore, more in-depth studies of crosstalk between the liver and bone marrow should be undertaken, using the methods established in this study, to determine the role of TRIM24 in activation of the inflammasome in a systemic or hepatic-specific manner.

TRIM24 and human NAFLD, NASH, and HCC.

Current biomarkers for NASH and HCC are virtually non-existent with little concrete evidence regarding biomarkers, mutations, or SNPs that are common in patients [171]. Early detection methods for disease have the potential to drastically reduce the incidence of late-stage disease through preventative therapy. Since we have such a striking, spontaneously progressive disease phenotype in our *Trim24*^{-/-} mice, TRIM24 has the potential as a biomarker of disease. Thus, patient samples (blood/tissue) from both non-obese and obese individuals with liver damage and HCC from collaborating clinics at the UT Medical Center could be used to establish baseline *TRIM24* expression levels as compared to healthy patients. To better understand inflammatory parameters affected in patients with disease, additional screening for immune populations and cytokine expression could also be performed. IHC staining for TRIM24 and immune factors to determine possible correlations between expression levels and disease progression could be performed on available human liver samples. Sequencing of these samples could also be utilized to determine the presence of mutant *Trim24*, possible related SNPS, or common gene targets that are observed in the *Trim24*^{-/-} mouse model. Due to the dimorphisms reported in previous studies [22, 38, 40], it will be important to analyze data keeping gender and ethnic backgrounds separate. These studies would be designed with the aim of understanding the mechanisms and triggers behind disease progression and the role of TRIM24 in the process.

CHAPTER VI

CONCLUSIONS

Conclusions

The “two-hit” hypothesis of NAFLD and NASH progression states that an initial, aberrant accumulation of hepatic lipid (steatosis) is the first step toward disease progression [21]. Next, the second hit is accumulation of dysregulated oxidative stress, inflammation, and cellular damage. Upon germline deletion of TRIM24, we discovered that both “hits” were present in our mouse model, which led to further characterization and dissection of regulatory mechanisms of TRIM24 in this study. In the first part of this work, I characterized the *Trim24*^{-/-} mouse model, showing that, upon loss of TRIM24, mice spontaneously develop hepatic steatosis, inflammation, hepatocellular damage and eventually HCC. These results, upon further biochemical and gene expression analysis (by RNA-seq and qPCR), identified key gene targets that are commonly misregulated in NAFLD and NASH progression. CHIP analysis showed direct enrichment of TRIM24 at both metabolic and inflammatory gene targets.

In the second part of this work, I described a cell population-specific, regulatory role for TRIM24 through isolation of both hepatic- and hematopoietic (bone marrow)-derived immune cells. These studies utilized both germline and liver-specific (*Albumin-Cre; Trim24*^{LoxP/LoxP}) *Trim24* deletion mice and showed that specific immune cell populations such as macrophages and myeloid lineage cells are misregulated in both sites. These results were further dissected by identification of increased markers of macrophage (M2) activation (tumor promoting/oncogenic) and identification of key inflammatory gene targets directly bound by TRIM24 (Nrf2 and Saa1) by integration of RNA- and ChIP-seq datasets.

I also established in this section that loss of TRIM24 causes misregulation of systemic glucose/insulin levels and decreased visceral white fat. These findings along with identification of TRIM24-bound gene targets involved in lipid and glucose metabolism (*Lpin1*, *Gck*, and *Gbe1*) from integration of RNA- and ChIP-seq datasets, suggest a direct role for TRIM24 in hepatic metabolism. Thus, my dissertation research demonstrated that TRIM24 is a key regulator of hepatic lipid and glucose metabolism and inflammation. Upon deletion of *Trim24*, the mouse model closely models the hallmarks of human NAFLD, non-obese NASH, and HCC. Taken together, this work supports the “two-hit” hypothesis and provides a novel model of spontaneous non-obese NAFLD/NASH/HCC progression. This project has provided the tools to further dissect the role of TRIM24 in metabolism and inflammation in multiple mouse models and organ systems (Diagram 8).

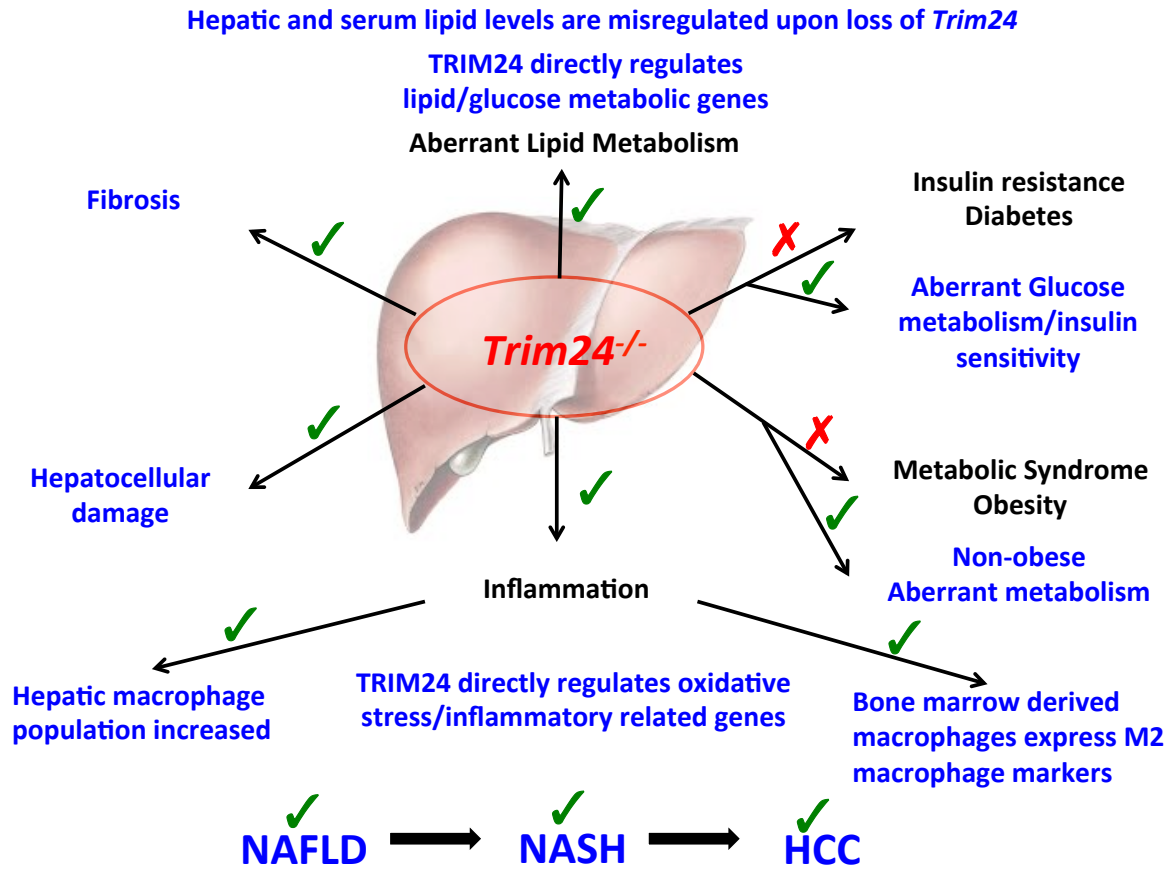


Diagram 8. Working model summarizing the effects of TRIM24 loss in the mouse model.

CONTRIBUTIONS:

I would like to thank the following people for their contributions to this dissertation:

- Dr. Shiming Jiang- for his guidance, expertise, and help with the characterization of the germline and liver specific *Trim24* deletion mouse models.

- Sabrina Stratton and Dr. Zeynep C. Akdemir- for their support, expertise, and help with ChIP and bioinformatics analysis.

- Kendra Allton and Hui Wei- for their help with genotyping and generation of MEFs.

- Dr. Ryan McCarthy- for his expertise with CyTOF and viSNE analysis and many helpful suggestions.

- Dr. Huiyuan Zhang- for her expertise and help with immune experiments in bone marrow derived macrophages, liver, and Flow Cytometry.

- Peirong Yang, Dr. Hussein Abbas, Dr. Vinod Pant, Dr. Sean Post, and Dr.

Guillermina Lozano -for their invaluable assistance and generosity while making the *Trim24^{-/-}* mouse.

-Dr. Richard Lee – for his expertise, generosity and help with the ALT/AST and hepatic lipid panels.

-Dr. Mihai Gagea – for his expertise in pathology and help in determining disease progression in our mouse models.

Without their generosity and support, this work would not have been possible.

Table 2: Sequences of 5' probe and 3' probe used for Southern blot

5' probe for Southern blot:

ggtaaccaaggaatgtgggtctatctgacaaactgtcactgtatcttatgaattcattgttattcagtaaattctgacattgc
agaaagacaggcttcacttcagctatfactttgtgtccaaaaaggactagagatgtcccccacactcatgtctgtca
cttagccatccagtgagggtttttcaatctacaaataatgttctgaaaacataaaatatctgggaagaaaacaggtg
ataaggaatggaaagatcatttaacttgaatcatgaactctccacctgagcatatgactctgaagaagaagcta
caaaccaaatgcttatggggaccagaggacaagaagactaaaccaagttggggggggggagggggaattctcatt
atcttcagtggaattgagaaatgttgaaggaatacagaggataagaggtagttctaggatccagtaaatagatgtct
atctagagagtttacttgccctgggtgggggtccagaagatcaccttcagttcaaatgagcttctatgagatctcaa
aatacagaagaaactgttagtcattcacttaggtacaatgtattacatcaaaaggatggaaatccatcagcagaag
aagctatatagggaagatgatgagaaaccaggc

3' probe for Southern blot:

cccattggtccagtcagaacataaagaggtggaatgtccttcttctggtgagcagggatcaattagctggggtatcgt
gacctcgggtcctagaatagagtttagtgatttctctggtgcttttacatcaaggagatctgtcaaacataaagtggc
ctgggcaagaatatagatggaggaacctctgcactgagttgcttgcacaaatacttgagttatgctgttgctattata
ataaacacctttttgtctctaactctgagttacttgccattgtcataagaaacttactatctgtgaaactgggattcttat
taggtgcaggaaaggtggaatctcatagtagttgtctcaaaggggcttgctgctggaaggaatgcaggataac
attaatcttattctatgtaacctgggtgacctctgactctgagtgctagggtcaaaggcatgctttatcaggctcaaatctt
aatcttaattgcaataatgttatgttgatgctgaggagtaagccttgtaaataaaagcactcactaccatgaagctccc
agttttaattcttagatgtattttgtatttctcattcccccccc

Table 3: Primers for real-time PCR analysis of mRNA expression

Genes	Sense	Antisense
18S RNA	TCAAGAACGAAAGTCGGAGGTT	GGACATCTAAGGGCATCACAG
Acaa1b/a*	GGGCTGACTGTGAATGAC	TGAGTAGCGTGACAACCT
Acaca*	AGCAGATCCGCAGCTTG	ACCTCTGCTCGCTGAGTGC
Acacb*	ATAGAGAAGGTGCTCATC	TTCATTACGGAACATCTC
Aco2	GAAGAACATTAACATTGTCCGTAA	CGCAGGTATGTCTTTCCC
Acox*	CCAAGACCCAAGAGTTCA	CAGGACTATCGCATGATTG
Acss3*	AGCCTAAGGTGGTTGTTACG	GCCTGTGCTGTCTATCC
Adar	GGAAGAAGACTCGGAGAA	ACTCAAGCAGTGTAGTAACT
ApoA5*	AAACAGTTGGAGCAAAGG	ATTGTTTCAATTGTAGAGGTCTT
Apob*	AACCAAGAACTCTGAAGA	CAGGGTAAAGAACAATTTG
Apobr *	GGGCTACATCAGGCTTTG	GGACTGTGTCTCCTACGA
ApoC1*	TCCTGATTGTGGTCGTAG	GTATGCTCTCCAATGTTT
ApoC2*	CGGTTCTTCTGGCTCTA	CGAGTCATCTTCTGGTTC
ApoC3*	GAGTCCGATATAGCTGTG	AGTAAACTTGCTCCAGTAG
Arg1**	GTGAAGAACCCACGGTCTGT	CTGGTTGTCAGGGGAGTGTT
Bax*	GATGCGTCCACCAAGAAG	CGTCAGCAATCATCTCT
B-myc	CATGGTGCAGGACTGTATGT	AAGCTTACAGTCCAAAGCCC
Casp12	AATCTTGGATACTCTGTGGTGTTA	CTGAGGACTGGTGCTCTG
Ccnd1	TCAAGTGCCTGCAGAAGG	GCTCCTCACAGACCTCCA
Ccr2	CTACTCCCTGGTATTCATC	CCAAGTTGAGCAGATAGA
Ces1d*	TCTTGGCTCCTTGAGATT	CATCCTGAGAGCATAG
Crbp1	ACGCTGAGCACTTTTCGGAA	TGCACACACTGGAGTTTGTC
Cyp26a1	CGGTTCACTTCATTCCATT	GTGGGGCTTGTCTTCATTGT
Cyp2c38	AACTTCAACCAATCCTTAACCAAT	GCTCCTTCACTGCTTCATAC
Ddit3*	GGGGCACCTATATCTCATCC	CTCCTCTGTCAGCCAAGC
Eno1	GTCCACTGGCATCTACGA	CCTGTGAGACACCCTTCC
Enpp1	CCGCTGCTTTTCAAAGGAC	TTGGTTCCACACAGGTCTC
Fasn	TTCCAAGACGAAAATGATGC	AATTGTGGGATCAGGAGAGC
Fizz**	TGCTGGGATGACTGCTACTG	AGCTGGGTTCTCCACCTCTT
Gck	TGGAGACCCATCAGGAGG	TCCAACCTTCTGAGCCTTCTG
Glut2	CCAGTTCGGCTATGACATCG	CCAGTGGAACACCCAAAACA
Hprt	TGGACTGATTATGGACAGGACTGA	GCACACAGAGGCCACAAT
Hsp90aa1	ATCGGACGCTCTGGATAA	CCTGTTTGTGGGAATGA
Icam1	CCGCAGGTCCAATTCACACT	CAGAGCGGCAGAGCAAAG
IL-33	GTTGACACATTGAGCATCC	CAGATTGGTCATTGTATGACTC
IL-4ra**	CCTCACACTCCACACCAATG	AGCCTGGGTTCTTGTAGGT
Irf9	TTCATCTATGGTGGCCGAGT	ACGCCTCTGTCAAGCTGATT
Irs1	AATAGCGTAACTGGACATC	CCTGGTTGTGAATTGTGA
Irs2	ACTTCCTGTCCCATCACTTGA	GCTTCACTCTTTCACGACTGT
Lcn13	GACGTCGGTGAATGAGCACT	CCGATCTCTGGCACAAACAT
Lpl	AGG ACC CCT GAA GAC AC	GGC ACC CAA CTC TCA TA
Mcat*	CTTCAGTGTGGGAGAGTTTG	TTCACCGCATAACAGACCTT
Me1	CCGCATCTCAACAAGGAC	GTCAGAGTTCAGTCGTTCCG

Mbl2	CAGGTCAAGGGCTCAGAG	CTCCTTTTCGGTCCCCTG
Mdh2	CATTGCCAACCCAGTGAA	GTTTCGCTCTGACGATGTC
Mgl2**	GGATCCCAAATTCCCAGTT	TCCCTCTTCTCCAGTGTGCT
Mttp*	TACCAACGAGGTAGATAT	ATGTATCCAGAGCCTTAA
Nox4*	ACACCTCTGCCTGCTCAT	ATGCTCTGCTTAAACACAATCCT
Pdk1	GGTCAGTGAATGCTTGTG	GGGTCCTGAGAAGATTGT
Pgm2	TCATTCTGACAGCCAGCCATAATC	GCTTCTGGAGCAGGACCC
Plin2*	AGCCACAAATTGCGGTTG	TGGTTCAGAATAGGCAGTCTT
Plin3*	CAGCAGCCGACTGAGAAG	CATTTCTTGAGCCCCAGACA
Plin5*	ACTAGACAAATTGGAAGAGAA	CTGTATCCTTGGCTGATG
Pnlip*	CTTAACAATGTCCACCTGAT	CCTGTGATCCTTCCAATG
Pnliprp1*	TCAACTACTCTGCTTCCA	CTGTAATCCTGCCAAGAC
Pnpla3*	GTCCACCAACTTCTTCCA	CCATCACCTTCACATCAGA
Retn	CAAGACTTCAACTCCCTGTTTCCA	GGGCAGGAGGCCAACTTA
Scd-1	TGG GTT GGC TGC TTG TG	GCG TGG GCA GGA TGA AG
Sc5d	AAGAACCAAGTCTCGCGTGAG	CAGTGAGACGGTGGGGATG
Stra6	GGGACTGGAGTCACTGTGT	GCCAGTGTGAGGAGAAGAGG
Tgm2	AAGAACCCACTTTCCGATCC	ACTTCAGCTTGTCACTACTGG
Tm7sf2	GGCTATGTGGCTGGTCAAT	ATGGTGGTGAGGACAGACT
Trim24-3'UTR*	AGAAGGAAGAGAAGGTAG	ACATCCAGATCACACTAA
Trim24-E11/13*	CCAGAGGTTGACTATGATTGT	TCAGGCACAGTTAGAGGAA
Trim24-E2/3*	ACACCACTGAAGTTCCTA	TCAACACACTCTACACAAA
Trim24-E7/8*	GCAAGCGGCTGATTACATACA	TGGTCACAGGAGGAAGCATCAC
Trim28*	ACATGCCACACTTCAGAAAAC	ACACCTGGCGGATCGA
Trim33*	GAAAACCTGCACAAGGCTTAAGC	GGTAAAGCAGAAGACGTTTACA
Vcam1*	GAATGAACACTCTTACCT	CACTGAATTGAATCTCTG
Vldlr	CGACGAGAAGAACTGTGTAA	CACTGCCATCTGTTAGGAA
Zfp445	GTGCAGTGTTCCTTCCATTCT	ACTCCATCGGAAGGCTTTTT

*Primers designed by Shiming Jiang, PhD, **Primers designed by Huiyuan Zhang, MD/PhD

Table 4: Primers for ChIP PCR analysis

Acacb*~(-3.6kb)	CTTGGCATGGAGGT CTTGA	CCTTGAACTCAGAGATCACTTT G
ApoA1*~ (2.0kb)	CTGGGGTCACAGGCTAT G	CAGCAAATGGCAAGTGTTCT
ApoA1* ~ (-3.2kb)	GGCTGGCACCATTG AAGG	GCACCAGAGACACCAAAC ATT
ApoC3* ~ (-0.15kb)	CTTTGTCCTTCTCTC ACTAATCC	CACACTGACCTCCACCTG
ApoC3* ~ (-2.9kb)	ACTCACGTCTCTGTC TGA	CTACCAATCAGCCTTACT AGC
ApoD1*~ (1.1kb)	GTGGCGAGGTGGTA ACAATG	TGTCTGAGAAGGGCACAG G
Bax * ~(-3.1kb)	CACACACCACAGAGAAGA CAAGGA	GCAATCCAGCCTGGCTCTCA
Casp12* ~(-1.1kb)	GGGTGGGAAGCAGAAAG C	TGGCAGAAGAGGAAGCAGAA C
Ccr2* ~ (-0.5kb)	CGTGAACTCATTGCT GGCAGATAG	ACCACGAGATGTTCTTACCACC T
Ccr2* ~(-1.0kb)	ACTCCAGGCAATCTGAAG C	GGACACACCTTGGCATGA
Cdkn1a	CGAGGAGGTGACTCATT GT	CAGGGAAAGGGGCTTCTG
Ddit3* ~ (-3.7kb)	GCATTGAGTCTCTGG CAC	CTACCTCCTCAGCGATGG
Gbe1	CCAGGGCGTGTGTGATT T	CAAGAGCAAACAGGAGGGT
Gck	AAGCCAGAGGACCTGAA TC	AGGAAGGAAGGAAGCCAAG
Icam* ~(-4.9kb)	AGATAGGCGCATCTC TGAGTTCA	CCCAGTGATTTCTTCGGTGGT TT
Icam* ~ (3.7kb)	ATCCGCAGAGCATT CTTAG	TGCCCTGTACCTCAGTCT
Il-1a* ~(-4.0kb)	TCTAGCCTGAACTAC ATGAAACCT	ACCACGCCCTGCTTACAT
Jun	CTACCAACGTGAGTGCT A	CGCTTCTGTAACAAAGTTTG
Lpin1	GGCAGAATCCCTTGAGA G	ACCACGAACTTCCAATCC
Mttp* ~ (700bp)	CACGCAACCACATTTTAA	CTCGGCCTCGTGGTCAG

	ACACAA	
Nfe2l2/Nrf2	GGGCTGTGTGTTCTGAG TA	CCTCTGTGACTGCCAACT
Pnpla* ~ (-3.5kb)	CGGGGTCTGGGAAT TGAG	TTAGGTTTGAAACTATTTG GGAC
Saa1	CGGAGTAGAGGAGATGA G	CGATAAGGACGATAGATACA TAT
Vldlr* ~ (-2.4kb)	GTCTGAACCTCTGAA CCTGTAAGC	CACAAGAGCCCTGCCTTA GTTAG
Non-specific (>5 kb from TSS)	GCAAGGGCAGTCAC ATTCA	GTCTCCATTTAGTTCCTGT TTCCA

*Primers designed by Sabrina Stratton

Table 5: Pathology report and diagnosis of aging *Trim24*^{-/-} mice

Genotype	WT	WT	Null	Null	WT	WT	Null	Null
Sex	M	M	M	M	F	F	F	F
Age	12 mo	12 mo	15 mo	15 mo	12 mo	12 mo	13 mo	13 mo
Terminal body weight (g)	35.7	46.27	30.01	30.14	35.65	30.79	25.04	39.08
Liver weight	1.61	2.24	2.22	3.94	1.63	1.5	2.41	2.83
Kidney weight	0.55	0.78	1.09	0.54	0.43	0.39	0.32	0.49
Spleen weight	0.36	0.12	0.08	0.15	0.2	0.12	0.09	0.1
Tumor weight (g)/size (mm)	N/A	N/A			N/A	N/A		
Gross observations	N/A	N/A	Multiple hepatic lesions	Multiple hepatic lesions	N/A	N/A	Multiple hepatic lesions	Multiple hepatic lesions
Organ Morphologic Diagnosis	Lesion Grade	Lesion Grade	Lesion Grade	Lesion Grade	Lesion Grade	Lesion Grade	Lesion Grade	Lesion Grade
Liver/Gall Bladder	A	N	A	A	A	N	A	A
Hepatocellular Carcinoma (HCC)			P					
Undifferentiated, invasive, malignant tumor, suspect Hepatoblastoma or HCC				P				
Hepatocellular Adenoma (HCA)				P			P	P
Focal nodular hyperplasia (FNH)				P				P

Foci of cellular alteration (FCA), eosinophilic			1	2			4	4
Hepatic fatty change or lipidosis/steatosis			1	1			1	3
Hepatic necrosis, focal, acute				2				1
Lipofuscin laden-macrophages, multifocal			1	2			2	1
Karyomegalic/polyploid nuclei, hepatocytes			4	4			1	3
Microgranulomas and/or Kupffer cell hyperplasia, multifocal				2				
Large numbers of intravascular lymphocytes	3							
Extramedullary hematopoiesis					1		2	1
Inflammation, gall bladder (cholecystitis)				3				
Kidneys	A	N	A	A	A	N	A	N
Chronic Progressive Nephropathy	1		4	4	1		1	
Vascular mineralization, multifocal			2	1			1	
Hydronephrosis			4					
Atrophy, diffuse			4					
Lung	A	N	A	A	N	N	A	A

Bronchioalveolar Adenoma				P				
Increased number of intravascular lymphocytes	2							
Mineralization/calcification, multifocal, alveolar/vascular			1	4			3	1
Spleen	A	N	N	A	A	A	N	N
Lymphoid hyperplasia	4				4	3		
Extramedullary hematopoiesis, increased				4				
Heart	N	N	N	A	N	N	A	N
Mineralization/calcification, multifocal, vascular, endocardium and/or myocardium				1			1	
Skeletal muscle	N	N	N	A	N	N	N	N
Vascular mineralization/calcification, multifocal				2				
Aorta (thoracic)	0	0	N	N	0	N	0	0
Adrenal Glands	N	N	N	N	N	A	A	A
Spindle cell hyperplasia, focal, subcapsular (incidental finding)						1	2	1
Brain and head tissues	N	N	A	A	N	N	A	N
Mineralization, multifocal,			1	2			1	

neuropil								
Myodegeneration, focal, skeletal muscle of head				2				
Nose	N	N	N	N	N	N	A	N
Osteoblasts hyperplasia and fibrosis, nasal/maxillary bones (consistent w/ fibrous osteodystrophy)							2	
Mineralization of dentin, teeth							3	
Eyes, Ears	N	N	N	N	N	N	A	A
Otitis, granulomatous, chronic (cholesterol granuloma) with foci of mineralization, tympanic bulae							2	3
Pituitary Gland	N	0	N	N	N	N	N	N
Sciatic Nerve	N	N	N	N	N	N	N	N
Spinal Column	N	N	N	A	N	N	A	N
Mineralization/saponification, multifocal, of subcutaneous and intermuscular brown fat				1			2	
Vascular mineralization, multifocal, skeletal muscle and brown fat				2				

Stomach	N	N	A	A	N	N	A	A
Squamous papilloma, forestomach							P	
Hyperplasia and hyperkeratosis of squamous epithelium, forestomach			2	1				2
Gastric polyp of glandular mucosa			P	P				
Hyperplasia, focal, glandular mucosa				2			1	1
Duodenum	N	N	N	N	N	N	N	N
Pancreas	N	N	N	N	N	N	N	N
Jejunum	N	N	N	N	N	N	N	N
Ileum	N	N	N	N	N	N	N	N
Cecum	N	N	N	N	N	N	N	N
Colon/Rectum	N	N	N	N	N	N	N	N
Mesenteric Lymph Node and Mesenterium	0	N	0	A	A	0	N	N
Lymphocytic hyperplasia, paracortical					3			
Plasmacytosis, medulla					1			
Vascular mineralization of blood vessels within the mesenteric adipose tissue				2				
Salivary	N	N	N	A	N	A	A	A

Glands								
Periductal and/or perivascular lymphocytic infiltration						2	3	1
Chronic abscess, cervical/submandibular region				4				
Mandibular Lymph Node	0	N	N	A	A	N	N	N
Lymphocytic hyperplasia, lymphoid follicle and/or paracortical				3	2			
Thymus	N	N	N		0	N	N	N
Tongue	N	N	N	N	N	N	A	A
Mineralization/calcification of tongue with granulomatous inflammation and fibrosis, focal							2	2
Esophagus	N	N	N	N	N	N	N	N
Trachea	N	N	N	N	0	N	N	N
Thyroid Gland	0	N	N	N	0	N	N	N
Parathyroid	0	0	N	0	0	0	0	A
Hyperplasia, diffuse								1
Skin	N	N	N	N	A	N	A	A
Focal subcutaneous neutrophilic panniculitis					1			
Superficial dermatitis, diffuse, minimal or mild							1	1

Mammary Gland	0	0	0	0	A	N	A	A
Vascular mineralization/ calcification, multifocal, small and medium arteries of subcutaneous and mammary gland tissue							1	2
Prostate	N	N	N	N	n/a	n/a	n/a	n/a
Seminal Vesicles	N	N	N	N	n/a	n/a	n/a	n/a
Urinary Bladder	N	N	0	N	0	0	I	N
Ureter	0	0	0	0	0	A	0	N
Periureteral lymphocytic infiltration, unilateral						3		
Ovary	n/a	n/a	n/a	n/a	N	0	N	N
Uterus	n/a	n/a	n/a	n/a	N	N	A	A
Endometrial cystic hyperplasia, endometrial mucosa							2	4
Adenomyosis, focal								P
Preputial Gland	N	N	N	N	n/a	n/a	n/a	n/a
Testes	N	N	N	N	n/a	n/a	n/a	n/a
Epididymides	N	N	N	N	n/a	n/a	n/a	n/a
Femur/Knee Joint	N	N	A	A	N	A	N	N
Hemosiderin laden macrophages,						2		

increased, bone marrow								
Erythroid hyperplasia, bone marrow			2			2		
Granulocytic hyperplasia, bone marrow				3				
Sternum	A	N	A	A	N	N	N	N
Lymphocytic hyperplasia, multifocal, bone marrow	1							
Erythroid hyperplasia, bone marrow			1					
Granulocytic hyperplasia, bone marrow				3				

LEGEND

N = No lesion observed (Normal tissue)

A = Abnormal tissue (Lesion present)

0 = No tissue present on the slide

P = The lesion is present, but not graded

S = Suspected/Presumptive lesion or diagnosis (needs more tests to confirm)

PMA = Postmortem autolysis

I = Inadequate section

n/a = not applicable

GRADING/SCORING OF HISTOLOGICAL LESIONS

Grade 0 = no histologic change (or normal tissue)

Grade 1 = minimal change, rare, occasional (or lesion affects less than 10% of the tissue)

Grade 2 = mild, slight, infrequent, random, sporadic (or lesion affects 10-20% of tissue)

Grade 3 = moderate, frequent, typical, common (or lesion affects 20-40% of tissue)

Grade 4 = marked, extensive, numerous, severe (or lesion affects 40-100% of tissue)

Table 6: Top up- and down-regulated categories from *Trim24*^{-/-} vs. *Trim24*^{+/+} RNA-seq

***Trim24*^{-/-} vs. *Trim24*^{+/+} top 5 (by p-value) up-regulated categories with associated genes**

Protein folding: HSP90AB1, HSP90AA1, FKBP4, AARS, HSPH1, HSP90B1, DNAJC16, DNAJB9, DNAJB11, DNAJA1, HSPA4L, HSPE1, DNAJB1, DNAJB4, AHSA1

Defense response: CXCL1, B4GALT1, PTPRC, MBL2, IFIH1, IRGM1, LYZ2, IL1R1, C4A, COLEC10, IFI47, B2M, DDX58, TNFRSF1A, SERPINA3N, SAA2, SAA1, BCL3, CLEC2H, MX2, ORM2, H47

mRNA metabolic process: TXNL4B, APOBEC1, PRPF4B, CRNKL1, PNPT1, DDX5, WBP4, SF3B3, PNN, DNAJB11, SNRPA, HNRNPC, PRPF38B, RBM25, ADAR, TXNL4A

Regulation of cell cycle: PTPRC, E2F4, ROCK2, ESR1, JUNB, CDKN1A, CCND1, YWHAH, CCND3, JUN, B230120H23RIK, MDM2, SIK1

EndR-nuclear signaling pathway: CCND1, AARS, HSPA5, NFE2L2, EIF2AK3

***Trim24*^{-/-} vs. *Trim24*^{+/+} top 5 (by p-value) down-regulated categories with associated genes**

Oxidation Reduction: CYB5R3, ACOX2, TM7SF2, SC5D, D2HGDH, ALDH1L1, UQCRC1, HIBADH, TDO2, AKR1C6, SRD5A1, PDHA1, NQO2, HPD, CYP2C54, CYP2D22, CYP2C29, QDPR, DECR2, CYP1A2, CYP2E1, ACADL, CDO1, CYP27A1, ALDH9A1, PRODH, ME1, CYP51, HSD3B3, CYP3A25, HSD17B2, HSD3B7, FDX1, HSD3B5, CYP2C40, ALDH3A2, ALDH1A1, FASN, HAAO, NSDHL, NOX4, BCKDHA, SCD1, CYP2C37, IDO2, CRYZ, PHYH, RDH11, SDHB, AKR1C19, PRODH2, CYP8B1, RDH16, CYP2C38, CYP2C39

Steroid Metabolic Process: CYB5R3, TM7SF2, CYP51, HSD3B3, SC5D, HSD17B2, HSD3B7, 0610007P14RIK, HSD3B5, STAT5B, SLC37A4, APOA2, INSIG2, AKR1C6, SRD5A1, SCARB1, NSDHL, SOAT2, FDPS, SCAP, EBPL, HMGCS2, SULT1B1, PON1, LIPC, SLC27A5

Lipid biosynthetic process: TM7SF2, CYB5R3, CYP51, HSD3B3, SC5D, HSD17B2, SGMS2, HSD3B7, 0610007P14RIK, HSD3B5, ALDH1A1, INSIG2, ELOVL5, AKR1C6, ELOVL3, ELOVL2, FASN, SCARB1, SRD5A1, ETNK2, AGPAT2, NSDHL, SCD1, FDPS, ACACB, LPCAT3, CHPT1, ACSM3, HMGCS2, RDH16, GPAM

Table 6: Top up- and down-regulated categories from *Trim24*^{-/-} vs. *Trim24*^{+/+} RNA-seq (continued)

Fatty acid metabolic process: SCD1, ACOX2, HACL1, SC5D, ECH1, CYP2D22, STAT5B, ADIPOR2, ACACB, ACADL, PHYH, ACSM3, APOA2, ELOVL5, ELOVL3, ELOVL2, FASN, ACOT12, LIPC, AACS, ACAA1B, GPAM, SLC27A2, SLC27A5

Steroid biosynthetic process: TM7SF2, CYB5R3, CYP51, HSD3B3, SC5D, HSD17B2, HSD3B7, 0610007P14RIK, HSD3B5, FDPS, HMGCS2, INSIG2, AKR1C6, SRD5A1, SCARB1

Table 7: Lipid and Inflammatory genes activated and repressed in Trim24^{-/-}

Category	Gene	Fold change at 3 weeks	Fold change at 10 weeks	3 weeks	10 week
Lipases	<i>Lpl</i>	2.86 fold	1.07 fold	Activated	No change
	<i>Pnpla3</i>	2.03 fold	4.34 fold	Activated	Activated
	<i>Pnlip</i>	1.64 fold	8.31 fold	Repressed	Activated
	<i>Pnlprp1</i>	1.55 fold	18.09 fold	Activated	Activated
Lipid Transport Receptors	<i>Apobr</i>	1.81 fold	1.83 fold	Activated	Activated
Pro-inflammatory Factors	<i>Ccr2</i>	2.76 fold	1.94 fold	Activated	Activated
	<i>Il-33</i>	1.73 fold	2.14 fold	Activated	Activated
	<i>Icam1</i>	1.29 fold	2.46 fold	No change	Activated
	<i>Vcam1</i>	1.95 fold	1.78 fold	Activated	No change
De Novo Lipid Synthesis	<i>Acaca</i>	2.19 fold	1.09 fold	Repressed	Repressed
	<i>Acacb</i>	10.71 fold	2.76 fold	Repressed	Repressed
	<i>Acss3</i>	1.88 fold	2.28 fold	Repressed	Repressed
	<i>Fasn</i>	38.17 fold	1.28 fold	Repressed	Repressed
	<i>Mcat</i>	1.57 fold	1.41 fold	Repressed	Repressed
	<i>Me1</i>	2.46 fold	2.28 fold	Repressed	Repressed
	<i>Scd1</i>	22.39 fold	4.55 fold	Repressed	Repressed
	Lipid Storage	<i>Apoa1</i>	1.26 fold	1.87 fold	Activated
<i>Apoa5</i>		1.67 fold	1.35 fold	Repressed	Repressed
<i>Apob</i>		2.63 fold	1. fold	Repressed	Repressed
<i>Apoc1</i>		.99 fold	1.36 fold	No change	Repressed
<i>Apoc2</i>		1.38 fold	1.10 fold	Repressed	No change
<i>Apoc3</i>		2.26 fold	1.50 fold	Repressed	Repressed
<i>Apod</i>		2.06 fold	3.33 fold	Activated	Repressed
Lipid Secretion		<i>Plin2</i>	2.20 fold	1.52 fold	Repressed
	<i>Plin3</i>	2.31 fold	1.58 fold	Repressed	Repressed
	<i>Plin5</i>	1.11 fold	2.59 fold	No change	Repressed
Lipid Transport/Receptors	<i>Mttp</i>	12.11 fold	1.66 fold	Repressed	Repressed
	<i>Vldlr</i>	1.79 fold	3.61 fold	Activated	Repressed
	<i>Ldlr</i>	3.34 fold	2.19 fold	Repressed	No change
	<i>Ces1d</i>	1.47 fold	2.75 fold	Repressed	Repressed
β-oxidation*	<i>Acaa1</i>	1.23 fold	2.01 fold	No change	Repressed
	<i>Acot1</i>	4.08 fold	23.44 fold	Repressed	Repressed
	<i>Acox1</i>	2.03 fold	1.93 fold	Repressed	No change
	<i>Hsd17b6</i>	2.20 fold	2.91 fold	Repressed	Activated
	<i>Nox4</i>	1.05 fold	2.34 fold	No change	Repressed

Repressed in Trim24^{-/-}, Activated in Trim24^{-/-}, No change = no significant change compared to WT, * Data not shown.

Table 8: Comparison of phenotypic characteristics in DE4 and DE1 *Trim24*^{-/-} mice

<i>Trim24</i> ^{dIE4/ dIE4} mice ¹	<i>Trim24</i> ^{dIE1/ dIE1} mice
1-5 wk Alterations in retinoic responsive gene expression: <i>Crbp1</i> , <i>Stra6</i> , <i>Tgm2</i> (3 wk – no change, 10 wk – upregulated), and <i>Cyp26a1</i> (3 wk – upregulated, 10 wk – upregulated).	3 wk, 10 wk Alterations in retinoic responsive gene expression: <i>Crbp1</i> (3 wk – downregulated, 10 wk – upregulated), <i>Stra6</i> (3 wk and 10 wk – no significant change), <i>Tgm2</i> (3 wk – no change, 10 wk – upregulated), and <i>Cyp26a1</i> (3 wk, 10 wk – no significant change).
2 wk No reported change in hepatic steatosis phenotype	2 wk Phenotype observed -first evidence of hepatic steatosis
14 wk Increased hepatocellular proliferation	10 wk Increase in hepatocellular proliferation
2M, 3M No steatosis/damage reported, no changes in peripheral fat accumulation reported. No data regarding ALT/AST levels. Changes in hepatic expression of inflammation pathway genes, controlled by RAR- α . <i>Acot1</i> – lipid metabolism gene, downregulated in <i>Trim24</i> ^{-/-} , no other fat/lipid metabolism genes misregulated (RNA-seq)	3 wk, 10 wk (2M) Misregulated gene expression in fat/lipid metabolism and transport pathways, evidence of hepatic steatosis and damage. Histological changes consistent with NASH, increased hepatocyte apoptosis and inflammation. ALT/AST levels indicative of liver damage.
3M Abnormal hypertrophic hepatocytes, enlarged nuclei	2M Abnormal hypertrophic hepatocytes with enlarged nuclei
4-6M No reported hepatic lipid accumulation, peripheral fat accumulation, or persistent fibrosis.	4-6 M Marked hepatic lipid accumulation, peripheral fat accumulation is less than WT. Persistent fibrosis.
7-8M Clear cell foci of altered hepatocytes (FCA) 13%	7-8 M Hepatic fibrotic changes with FCA
9M 53% HCA, 12M 20% HCC, 13-19 M 41% HCC, 19-29 M 80% HCC	9-21M 26% HCA, 33% HCC with HCA, 22% HCC without HCA, 19% Other
9-29 M No change in pancreas, spleen, intestine, testis, uterus, 80% male have hepatic tumors, 69% female have hepatic tumors, Mets to the lung (n=2) (3M) Calcification reported 100% in kidney and tongue, 6% in brown fat, 13% in snout dermis, 20% in heart, 30% in retina, and 65% in thyroid	9-21M Abnormalities reported in lungs, kidneys, spleen, and heart. No abnormalities reported in pancreas, intestine, testis. 100% hepatic tumors. Hyperplasia reported in uterus. No mets (9-21M) Calcification/mineralization reported in kidney, tongue, skeletal muscle, lung, heart, mammary gland

Table 9: *Trim24* variants and predicted products upon deletion of E4

***Trim24* Variant 1**

1 ggtggtccaa ggggcccag agaaaggctg ctaggcacgg gcgggcgcg tgggcggaat
61 cgagcgtctc ggtggcggtt tgcctatcgg cccgcgcggc ggcgtcgcgg tgcgggaacc
121 ggtccccgtt gacagctccg cgtctccgg ccgcgccact cgggaggtgg ctctctcct
181 gtgtccctc cgcgagtcg ttcggcctcg gagaagcggg aggcggcggc ggctcggag
241 gtcgtcgggg gcggcggcg gtgagcgcgc tcccgctcc cggcggcgg cgcaggaca
301 atggaggtgg ctgtggagaa ggcggcggcg gcagcggctc cggccggagg cccgcagcg
361 gcggcggcga gcggggagaa tgaggccgag agccggcagg gcccgactc ggagagcggc
421 ggcgaggcgt cccggctcaa cctgtggac acttgcgcc tgtccacca gaacatccag
481 agccgggtgc ccaagctgct gccctgctg cactcgttct gccagcgtg ttgcccgcg
541 ccgcagcgt atctatgct gacggcgccc gcgctgggct cggcagagac cctccacc
601 gctccccccc ccgccccgc cccgggctcc cggccggtg gtcctcggc attcggacc
661 caagtggag tcattcgatg ccagtttg agtcaagagt gtgctgagag acacatcata
721 gacaactttt ttgtaagga caccactgaa gttcctagta gtacagtaga aaagtcta
781 caggtatgta caagctgtga agacaatgca gaagctaag gttttgtgt agagtgtt
841 gaatggctct gcaagacatg tattagagct caccagagg tgaagttcac aaaagaccac
901 acagtcaggc agaaagaaga agtatctca gaggcagttg ggtgaccag tcagcgacca
961 gtgtttgtc cctccataa aaaggagcag ttgaaacttt actgtgaaac atgtgataa
1021 ctgacctgtc gagactgcca gctgctagaa cacaaagaac acaggtatca atttatagaa
1081 gaagctttc agaatcaaaa agtgatcata gatactctaa tcaccaaact gatggaaaa
1141 acaaaatata taaagtatac aggaatcag atcaaaaata g

***Trim24* Variant 1 with E4 deletion**

1 ggtggtccaa ggggcccag agaaaggctg ctaggcacgg gcgggcgcg tgggcggaat
61 cgagcgtctc ggtggcggtt tgcctatcgg cccgcgcggc ggcgtcgcgg tgcgggaacc
121 ggtccccgtt gacagctccg cgtctccgg ccgcgccact cgggaggtgg ctctctcct
181 gtgtccctc cgcgagtcg ttcggcctcg gagaagcggg aggcggcggc ggctcggag
241 gtcgtcgggg gcggcggcg gtgagcgcgc tcccgctcc cggcggcgg cgcaggaca
301 atggaggtgg ctgtggagaa ggcggcggcg gcagcggctc cggccggagg cccgcagcg
361 gcggcggcga gcggggagaa tgaggccgag agccggcagg gcccgactc ggagagcggc
421 ggcgaggcgt cccggctcaa cctgtggac acttgcgcc tgtccacca gaacatccag
481 agccgggtgc ccaagctgct gccctgctg cactcgttct gccagcgtg ttgcccgcg
541 ccgcagcgt atctatgct gacggcgccc gcgctgggct cggcagagac cctccacc
601 gctccccccc ccgccccgc cccgggctcc cggccggtg gtcctcggc attcggacc
661 caagtggag tcattcgatg ccagtttg agtcaagagt gtgctgagag acacatcata
721 gacaactttt ttgtaagga caccactgaa gttcctagta gtacagtaga aaagtcta
781 caggtatgta caagctgtga agacaatgca gaagctaag gttttgtgt agagtgtt
841 gaatggctct gcaagacatg tattagagct caccagagg tgaagttcac aaaagaccac
901 acagtcaggc agaaagaaga agtatctca gatactctaa atttatagaa
1081 gaagctttc agaatcaaaa agtgatcata gatactctaa tcaccaaact gatggaaaa
1141 acaaaatata taaagtatac aggaatcag atcaaaaata g

Table 9: *Trim24* variants and predicted products upon deletion of E4 (continued)

***Trim24* Variant 3**

1 gacatcat gcagtctcac cacttggtag ttgtactttg gagaccagc cttaacagg
 61 ggcaccttg gggccactag ctattcaact atggcagata ttttgatta cactttatc
 121 ggtgggtg gagatgctg tccacatgc gcatgtgaa gtcagaggat aactggaaa
 181 agtcagttct tccatcctg tttctgtccc atggataaaa ctgctgtcac tggatgag
 241 caagttggag tcattcgatg cccagttgc agtcaagagt gtgctgagag acacatcata
 301 gacaactttt ttgtgaagga caccactgaa gttcctagta gtacagtaga aaagtcta
 361 caggtatgta caagctgtga agacaatgca gaagctaag ggtttgtgt agagtgtgt
 421 gaatggctct gcaagacatg tattagagct caccagaggg tgaagttcac aaaagaccac
 481 acagtcaggc agaaagaaga agtatctcca gaggcagttg gggtagaccag tcagcgacca
 541 gtgtttgtc ccttccataa aaaggagcag ttgaaacttt actgtgaaac atgtgataaa
 601 ctgacctgtc gagactgcca gctgctagaa cacaaagaac acaggtatca atttatagaa
 661 gaagctttc agaatcaaaa agtgatcata gatactctaa tcaccaaact gatggaaaa
 721 acaaaatata taaagtatac aggaaatcag atccaaaata g

***Trim24* Variant 3 with E4 deletion**

1 gacatcat gcagtctcac cacttggtag ttgtactttg gagaccagc cttaacagg
 61 ggcaccttg gggccactag ctattcaact atggcagata ttttgatta cactttatc
 121 ggtgggtg gagatgctg tccacatgc gcatgtgaa gtcagaggat aactggaaa
 181 agtcagttct tccatcctg tttctgtccc atggataaaa ctgctgtcac tggatgag
 241 caagttggag tcattcgatg cccagttgc agtcaagagt gtgctgagag acacatcata
 301 gacaactttt ttgtgaagga caccactgaa gttcctagta gtacagtaga aaagtcta
 361 caggtatgta caagctgtga agacaatgca gaagctaag ggtttgtgt agagtgtgt
 421 gaatggctct gcaagacatg tattagagct caccagaggg tgaagttcac aaaagaccac
 481 acagtcaggc agaaagaaga agtatctcca gta tca atttatagaa
 661 gaagctttc agaatcaaaa agtgatcata gatactctaa tcaccaaact gatggaaaa
 721 acaaaatata taaagtatac aggaaatcag atccaaaata g

Key:

Variant 1:

E1 – 301-664 (from start site), E2 – 665-783, E3 – 784-931, E4 – 932-1064,
 E5 – 1065-1181 Splice site Stop codon

Variant 3:

E1 – 91-244 (from start site), E2 – 245-363, E3 – 364-511, E4 – 512-644,
 E5 – 645-761 Splice site Stop codon

Table 14. Flow Cytometry Antibodies

Antibody/Cell Marker	Surface	Target	Compnay
CD45*- PB		Hematopoietic cells	eBioscience
Ly6G (Gr1)- FITC		Lymphoid lineage	eBioscience
F4/80- Precp		Macrophages	eBioscience
Cd11b-PE		Myeloid lineage	eBioscience
Cd11c-PE-Cy7		Dendritic cells	eBioscience
Cd3-APC-Cy7		T cells	eBioscience
B220 -APC		B cells	Becton Dickson

***Not included in analysis of bone marrow cells**

Table 15. CyTOF Antibodies

Antibody/Cell Surface Marker	Target	Company
CD45	Hematopoietic cells	DVS
Ly6G (Gr1)	Lymphoid lineage	DVS
Cd11b	Myeloid lineage	DVS
Cd11c	Dendritic cells	DVS
*F4/80	Macrophages	Biolegend
*Arg1	M2 Macrophages	Biolegend
*Cd14	Monocytes/Macrophages/Dendritic cells/Neutrophils	Biolegend
B220	B cells	DVS
Cd3	T cells	eBioscience
Cd45RA	Lymphocyte	DVS
Cd117	Hematopoietic cells	DVS
Cyclin D	Cell Cycle	BD Biosciences
IFN γ	M2 Macrophages	DVS
pRB	Cell Cycle	BD Biosciences
TRIM24/28	-	Proteintech
p53	-	Biolegend

***Currently validating for future experiments**

Appendix 1: Solutions for ChIP

2X SM2 Buffer

0.5M Sucrose/Dextrose (Sigma/Fisher)

80mM KCl (Fisher)

20mM HEPES (pH 7.9) (Fisher)

6mM CaCl (Sigma)

H₂O (to 5 mL)

10X EDTA/EGTA Stop Solution

0.5M EDTA (Fisher)

0.1M EGTA (Sigma)

H₂O (to 1 mL)

Cell Lysis buffer

5mM PIPES pH 8.0 (Sigma)

85mM KCl (Fisher)

0.5% NP40 (Fluka)

PI's (fresh) (Sigma)

H₂O (to 10 mL)

Appendix 1: Solutions for ChIP (continued)

Nuclei Lysis Buffer

50mM Tris-Cl pH 8.1 (Fisher)

10mM EDTA (Fisher)

1% SDS (Bio Rad)

PI's (fresh) (Sigma)

H2O (to 10 mL)

Lysis Buffer

150mM NaCl (Fisher)

25mM Tris pH 7.5 (Fisher)

5mM EDTA (Fisher)

1% Triton X 100 (Fisher)

0.1% SDS (Bio Rad)

0.5% Deoxycholate (Fisher)

PI's (fresh) (Sigma)

H2O (to 10 mL)

High Salt Buffer (see previous for manufacturers)

50mM Tris pH 8.0

500mM NaCl

0.1% SDS

0.5% Deoxycholate

1% NP40

1mM EDTA

PI's (fresh)

H₂O (to 10 mL)

RIPA (see previous for manufacturers)

50mM Tris pH 8.0

150mM NaCl

0.1% SDS

0.5% Deoxycholate

1% NP40

1mM EDTA

PI's (fresh)

H₂O (to 10 mL)

LiCl Wash

50mM Tris pH 8.0

1mM EDTA

250mM LiCl (Fisher)

1% NP40

0.5% Deoxycholate

PI's (fresh)

H₂O (to 10 mL)

TE Buffer

10 mM Tris-HCL pH 7.5

1 mM EDTA pH 8.0

H₂O (to 500 mL)

Bibliography

- [1] Kurinna S, Barton MC. Hierarchies of transcriptional regulation during liver regeneration. *Progress in molecular biology and translational science* 2010;97:201-227.
- [2] Sabine Colnot and Perret C. Liver Zonation. In: Monga SPS, editor. *Molecular Pathogenesis of Liver Diseases*: Springer US; 2011. p. 7-16.
- [3] Krishna M. Microscopic Anatomy of the Liver. In: Mayo Clinic F, editor.: *AASLD*; 2013.
- [4] Katz N, Teutsch HF, Sasse D, Jungermann K. Heterogeneous distribution of glucose-6-phosphatase in microdissected periportal and perivenous rat liver tissue. *FEBS letters* 1977;76:226-230.
- [5] Jungermann K, Kietzmann T. Zonation of parenchymal and nonparenchymal metabolism in liver. *Annual review of nutrition* 1996;16:179-203.
- [6] Blaner WS, O'Byrne SM, Wongsiriroj N, Kluwe J, D'Ambrosio DM, Jiang H, Schwabe RF, Hillman EM, Piantedosi R, Libien J. Hepatic stellate cell lipid droplets: a specialized lipid droplet for retinoid storage. *Biochimica et biophysica acta* 2009;1791:467-473.
- [7] Lee UE, Friedman SL. Mechanisms of hepatic fibrogenesis. *Best practice & research Clinical gastroenterology* 2011;25:195-206.
- [8] Brenner DA, Waterboer T, Choi SK, Lindquist JN, Stefanovic B, Burchardt E, Yamauchi M, Gillan A, Rippe RA. New aspects of hepatic fibrosis. *Journal of hepatology* 2000;32:32-38.

- [9] Yang C, Zeisberg M, Mosterman B, Sudhakar A, Yerramalla U, Holthaus K, Xu L, Eng F, Afdhal N, Kalluri R. Liver fibrosis: insights into migration of hepatic stellate cells in response to extracellular matrix and growth factors. *Gastroenterology* 2003;124:147-159.
- [10] Zeisberg M, Yang C, Martino M, Duncan MB, Rieder F, Tanjore H, Kalluri R. Fibroblasts derive from hepatocytes in liver fibrosis via epithelial to mesenchymal transition. *The Journal of biological chemistry* 2007;282:23337-23347.
- [11] Wilson JW, Groat CS, Leduc EH. Histogenesis of the Liver. *Annals of the New York Academy of Sciences* 1963;111:8-24.
- [12] Bilzer M, Roggel F, Gerbes AL. Role of Kupffer cells in host defense and liver disease. *Liver international : official journal of the International Association for the Study of the Liver* 2006;26:1175-1186.
- [13] Parker GA, Picut CA. Liver immunobiology. *Toxicologic pathology* 2005;33:52-62.
- [14] Furth Rv. *Mononuclear phagocytes: biology of monocytes and macrophages*: Kluwer Academic Publishers; 1992.
- [15] Bouwens L, Baekeland M, Wisse E. Importance of local proliferation in the expanding Kupffer cell population of rat liver after zymosan stimulation and partial hepatectomy. *Hepatology* 1984;4:213-219.
- [16] Malik R, Selden C, Hodgson H. The role of non-parenchymal cells in liver growth. *Seminars in cell & developmental biology* 2002;13:425-431.
- [17] Jump DB, Tripathy S, Depner CM. Fatty acid-regulated transcription factors in the liver. *Annual review of nutrition* 2013;33:249-269.

- [18] Yamada Y, Kirillova I, Peschon JJ, Fausto N. Initiation of liver growth by tumor necrosis factor: deficient liver regeneration in mice lacking type I tumor necrosis factor receptor. *Proceedings of the National Academy of Sciences of the United States of America* 1997;94:1441-1446.
- [19] Cressman DE, Greenbaum LE, DeAngelis RA, Ciliberto G, Furth EE, Poli V, Taub R. Liver failure and defective hepatocyte regeneration in interleukin-6-deficient mice. *Science* 1996;274:1379-1383.
- [20] Wuestefeld T, Klein C, Streetz KL, Betz U, Lauber J, Buer J, Manns MP, Muller W, Trautwein C. Interleukin-6/glycoprotein 130-dependent pathways are protective during liver regeneration. *The Journal of biological chemistry* 2003;278:11281-11288.
- [21] Day CP, James OF. Steatohepatitis: a tale of two "hits"? *Gastroenterology* 1998;114:842-845.
- [22] Pan JJ, Fallon MB. Gender and racial differences in nonalcoholic fatty liver disease. *World journal of hepatology* 2014;6:274-283.
- [23] Larter CZ, Chitturi S, Heydet D, Farrell GC. A fresh look at NASH pathogenesis. Part 1: the metabolic movers. *Journal of gastroenterology and hepatology* 2010;25:672-690.
- [24] Myers RP. Noninvasive diagnosis of nonalcoholic fatty liver disease. *Annals of hepatology* 2009;8 Suppl 1:S25-33.
- [25] Brunt EM. Histopathology of non-alcoholic fatty liver disease. *Clinics in liver disease* 2009;13:533-544.

- [26] Takahashi Y, Soejima Y, Fukusato T. Animal models of nonalcoholic fatty liver disease/nonalcoholic steatohepatitis. *World journal of gastroenterology : WJG* 2012;18:2300-2308.
- [27] Adams LA, Angulo P. Recent concepts in non-alcoholic fatty liver disease. *Diabetic medicine : a journal of the British Diabetic Association* 2005;22:1129-1133.
- [28] Harrison SA, Torgerson S, Hayashi PH. The natural history of nonalcoholic fatty liver disease: a clinical histopathological study. *The American journal of gastroenterology* 2003;98:2042-2047.
- [29] Cohen JC, Horton JD, Hobbs HH. Human fatty liver disease: old questions and new insights. *Science* 2011;332:1519-1523.
- [30] Teli MR, Day CP, Burt AD, Bennett MK, James OF. Determinants of progression to cirrhosis or fibrosis in pure alcoholic fatty liver. *Lancet* 1995;346:987-990.
- [31] McCullough AJ. Pathophysiology of nonalcoholic steatohepatitis. *Journal of clinical gastroenterology* 2006;40 Suppl 1:S17-29.
- [32] Takaki A, Kawai D, Yamamoto K. Multiple hits, including oxidative stress, as pathogenesis and treatment target in non-alcoholic steatohepatitis (NASH). *International journal of molecular sciences* 2013;14:20704-20728.
- [33] Peverill W, Powell LW, Skoien R. Evolving concepts in the pathogenesis of NASH: beyond steatosis and inflammation. *International journal of molecular sciences* 2014;15:8591-8638.
- [34] Kawamura Y, Arase Y, Ikeda K, Seko Y, Imai N, Hosaka T, Kobayashi M, Saitoh S, Sezaki H, Akuta N, Suzuki F, Suzuki Y, Ohmoto Y, Amakawa K, Tsuji H,

Kumada H. Large-scale long-term follow-up study of Japanese patients with non-alcoholic Fatty liver disease for the onset of hepatocellular carcinoma. *The American journal of gastroenterology* 2012;107:253-261.

[35] Riordan JD, Nadeau JH. Modeling progressive non-alcoholic fatty liver disease in the laboratory mouse. *Mammalian genome : official journal of the International Mammalian Genome Society* 2014.

[36] Romeo S, Kozlitina J, Xing C, Pertsemlidis A, Cox D, Pennacchio LA, Boerwinkle E, Cohen JC, Hobbs HH. Genetic variation in PNPLA3 confers susceptibility to nonalcoholic fatty liver disease. *Nature genetics* 2008;40:1461-1465.

[37] Yuan X, Waterworth D, Perry JR, Lim N, Song K, Chambers JC, Zhang W, Vollenweider P, Stirnadel H, Johnson T, Bergmann S, Beckmann ND, Li Y, Ferrucci L, Melzer D, Hernandez D, Singleton A, Scott J, Elliott P, Waeber G, Cardon L, Frayling TM, Kooner JS, Mooser V. Population-based genome-wide association studies reveal six loci influencing plasma levels of liver enzymes. *American journal of human genetics* 2008;83:520-528.

[38] Li Q, Qu HQ, Rentfro AR, Grove ML, Mirza S, Lu Y, Hanis CL, Fallon MB, Boerwinkle E, Fisher-Hoch SP, McCormick JB. PNPLA3 polymorphisms and liver aminotransferase levels in a Mexican American population. *Clinical and investigative medicine Medecine clinique et experimentale* 2012;35:E237-245.

[39] Wagenknecht LE, Scherzinger AL, Stamm ER, Hanley AJ, Norris JM, Chen YD, Bryer-Ash M, Haffner SM, Rotter JI. Correlates and heritability of nonalcoholic fatty liver disease in a minority cohort. *Obesity* 2009;17:1240-1246.

- [40] Younossi ZM, Stepanova M, Negro F, Hallaji S, Younossi Y, Lam B, Srishord M. Nonalcoholic fatty liver disease in lean individuals in the United States. *Medicine* 2012;91:319-327.
- [41] Brunt EM, Kleiner DE, Wilson LA, Belt P, Neuschwander-Tetri BA, Network NCR. Nonalcoholic fatty liver disease (NAFLD) activity score and the histopathologic diagnosis in NAFLD: distinct clinicopathologic meanings. *Hepatology* 2011;53:810-820.
- [42] Kleiner DE, Brunt EM, Van Natta M, Behling C, Contos MJ, Cummings OW, Ferrell LD, Liu YC, Torbenson MS, Unalp-Arida A, Yeh M, McCullough AJ, Sanyal AJ, Nonalcoholic Steatohepatitis Clinical Research N. Design and validation of a histological scoring system for nonalcoholic fatty liver disease. *Hepatology* 2005;41:1313-1321.
- [43] Bedossa P, Poitou C, Veyrie N, Bouillot JL, Basdevant A, Paradis V, Tordjman J, Clement K. Histopathological algorithm and scoring system for evaluation of liver lesions in morbidly obese patients. *Hepatology* 2012;56:1751-1759.
- [44] McPherson S, Stewart SF, Henderson E, Burt AD, Day CP. Simple non-invasive fibrosis scoring systems can reliably exclude advanced fibrosis in patients with non-alcoholic fatty liver disease. *Gut* 2010;59:1265-1269.
- [45] Vallet-Pichard A, Mallet V, Nalpas B, Verkarre V, Nalpas A, Dhalluin-Venier V, Fontaine H, Pol S. FIB-4: an inexpensive and accurate marker of fibrosis in HCV infection. comparison with liver biopsy and fibrotest. *Hepatology* 2007;46:32-36.

- [46] Wieckowska A, McCullough AJ, Feldstein AE. Noninvasive diagnosis and monitoring of nonalcoholic steatohepatitis: present and future. *Hepatology* 2007;46:582-589.
- [47] Schwenger KJ, Allard JP. Clinical approaches to non-alcoholic fatty liver disease. *World journal of gastroenterology : WJG* 2014;20:1712-1723.
- [48] Attar BM, Van Thiel DH. Current concepts and management approaches in nonalcoholic fatty liver disease. *TheScientificWorldJournal* 2013;2013:481893.
- [49] Meroni G, Diez-Roux G. TRIM/RBCC, a novel class of 'single protein RING finger' E3 ubiquitin ligases. *BioEssays : news and reviews in molecular, cellular and developmental biology* 2005;27:1147-1157.
- [50] Wang C, Rauscher FJ, 3rd, Cress WD, Chen J. Regulation of E2F1 function by the nuclear corepressor KAP1. *The Journal of biological chemistry* 2007;282:29902-29909.
- [51] Beckstead R, Ortiz JA, Sanchez C, Prokopenko SN, Chambon P, Losson R, Bellen HJ. Bonus, a Drosophila homolog of TIF1 proteins, interacts with nuclear receptors and can inhibit betaFTZ-F1-dependent transcription. *Molecular cell* 2001;7:753-765.
- [52] Zeng L, Yap KL, Ivanov AV, Wang X, Mujtaba S, Plotnikova O, Rauscher FJ, 3rd, Zhou MM. Structural insights into human KAP1 PHD finger-bromodomain and its role in gene silencing. *Nature structural & molecular biology* 2008;15:626-633.
- [53] Zhong S, Delva L, Rachez C, Cenciarelli C, Gandini D, Zhang H, Kalantry S, Freedman LP, Pandolfi PP. A RA-dependent, tumour-growth suppressive

transcription complex is the target of the PML-RARalpha and T18 oncoproteins. *Nature genetics* 1999;23:287-295.

[54] Le Douarin B, Zechel C, Garnier JM, Lutz Y, Tora L, Pierrat P, Heery D, Gronemeyer H, Chambon P, Losson R. The N-terminal part of TIF1, a putative mediator of the ligand-dependent activation function (AF-2) of nuclear receptors, is fused to B-raf in the oncogenic protein T18. *The EMBO journal* 1995;14:2020-2033.

[55] Le Douarin B, Nielsen AL, Garnier JM, Ichinose H, Jeanmougin F, Losson R, Chambon P. A possible involvement of TIF1 alpha and TIF1 beta in the epigenetic control of transcription by nuclear receptors. *The EMBO journal* 1996;15:6701-6715.

[56] Klugbauer S, Rabes HM. The transcription coactivator HTIF1 and a related protein are fused to the RET receptor tyrosine kinase in childhood papillary thyroid carcinomas. *Oncogene* 1999;18:4388-4393.

[57] Allton K, Jain AK, Herz HM, Tsai WW, Jung SY, Qin J, Bergmann A, Johnson RL, Barton MC. Trim24 targets endogenous p53 for degradation. *Proc Natl Acad Sci U S A* 2009;106:11612-11616.

[58] Tisserand J, Khetchoumian K, Thibault C, Dembele D, Chambon P, Losson R. Tripartite motif 24 (Trim24/Tif1alpha) tumor suppressor protein is a novel negative regulator of interferon (IFN)/signal transducers and activators of transcription (STAT) signaling pathway acting through retinoic acid receptor alpha (Raralpha) inhibition. *The Journal of biological chemistry* 2011;286:33369-33379.

[59] Tsai WW, Wang Z, Yiu TT, Akdemir KC, Xia W, Winter S, Tsai CY, Shi X, Schwarzer D, Plunkett W, Aronow B, Gozani O, Fischle W, Hung MC, Patel DJ,

Barton MC. TRIM24 links a non-canonical histone signature to breast cancer. *Nature* 2010;468:927-932.

[60] Tisserand J, Khetchoumian K, Thibault C, Dembele D, Chambon P, Losson R. Tripartite motif 24 (Trim24/Tif1alpha) tumor suppressor protein is a novel negative regulator of interferon (IFN)/signal transducers and activators of transcription (STAT) signaling pathway acting through retinoic acid receptor alpha (Raralpha) inhibition. *The Journal of biological chemistry* 2011;286:33369-33379.

[61] Venturini L, You J, Stadler M, Galien R, Lallemand V, Koken MH, Mattei MG, Ganser A, Chambon P, Losson R, de The H. TIF1gamma, a novel member of the transcriptional intermediary factor 1 family. *Oncogene* 1999;18:1209-1217.

[62] vom Baur E, Zechel C, Heery D, Heine MJ, Garnier JM, Vivat V, Le Douarin B, Gronemeyer H, Chambon P, Losson R. Differential ligand-dependent interactions between the AF-2 activating domain of nuclear receptors and the putative transcriptional intermediary factors mSUG1 and TIF1. *The EMBO journal* 1996;15:110-124.

[63] Thenot S, Bonnet S, Boulahtouf A, Margeat E, Royer CA, Borgna JL, Cavailles V. Effect of ligand and DNA binding on the interaction between human transcription intermediary factor 1alpha and estrogen receptors. *Molecular endocrinology* 1999;13:2137-2150.

[64] Teyssier C, Ou CY, Khetchoumian K, Losson R, Stallcup MR. Transcriptional intermediary factor 1alpha mediates physical interaction and functional synergy between the coactivator-associated arginine methyltransferase 1 and glucocorticoid

receptor-interacting protein 1 nuclear receptor coactivators. *Molecular endocrinology* 2006;20:1276-1286.

[65] Khetchoumian K, Teletin M, Tisserand J, Herquel B, Ouararhni K, Losson R. Trim24 (Tif1 alpha): an essential 'brake' for retinoic acid-induced transcription to prevent liver cancer. *Cell cycle* 2008;7:3647-3652.

[66] Ignat M, Teletin M, Tisserand J, Khetchoumian K, Dennefeld C, Chambon P, Losson R, Mark M. Arterial calcifications and increased expression of vitamin D receptor targets in mice lacking TIF1alpha. *Proceedings of the National Academy of Sciences of the United States of America* 2008;105:2598-2603.

[67] Pathiraja TN, K.N. Thakkar, S. Jiang, S. Stratton, Z. Liu, M. Gagea, S. Xi, P. Shah, L. Phan, M-H. Lee, J. Andersen, M. Stampfer, and Michelle C. Barton. TRIM24 links glucose metabolism with transformation of human mammary epithelial cells. *Oncogene* 2014;In Press.

[68] Jain AK, Allton K, Duncan AD, Barton MC. TRIM24 is a p53-Induced E3-Ubiquitin Ligase that undergoes ATM-Mediated Phosphorylation and Autodegradation during DNA Damage. *Molecular and cellular biology* 2014.

[69] Crooke RM, Graham MJ, Lemonidis KM, Whipple CP, Koo S, Perera RJ. An apolipoprotein B antisense oligonucleotide lowers LDL cholesterol in hyperlipidemic mice without causing hepatic steatosis. *J Lipid Res* 2005;46:872-884.

[70] Carr TP, Andresen CJ, Rudel LL. Enzymatic determination of triglyceride, free cholesterol, and total cholesterol in tissue lipid extracts. *Clin Biochem* 1993;26:39-42.

- [71] Amir el AD, Davis KL, Tadmor MD, Simonds EF, Levine JH, Bendall SC, Shenfeld DK, Krishnaswamy S, Nolan GP, Pe'er D. viSNE enables visualization of high dimensional single-cell data and reveals phenotypic heterogeneity of leukemia. *Nature biotechnology* 2013;31:545-552.
- [72] Kurinna S, Stratton SA, Tsai WW, Akdemir KC, Gu W, Singh P, Goode T, Darlington GJ, Barton MC. Direct activation of forkhead box O3 by tumor suppressors p53 and p73 is disrupted during liver regeneration in mice. *Hepatology* 2010;52:1023-1032.
- [73] Trapnell C, Pachter L, Salzberg SL. TopHat: discovering splice junctions with RNA-Seq. *Bioinformatics* 2009;25:1105-1111.
- [74] Robinson MD, McCarthy DJ, Smyth GK. edgeR: a Bioconductor package for differential expression analysis of digital gene expression data. *Bioinformatics* 2010;26:139-140.
- [75] Thorvaldsdottir H, Robinson JT, Mesirov JP. Integrative Genomics Viewer (IGV): high-performance genomics data visualization and exploration. *Brief Bioinform* 2012.
- [76] Robinson JT, Thorvaldsdottir H, Winckler W, Guttman M, Lander ES, Getz G, Mesirov JP. Integrative genomics viewer. *Nat Biotechnol* 2011;29:24-26.
- [77] Machanick P, Bailey TL. MEME-ChIP: motif analysis of large DNA datasets. *Bioinformatics* 2011;27:1696-1697.
- [78] Thomas-Chollier M, Hufton A, Heinig M, O'Keeffe S, Masri NE, Roider HG, Manke T, Vingron M. Transcription factor binding predictions using TRAP for the analysis of ChIP-seq data and regulatory SNPs. *Nat Protoc* 2011;6:1860-1869.

- [79] Chambon M, Orsetti B, Berthe ML, Bascoul-Mollevi C, Rodriguez C, Duong V, Gleizes M, Thenot S, Bibeau F, Theillet C, Cavailles V. Prognostic significance of TRIM24/TIF-1alpha gene expression in breast cancer. *Am J Pathol* 2011;178:1461-1469.
- [80] Cui Z, Cao W, Li J, Song X, Mao L, Chen W. TRIM24 overexpression is common in locally advanced head and neck squamous cell carcinoma and correlates with aggressive malignant phenotypes. *PLoS One* 2013;8:e63887.
- [81] Li H, Sun L, Tang Z, Fu L, Xu Y, Li Z, Luo W, Qiu X, Wang E. Overexpression of TRIM24 Correlates with Tumor Progression in Non-Small Cell Lung Cancer. *PLoS One* 2012;7:e37657.
- [82] Zhang LH, Yin AA, Cheng JX, Huang HY, Li XM, Zhang YQ, Han N, Zhang X. TRIM24 promotes glioma progression and enhances chemoresistance through activation of the PI3K/Akt signaling pathway. *Oncogene* 2014.
- [83] Liu X, Huang Y, Yang D, Li X, Liang J, Lin L, Zhang M, Zhong K, Liang B, Li J. Overexpression of TRIM24 is associated with the onset and progress of human hepatocellular carcinoma. *PloS one* 2014;9:e85462.
- [84] Khetchoumian K, Teletin M, Tisserand J, Mark M, Herquel B, Ignat M, Zucman-Rossi J, Cammas F, Lerouge T, Thibault C, Metzger D, Chambon P, Losson R. Loss of Trim24 (Tif1alpha) gene function confers oncogenic activity to retinoic acid receptor alpha. *Nat Genet* 2007;39:1500-1506.
- [85] Herquel B, Ouarrhni K, Martianov I, Le Gras S, Ye T, Keime C, Lerouge T, Jost B, Cammas F, Losson R, Davidson I. Trim24-repressed VL30 retrotransposons regulate gene expression by producing noncoding RNA. *Nat Struct Mol Biol* 2013.

- [86] Matsui T, Leung D, Miyashita H, Maksakova IA, Miyachi H, Kimura H, Tachibana M, Lorincz MC, Shinkai Y. Proviral silencing in embryonic stem cells requires the histone methyltransferase ESET. *Nature* 2010;464:927-931.
- [87] Hatakeyama S. TRIM proteins and cancer. *Nat Rev Cancer* 2011;11:792-804.
- [88] Freemont PS. The RING finger. A novel protein sequence motif related to the zinc finger. *Annals of the New York Academy of Sciences* 1993;684:174-192.
- [89] Herquel B, Ouarrhni K, Khetchoumian K, Ignat M, Teletin M, Mark M, Bechade G, Van Dorsselaer A, Sanglier-Cianferani S, Hamiche A, Cammas F, Davidson I, Losson R. Transcription cofactors TRIM24, TRIM28, and TRIM33 associate to form regulatory complexes that suppress murine hepatocellular carcinoma. *Proc Natl Acad Sci U S A* 2011;108:8212-8217.
- [90] Fon Tacer K, Rozman D. Nonalcoholic Fatty liver disease: focus on lipoprotein and lipid deregulation. *J Lipids* 2011;2011:783976.
- [91] Trapnell C, Williams BA, Pertea G, Mortazavi A, Kwan G, van Baren MJ, Salzberg SL, Wold BJ, Pachter L. Transcript assembly and quantification by RNA-Seq reveals unannotated transcripts and isoform switching during cell differentiation. *Nat Biotechnol* 2010;28:511-515.
- [92] Jenuwein T, Allis CD. Translating the histone code. *Science* 2001;293:1074-1080.
- [93] Ruthenburg AJ, Li H, Patel DJ, Allis CD. Multivalent engagement of chromatin modifications by linked binding modules. *Nat Rev Mol Cell Biol* 2007;8:983-994.
- [94] Katzenellenbogen BS. Estrogen receptors: bioactivities and interactions with cell signaling pathways. *Biol Reprod* 1996;54:287-293.

- [95] Cheskis BJ, Greger JG, Nagpal S, Freedman LP. Signaling by estrogens. *J Cell Physiol* 2007;213:610-617.
- [96] Huang da W, Sherman BT, Lempicki RA. Bioinformatics enrichment tools: paths toward the comprehensive functional analysis of large gene lists. *Nucleic Acids Res* 2009;37:1-13.
- [97] Chavez AO, Kamath S, Jani R, Sharma LK, Monroy A, Abdul-Ghani MA, Centonze VE, Sathyanarayana P, Coletta DK, Jenkinson CP, Bai Y, Folli F, Defronzo RA, Tripathy D. Effect of short-term free Fatty acids elevation on mitochondrial function in skeletal muscle of healthy individuals. *J Clin Endocrinol Metab* 2010;95:422-429.
- [98] Carroll JS, Liu XS, Brodsky AS, Li W, Meyer CA, Szary AJ, Eeckhoute J, Shao W, Hestermann EV, Geistlinger TR, Fox EA, Silver PA, Brown M. Chromosome-wide mapping of estrogen receptor binding reveals long-range regulation requiring the forkhead protein FoxA1. *Cell* 2005;122:33-43.
- [99] Kato S, Sasaki H, Suzawa M, Masushige S, Tora L, Chambon P, Gronemeyer H. Widely spaced, directly repeated PuGGTCA elements act as promiscuous enhancers for different classes of nuclear receptors. *Mol Cell Biol* 1995;15:5858-5867.
- [100] Amengual J, Ribot J, Bonet ML, Palou A. Retinoic acid treatment increases lipid oxidation capacity in skeletal muscle of mice. *Obesity* 2008;16:585-591.
- [101] Hoekstra M, Li Z, Kruijt JK, Van Eck M, Van Berkel TJ, Kuiper J. The expression level of non-alcoholic fatty liver disease-related gene PNPLA3 in hepatocytes is highly influenced by hepatic lipid status. *J Hepatol* 2010;52:244-251.

- [102] Starley BQ, Calcagno CJ, Harrison SA. Nonalcoholic fatty liver disease and hepatocellular carcinoma: a weighty connection. *Hepatology* 2010;51:1820-1832.
- [103] Hebbard L, George J. Animal models of nonalcoholic fatty liver disease. *Nat Rev Gastroenterol Hepatol* 2011;8:35-44.
- [104] Zhang XQ, Xu CF, Yu CH, Chen WX, Li YM. Role of endoplasmic reticulum stress in the pathogenesis of nonalcoholic fatty liver disease. *World journal of gastroenterology : WJG* 2014;20:1768-1776.
- [105] Khetchoumian K, Teletin M, Tisserand J, Mark M, Herquel B, Ignat M, Zucman-Rossi J, Cammas F, Lerouge T, Thibault C, Metzger D, Chambon P, Losson R. Loss of Trim24 (Tif1alpha) gene function confers oncogenic activity to retinoic acid receptor alpha. *Nature genetics* 2007;39:1500-1506.
- [106] Miki T, Fleming TP, Crescenzi M, Molloy CJ, Blam SB, Reynolds SH, Aaronson SA. Development of a highly efficient expression cDNA cloning system: application to oncogene isolation. *Proc Natl Acad Sci U S A* 1991;88:5167-5171.
- [107] Le Douarin B, Zechel C, Garnier JM, Lutz Y, Tora L, Pierrat P, Heery D, Gronemeyer H, Chambon P, Losson R. The N-terminal part of TIF1, a putative mediator of the ligand-dependent activation function (AF-2) of nuclear receptors, is fused to B-raf in the oncogenic protein T18. *Embo J* 1995;14:2020-2033.
- [108] Breuhahn K, Vreden S, Haddad R, Beckebaum S, Stippel D, Flemming P, Nussbaum T, Caselmann WH, Haab BB, Schirmacher P. Molecular profiling of human hepatocellular carcinoma defines mutually exclusive interferon regulation and insulin-like growth factor II overexpression. *Cancer Res* 2004;64:6058-6064.

- [109] Malaguarnera M, Di Rosa M, Nicoletti F, Malaguarnera L. Molecular mechanisms involved in NAFLD progression. *J Mol Med (Berl)* 2009;87:679-695.
- [110] Kim NH, Kim JH, Kim YJ, Yoo HJ, Kim HY, Seo JA, Kim NH, Choi KM, Baik SH, Choi DS, Kim SG. Clinical and metabolic factors associated with development and regression of nonalcoholic fatty liver disease in nonobese subjects. *Liver international : official journal of the International Association for the Study of the Liver* 2014;34:604-611.
- [111] Geissmann F, Gordon S, Hume DA, Mowat AM, Randolph GJ. Unravelling mononuclear phagocyte heterogeneity. *Nature reviews Immunology* 2010;10:453-460.
- [112] Murray PJ, Wynn TA. Protective and pathogenic functions of macrophage subsets. *Nature reviews Immunology* 2011;11:723-737.
- [113] Gordon S, Taylor PR. Monocyte and macrophage heterogeneity. *Nature reviews Immunology* 2005;5:953-964.
- [114] Mosmann TR, Cherwinski H, Bond MW, Giedlin MA, Coffman RL. Two types of murine helper T cell clone. I. Definition according to profiles of lymphokine activities and secreted proteins. *Journal of immunology* 1986;136:2348-2357.
- [115] Mills CD, Kincaid K, Alt JM, Heilman MJ, Hill AM. M-1/M-2 macrophages and the Th1/Th2 paradigm. *Journal of immunology* 2000;164:6166-6173.
- [116] Martinez FO, Gordon S. The M1 and M2 paradigm of macrophage activation: time for reassessment. *F1000prime reports* 2014;6:13.
- [117] Wynn TA, Barron L. Macrophages: master regulators of inflammation and fibrosis. *Seminars in liver disease* 2010;30:245-257.

- [118] Wynn TA. Fibrotic disease and the T(H)1/T(H)2 paradigm. *Nature reviews Immunology* 2004;4:583-594.
- [119] Odegaard JI, Chawla A. Alternative macrophage activation and metabolism. *Annual review of pathology* 2011;6:275-297.
- [120] Lumeng CN, Deyoung SM, Saltiel AR. Macrophages block insulin action in adipocytes by altering expression of signaling and glucose transport proteins. *American journal of physiology Endocrinology and metabolism* 2007;292:E166-174.
- [121] de Visser KE, Korets LV, Coussens LM. De novo carcinogenesis promoted by chronic inflammation is B lymphocyte dependent. *Cancer cell* 2005;7:411-423.
- [122] Yang XD, Ai W, Asfaha S, Bhagat G, Friedman RA, Jin G, Park H, Shykind B, Diacovo TG, Falus A, Wang TC. Histamine deficiency promotes inflammation-associated carcinogenesis through reduced myeloid maturation and accumulation of CD11b+Ly6G+ immature myeloid cells. *Nature medicine* 2011;17:87-95.
- [123] Sierra JR, Corso S, Caione L, Cepero V, Conrotto P, Cignetti A, Piacibello W, Kumanogoh A, Kikutani H, Comoglio PM, Tamagnone L, Giordano S. Tumor angiogenesis and progression are enhanced by Sema4D produced by tumor-associated macrophages. *The Journal of experimental medicine* 2008;205:1673-1685.
- [124] Nardin A, Abastado JP. Macrophages and cancer. *Frontiers in bioscience : a journal and virtual library* 2008;13:3494-3505.
- [125] Kryczek I, Zou L, Rodriguez P, Zhu G, Wei S, Mottram P, Brumlik M, Cheng P, Curiel T, Myers L, Lackner A, Alvarez X, Ochoa A, Chen L, Zou W. B7-H4

expression identifies a novel suppressive macrophage population in human ovarian carcinoma. *The Journal of experimental medicine* 2006;203:871-881.

[126] Andreu P, Johansson M, Affara NI, Pucci F, Tan T, Junankar S, Korets L, Lam J, Tawfik D, DeNardo DG, Naldini L, de Visser KE, De Palma M, Coussens LM. FcRgamma activation regulates inflammation-associated squamous carcinogenesis. *Cancer cell* 2010;17:121-134.

[127] Cortez-Pinto H, de Moura MC, Day CP. Non-alcoholic steatohepatitis: from cell biology to clinical practice. *Journal of hepatology* 2006;44:197-208.

[128] Marra F, Gastaldelli A, Svegliati Baroni G, Tell G, Tiribelli C. Molecular basis and mechanisms of progression of non-alcoholic steatohepatitis. *Trends in molecular medicine* 2008;14:72-81.

[129] Tilg H. The role of cytokines in non-alcoholic fatty liver disease. *Digestive diseases* 2010;28:179-185.

[130] Sica A, Invernizzi P, Mantovani A. Macrophage plasticity and polarization in liver homeostasis and pathology. *Hepatology* 2014;59:2034-2042.

[131] Tirone TA, Brunicardi FC. Overview of glucose regulation. *World journal of surgery* 2001;25:461-467.

[132] Gerich JE. Lilly lecture 1988. Glucose counterregulation and its impact on diabetes mellitus. *Diabetes* 1988;37:1608-1617.

[133] Owen OE, Felig P, Morgan AP, Wahren J, Cahill GF, Jr. Liver and kidney metabolism during prolonged starvation. *The Journal of clinical investigation* 1969;48:574-583.

- [134] Cahill GF, Jr. Starvation in man. *The New England journal of medicine* 1970;282:668-675.
- [135] Szablewski L. *Glucose Homeostasis and Insulin Resistance*: Bentham Science Publishers; 2011.
- [136] Karim S, Adams DH, Lalor PF. Hepatic expression and cellular distribution of the glucose transporter family. *World journal of gastroenterology : WJG* 2012;18:6771-6781.
- [137] Ward PS, Thompson CB. Metabolic reprogramming: a cancer hallmark even warburg did not anticipate. *Cancer cell* 2012;21:297-308.
- [138] DeBerardinis RJ. Is cancer a disease of abnormal cellular metabolism? New angles on an old idea. *Genetics in medicine : official journal of the American College of Medical Genetics* 2008;10:767-777.
- [139] Schulze A, Harris AL. How cancer metabolism is tuned for proliferation and vulnerable to disruption. *Nature* 2012;491:364-373.
- [140] Bard-Chapeau EA, Nguyen AT, Rust AG, Sayadi A, Lee P, Chua BQ, New LS, de Jong J, Ward JM, Chin CK, Chew V, Toh HC, Abastado JP, Benoukraf T, Soong R, Bard FA, Dupuy AJ, Johnson RL, Radda GK, Chan EC, Wessels LF, Adams DJ, Jenkins NA, Copeland NG. Transposon mutagenesis identifies genes driving hepatocellular carcinoma in a chronic hepatitis B mouse model. *Nature genetics* 2014;46:24-32.
- [141] Farrell GC, Larter CZ. Nonalcoholic fatty liver disease: from steatosis to cirrhosis. *Hepatology* 2006;43:S99-S112.

- [142] Namani A, Li Y, Wang XJ, Tang X. Modulation of NRF2 signaling pathway by nuclear receptors: Implications for cancer. *Biochimica et biophysica acta* 2014;1843:1875-1885.
- [143] Guo L, Guo Y, Xiao S, Shi X. Protein kinase p-JNK is correlated with the activation of AP-1 and its associated Jun family proteins in hepatocellular carcinoma. *Life sciences* 2005;77:1869-1878.
- [144] Hahn ME. Aryl hydrocarbon receptors: diversity and evolution. *Chemico-biological interactions* 2002;141:131-160.
- [145] Marhenke S, Buitrago-Molina LE, Endig J, Orlik J, Schweitzer N, Klett S, Longerich T, Geffers R, Sanchez Munoz A, Dorrell C, Katz SF, Lechel A, Weng H, Krech T, Lehmann U, Dooley S, Rudolph KL, Manns MP, Vogel A. p21 promotes sustained liver regeneration and hepatocarcinogenesis in chronic cholestatic liver injury. *Gut* 2014;63:1501-1512.
- [146] Thomsen KL, Hebbard L, Glavind E, Clouston A, Vilstrup H, George J, Gronbaek H. Non-alcoholic steatohepatitis weakens the acute phase response to endotoxin in rats. *Liver international : official journal of the International Association for the Study of the Liver* 2014.
- [147] Feng ZP, Li XY, Jiang R, Deng HC, Yang M, Zhou Q, Que WJ, Du J. Associations of SAA1 gene polymorphism with lipid levels and osteoporosis in Chinese women. *Lipids in health and disease* 2013;12:39.
- [148] Song C, Hsu K, Yamen E, Yan W, Fock J, Witting PK, Geczy CL, Freedman SB. Serum amyloid A induction of cytokines in monocytes/macrophages and lymphocytes. *Atherosclerosis* 2009;207:374-383.

- [149] Welsby I, Hutin D, Gueydan C, Kruys V, Rongvaux A, Leo O. PARP12, an Interferon Stimulated Gene Involved in the Control of Protein Translation and Inflammation. *The Journal of biological chemistry* 2014.
- [150] Goldstein I, Yizhak K, Madar S, Goldfinger N, Ruppin E, Rotter V. p53 promotes the expression of gluconeogenesis-related genes and enhances hepatic glucose production. *Cancer & metabolism* 2013;1:9.
- [151] Wortmann M, Peters AS, Hakimi M, Bockler D, Dihlmann S. Glyoxalase I (Glo1) and its metabolites in vascular disease. *Biochemical Society transactions* 2014;42:528-533.
- [152] Kohler UA, Kurinna S, Schwitter D, Marti A, Schafer M, Hellerbrand C, Speicher T, Werner S. Activated Nrf2 impairs liver regeneration in mice by activation of genes involved in cell-cycle control and apoptosis. *Hepatology* 2013.
- [153] Ikeda Y, Sugawara A, Taniyama Y, Uruno A, Igarashi K, Arima S, Ito S, Takeuchi K. Suppression of rat thromboxane synthase gene transcription by peroxisome proliferator-activated receptor gamma in macrophages via an interaction with NRF2. *The Journal of biological chemistry* 2000;275:33142-33150.
- [154] Wang XJ, Sun Z, Villeneuve NF, Zhang S, Zhao F, Li Y, Chen W, Yi X, Zheng W, Wondrak GT, Wong PK, Zhang DD. Nrf2 enhances resistance of cancer cells to chemotherapeutic drugs, the dark side of Nrf2. *Carcinogenesis* 2008;29:1235-1243.
- [155] Mitsuishi Y, Taguchi K, Kawatani Y, Shibata T, Nukiwa T, Aburatani H, Yamamoto M, Motohashi H. Nrf2 redirects glucose and glutamine into anabolic pathways in metabolic reprogramming. *Cancer cell* 2012;22:66-79.

- [156] Niture SK, Jaiswal AK. Nrf2 protein up-regulates antiapoptotic protein Bcl-2 and prevents cellular apoptosis. *The Journal of biological chemistry* 2012;287:9873-9886.
- [157] Niture SK, Jaiswal AK. Nrf2-induced antiapoptotic Bcl-xL protein enhances cell survival and drug resistance. *Free radical biology & medicine* 2013;57:119-131.
- [158] Csaki LS, Dwyer JR, Li X, Nguyen MH, Dewald J, Brindley DN, Lusic AJ, Yoshinaga Y, de Jong P, Fong L, Young SG, Reue K. Lipin-1 and lipin-3 together determine adiposity in vivo. *Molecular metabolism* 2014;3:145-154.
- [159] Velho G, Petersen KF, Perseghin G, Hwang JH, Rothman DL, Pueyo ME, Cline GW, Froguel P, Shulman GI. Impaired hepatic glycogen synthesis in glucokinase-deficient (MODY-2) subjects. *The Journal of clinical investigation* 1996;98:1755-1761.
- [160] Magnuson MA, Andreone TL, Printz RL, Koch S, Granner DK. Rat glucokinase gene: structure and regulation by insulin. *Proceedings of the National Academy of Sciences of the United States of America* 1989;86:4838-4842.
- [161] Beyoglu D, Idle JR. The metabolomic window into hepatobiliary disease. *Journal of hepatology* 2013;59:842-858.
- [162] Medina RA, Owen GI. Glucose transporters: expression, regulation and cancer. *Biological research* 2002;35:9-26.
- [163] Godoy A, Ulloa V, Rodriguez F, Reinicke K, Yanez AJ, Garcia Mde L, Medina RA, Carrasco M, Barberis S, Castro T, Martinez F, Koch X, Vera JC, Poblete MT, Figueroa CD, Peruzzo B, Perez F, Nualart F. Differential subcellular distribution of glucose transporters GLUT1-6 and GLUT9 in human cancer: ultrastructural

localization of GLUT1 and GLUT5 in breast tumor tissues. *Journal of cellular physiology* 2006;207:614-627.

[164] Kurata T, Oguri T, Isobe T, Ishioka S, Yamakido M. Differential expression of facilitative glucose transporter (GLUT) genes in primary lung cancers and their liver metastases. *Japanese journal of cancer research : Gann* 1999;90:1238-1243.

[165] Miura K, Yang L, van Rooijen N, Ohnishi H, Seki E. Hepatic recruitment of macrophages promotes nonalcoholic steatohepatitis through CCR2. *Am J Physiol Gastrointest Liver Physiol* 2012;302:G1310-1321.

[166] Lujambio A, Akkari L, Simon J, Grace D, Tschaharganeh DF, Bolden JE, Zhao Z, Thapar V, Joyce JA, Krizhanovsky V, Lowe SW. Non-cell-autonomous tumor suppression by p53. *Cell* 2013;153:449-460.

[167] Petrasek J, Bala S, Csak T, Lippai D, Kodys K, Menashy V, Barrieau M, Min SY, Kurt-Jones EA, Szabo G. IL-1 receptor antagonist ameliorates inflammasome-dependent alcoholic steatohepatitis in mice. *The Journal of clinical investigation* 2012;122:3476-3489.

[168] Stienstra R, Joosten LA, Koenen T, van Tits B, van Diepen JA, van den Berg SA, Rensen PC, Voshol PJ, Fantuzzi G, Hijmans A, Kersten S, Muller M, van den Berg WB, van Rooijen N, Wabitsch M, Kullberg BJ, van der Meer JW, Kanneganti T, Tack CJ, Netea MG. The inflammasome-mediated caspase-1 activation controls adipocyte differentiation and insulin sensitivity. *Cell metabolism* 2010;12:593-605.

[169] Stienstra R, Saudale F, Duval C, Keshtkar S, Groener JE, van Rooijen N, Staels B, Kersten S, Muller M. Kupffer cells promote hepatic steatosis via

interleukin-1beta-dependent suppression of peroxisome proliferator-activated receptor alpha activity. *Hepatology* 2010;51:511-522.

[170] Uygun BE, Soto-Gutierrez A, Yagi H, Izamis ML, Guzzardi MA, Shulman C, Milwid J, Kobayashi N, Tilles A, Berthiaume F, Hertl M, Nahmias Y, Yarmush ML, Uygun K. Organ reengineering through development of a transplantable recellularized liver graft using decellularized liver matrix. *Nature medicine* 2010;16:814-820.

[171] Farrell GC, van Rooyen D, Gan L, Chitturi S. NASH is an Inflammatory Disorder: Pathogenic, Prognostic and Therapeutic Implications. *Gut and liver* 2012;6:149-171.

VITA

Lindsey Ann Cauthen Minter was born in Woodville, Texas on November 21, 1984, the daughter of Pamela McCullough Cauthen and Timothy Mason Cauthen. Following her graduation from Cathedral Christian High School, Beaumont, Texas in 2002, she entered Lamar University in Beaumont, Texas. She received the degrees of Bachelor of Science with a major in biology, minor in chemistry, and Bachelor of Arts in music, with concentrations in piano and voice, both summa cum laude, from Lamar in May, 2007. Following her college graduation, she worked for a year as a research technician in the Department of Reproductive Biology and Physiology at Texas A&M University. During this time, she applied and was accepted to The University of Texas MD Anderson Cancer Center Graduate School of Biomedical Sciences at Houston and began her studies in 2008. She joined the laboratory of Dr. Michelle C. Barton in 2009. She married her husband, Andrew, in 2012.

Permanent Address:

13135 7th Street

Santa Fe, Texas 77510